

POLITECNICO DI TORINO

Collegio di Ingegneria Chimica e dei Materiali

**Master of Science Course
in Materials Engineering**

Master of Science Thesis

**Deposition and characterization of thin films made
with active layer from end life first generation solar cells**



Tutors

Prof. Matteo Pavese

Prof. Isabel Ferreira

Candidate

Francesco Toscano

October 2023

This page is intentionally left blank

Index:

Abstract	5
Introduction	6
First generation solar cells.....	12
Processes.....	13
Devices.....	17
Second generation solar cells.....	21
Amorphous silicon.....	21
Cadmium telluride.....	22
CIGS.....	23
Third generation solar cells.....	24
Organic solar cells.....	25
Dye sensitized solar cells.....	26
Quantum dot solar cells	27
Perovskite solar cells	28
Heterojunction solar cells.....	31
Silicon partners.....	31
Record heterojunction.....	32
Recycling processes.....	33
Semiconductor recycling.....	34
Other materials recycling.....	34
Materials and methods	34
Materials.....	35
Useful instruments.....	36
Jaasco spectrophotometer.....	37
Thermal evaporator.....	39
Hall effect measurement.....	42
Seebeck and voltage measurement.....	43
I-V curves measurement.....	44
Results and discussion	45
Influence of thickness.....	46
Deposition.....	46
Spectrophotometer.....	49
Seebeck and Voltage measurement.....	51
I-V curves measurement.....	53
Hall effect measurement.....	55
Discussion of results.....	56
Shutter and Al-bottom configurations.....	57

Deposition.....	57
Spectrophotometer.....	59
Seebeck and voltage measurement.....	61
I-V curves measurement.....	64
Hall effect measurement.....	66
Discussion of results.....	67
P-N junction.....	68
Deposition.....	70
Spectrophotometer.....	71
Seebeck and voltage measurement.....	74
I-V curves measurement.....	76
Hall effect measurement.....	78
Discussion of results.....	79
Conclusions.....	81
Energetic and economic considerations.....	81
Environmental considerations.....	84
Final considerations.....	87
Ringraziamenti.....	89
Bibliography.....	90

Abstract:

Photovoltaic technology is one of the most promising technology of the present and the near future. Nowadays several different solar cells are available in the market in order to try to meet the demand of different sectors which requires devices with different performance, thickness and flexibility to entirely cover the demand. However, the biggest part of the market share belongs to the crystalline silicon solar cells with over the 90% of the demand covered [1]. Furthermore, the demand of solar energy is estimated to grow another 60% in 2030, reaching 31600 TWh [1]. With these premises, it is evident that silicon solar panels are massively impacting the environment in a way that is not always positive: although it is true that renewable energy sources such as the solar one currently seems the best solution to keep our energy needs away from fossil fuels, there are still negative evidences concerning researchers all over the world, especially because of the massive pollution generated during the production of the silicon and the assembly of the photovoltaic module. During the production of silicon modules, in fact, a lot of chemicals are used in order to purify, deposit, build contacts, and all the other necessary steps to produce the final result. Another major concern regards the disposal of the photovoltaic modules after their lifetime: it can be assumed that the lifetime of a solar panel varies from 15 to 30 years according to the initial year of installation, which underlines the technological improvements made year by year in the solar sector [2].

After this amount of time, the easiest way to dispose of solar modules is the landfilling, which is also the most negatively impacting from an environmental point of view.

In order to avoid it and find the most useful way to give a new birth to the various materials used in the photovoltaic technology, many recycling processes were ideated, with the active layer of silicon as the heart of these processes. Usually the followed path is the leaching: through the use of chemicals the active layer is purified from all the contacts and materials that were needed during the working time of the PV.

Although it is an easy way to recycle silicon, it is still not environmentally friendly under all aspects: the use of chemicals such as toxic gases and strong acids it is always associated with some damage. In this work will be discussed the possibility to generate new value for crystalline solar cells trying to exploit the semiconductor active layer just with thermochemical processes. Not just recycle into new solar cells will be discussed, but also the possibility to exploit the new silicon for other applications such as sensors or optical devices.

The characterization will be conducted on thin films of the recycled material after depositions through thermal evaporation, and several experimental setups will be used for its characterization, such as Hall effect measurement, Jaasco spectrophotometer, Seebeck coefficient measurement, $I-V$ curves experimental setup and $V-t$ curves experimental setup in order to explore the potential of the deposited materials with and without further treatments and of simple p-n junctions built with a monolayer of the same material, recycled active layer from first generation solar cells waste.

1)Introduction:

Although the materials used in this study come from the crystalline silicon solar cells, it is indeed needed a general view of all the devices available on the market, which can vary not just because of the materials used, but also in the working mechanism and in the building processes. The division of different solar cells technologies is not universal, but the majority describes them as divided in four different types of technologies: the first generation is composed of polycrystalline and monocrystalline solar cells, the second generation regards all the thin films devices, ranging from amorphous silicon to cadmium telluride and CIGS (copper indium gallium diselenide), while the third generation includes the latest advancements in the field, such as organic solar cells, dye sensitized solar cells, quantum dot solar cells and perovskite solar cells [3]. The fourth generation of solar cells regards the multiple junctions or tandem solar cells, which were ideated to overcome the limit of the active layer of the solar panels: the band gap. It is a parameter fundamental to understand the energy that incident photons must have to start the photovoltaic effect, making the carriers “jump” from the valence band to the conduction band, thus creating the photoelectric effect. In effect, the simplest solar cell can be seen like a p-n junction, that is a junction between two semiconductor materials or one material doped differently in different regions [4]: when the light rays hit the junction, the photons with energy equal or higher than the band gap generate a separation of charge between electrons and holes, the two carriers of the solar cell: these two carriers cannot recombine immediately in a p-n junction because of the intrinsic electric field created in the junction itself [5]: for that reason, they can be harvested simply using two metal contacts in the bottom and in the top of the solar cell.

Although the solar cell has a structure far more complex than this, and lot of changes in the design can give better performances, at the bottom of the technology this will be always the effect exploited, with a little difference for organic solar cells, has it will be further investigated later. What about the energy that can be harvested? It is a common estimation that the sun’s energy that arrives at the Earth’s surface is approximately 1000 W/m^2 , available without any cost and more than enough to cover the human needs [4].

The only two limitations of the solar energy harvesting consist in the fact that solar energy is not available at night for obvious reasons, and it’s not always uniform throughout days and seasons of the year: according to the position and the hour of the day a lot of changes can occur in the light incident a solar panel [4].

However, as it can be seen in the figure below, the band gap can be seen as a little amount of energy that is needed for a semiconductor material in order to generate the carriers, while for other classes of materials, such as metals and dielectrics, the situation is different: metals have the two bands partially overlapped, which means they don’t need energy to generate free

carriers while dielectrics have a band gap that is too high to reach, which means that is very difficult to generate free carriers and they act as insulators [6].

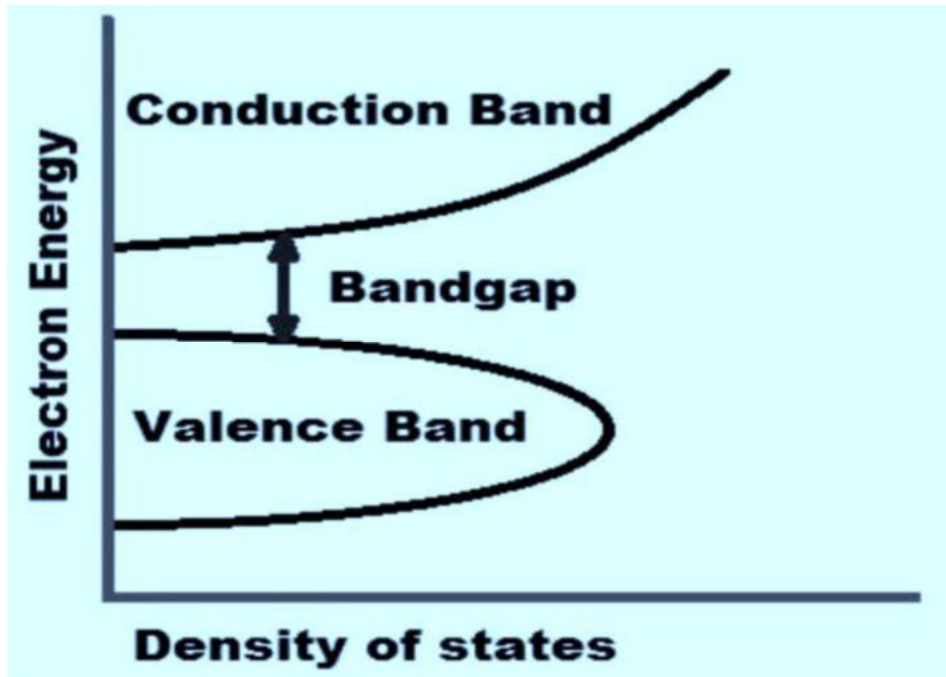


Fig 1.1: schematic of the band gap [6]

Cell type	Bandgap (eV)	V_{oc} (V)	FF (%)
Si	1.12	0.71	82.8
GaAs	1.42	1.11	85.9
InP	1.28	0.88	85.4
CIGS	1.15	0.71	79.2
CdTe	1.45	0.84	75.5
a-Si	1.73	0.89	67
DSC (black dye)	1.3	0.74	68
DSC (N719)	1.6	0.82	74
DSC (YD2-o-c8 + Y123) ^a	1.7	0.93	74
Organic Polymer (Konarka)	1.65	0.82	70.2
Organic Small Molecule (Mitsubishi)	1.66	0.90	66.1

Fig 1.2: list of band gaps for several materials [6]

According to the previous figure, the choice of the material strongly influence the final efficiency of the solar cells: one of the general rules to design an efficient solar panel is the utilization of a material with a band gap between 1.1 eV and 1.7 eV, preferably direct [7]. This range perfectly suits with the solar spectrum range, making possible the harvest of the greatest part of the solar photons.

In fact, if the solar spectrum is considered, it is evident how, independently on the AM (air mass) the majority of the energy available comes from the visible light (ranging from 400 to 750 nm) and the near IR [8]:it has also to be said that in case of space applications the solar spectra is slightly different (moved on higher energies), because solar rays are not filtered by the atmosphere [8], so if solar technology is needed for solar space applications the choice of the material might change according to this.

Schockley and Queisser have plotted the maximum theoretical efficiency that can be reached by a single junction solar cell according to its band gap considering all the inevitable losses of the system. The loss of efficiency in a solar cell is due to both intrinsic and extrinsic losses [9]: the extrinsic losses can, in principle, be eliminated because they are due to absorption of the inactive window layer, series resistance of the different materials that compose the panel and impurities and defects that can be generated during the manufacturing process. On the contrary, the intrinsic losses are caused by various side effects happening in the system during its work life.

If no new entropy is generated, the solar cell can be seen as an heat engine which has an efficiency of 95% (the Carnot efficiency) [9].The math explanation for this rely on the equation [10]:

$$\frac{T_{sun} - T_{cell}}{T_{sun}} = 95\%$$

In which we considered $T_{sun} = 6000$ K, $T_{cell} = 300$ K.

This means that even if the device was ideal, and it needs conditions not manageable to reach in real life, the efficiency would not be unitary.

The loss factors to take into account are the recombination of electron/hole pairs, which lower the efficiency by another 1% [9], the mismatch between the angle of incident and emitted radiation, which lower the efficiency of another 9% [9], shadowing effect and reflection of the incident photons, [9] and the two most important losses: the transparency of the solar cell absorber to photons which have an energy below the band gap of the material (which is one of the main reason for multijunction solar cells to be created) and the thermalization losses that happen when an incident photon with an higher energy compared to the band gap excite the layer: in fact the electrons and holes created with these photons thermalize with the lattice, generating an energy dispersion before being extracted at the band edges. Furthermore, some of the incident photons, after the thermalization, can also be re-emitted as new photons of littler wavelength [11].

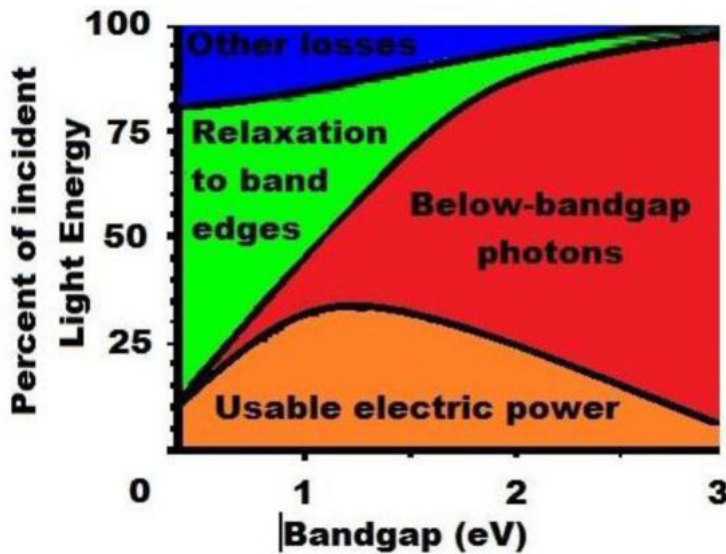


Fig 1.3: A schematic representation of the possible losses in a solar panel [6]

Surprisingly, the sight of efficiency as a function of the band gap doesn't crown the silicon as the most efficient active layer, although its efficiency is very near the theoretical maximum level: in fact GaAs (gallium arsenide) has a maximum efficiency estimated at 33.2% [12], thanks to its bandgap of 1.42 eV, against the approximately 32% of silicon [12].

So why silicon solar panels are the majority in the market? The answer must be searched in the other characteristics that make a semiconductor or another type of material perfect for the application:

- Readily available and non toxic material
- Cheap and available for mass production
- Good PV conversion efficiency
- Long term stability factor

All this other factors to take into account along with the high cost of GaAs production, make the silicon the most easy going and functional path nowadays, although, as it will be shown later, there are many efforts in the academies and industries in order to find alternative solutions, especially in order to find a way to overcome the Shockley-Queisser limit and to design flexible solar cells, suitable to cover any surface and also to be integrated in the textiles of clothes [13]. One of the problems of crystalline silicon, for example, is the indirect band gap, which makes necessary to thicken the absorbing layer: in fact, the use of a direct band gap material, lowers the cost of the photo-absorbing material because a thinner layer is needed to absorb sufficient amount of light for photoconversion [13].

After talking about the materials properties, it is useful to have a glance on how can be calculated the power emitted by a solar cell: the first thing to do is to collect data for the short-circuit current I_{sc} and the open circuit voltage V_{oc} [14], which can be calculated by a simple characterization of the material in a laboratory, or simulated by software. Unfortunately, the plot of $I-V$ curve shows that these two numbers are not the maximum values possible, which, according to [14] in equation terms means that:

$$\frac{I_{sc} * V_{oc}}{I_{max} * V_{max}} < 1$$

That also means it can be used a fill factor FF , that can range from 0 to 1, in order to adjust the equation considering that the curve is not rectangular but has a rounded shape.

If we indicate the maximum incident power of the sun as P_{in} , a factor of efficiency can be obtained according to [14]:

$$\frac{I_{sc} * V_{oc} * FF}{P_{in}} = \eta$$

Which, of course, can be demonstrated to be linked to the temperature according to [15]:

$$J_0 = J_{sc} * \left(\exp \left[\frac{q * V_{oc}}{Kb * T} \right] - 1 \right)$$

Where J indicates a density current instead of a current, q is the elementary charge, Kb is the Stefan-Boltzmann constant, and T is the temperature of the cell.

Finally, it has to be said that these parameters should't be seen as untangled from the elementary properties of the material: the fact that both I_{sc} and V_{oc} can be extrapolated from experimental curves, makes easy to understand that they are properties depending on the materials used to build the junction. All the parameters are found for SC (standard conditions), for values of Air Mass=1.5, $T_{cell}=298.15$ K, Irradiance power=1000 W/m². [3]

In the figure below, it is shown the trend and the evolution of different solar systems based on the four generations that will be analysed consequently: this graph should be seen as a guide in order to understand the latest advancements and in which direction the future will be directed. The technologies taken into consideration will be:

- Crystalline silicon solar cells
- Thin film technologies, considering also amorphous silicon thin films
- Multijunction solar cells, with 2, 3 or 4 junctions
- Single junction GaAs solar cells
- Organic solar cells
- Dye sensitized solar cells
- Quantum dot solar cells
- Perovskite solar cells

In some of them the word concentrator is written, which means that a structure, usually glassy, is used to concentrate the sun rays on the active layer [10].

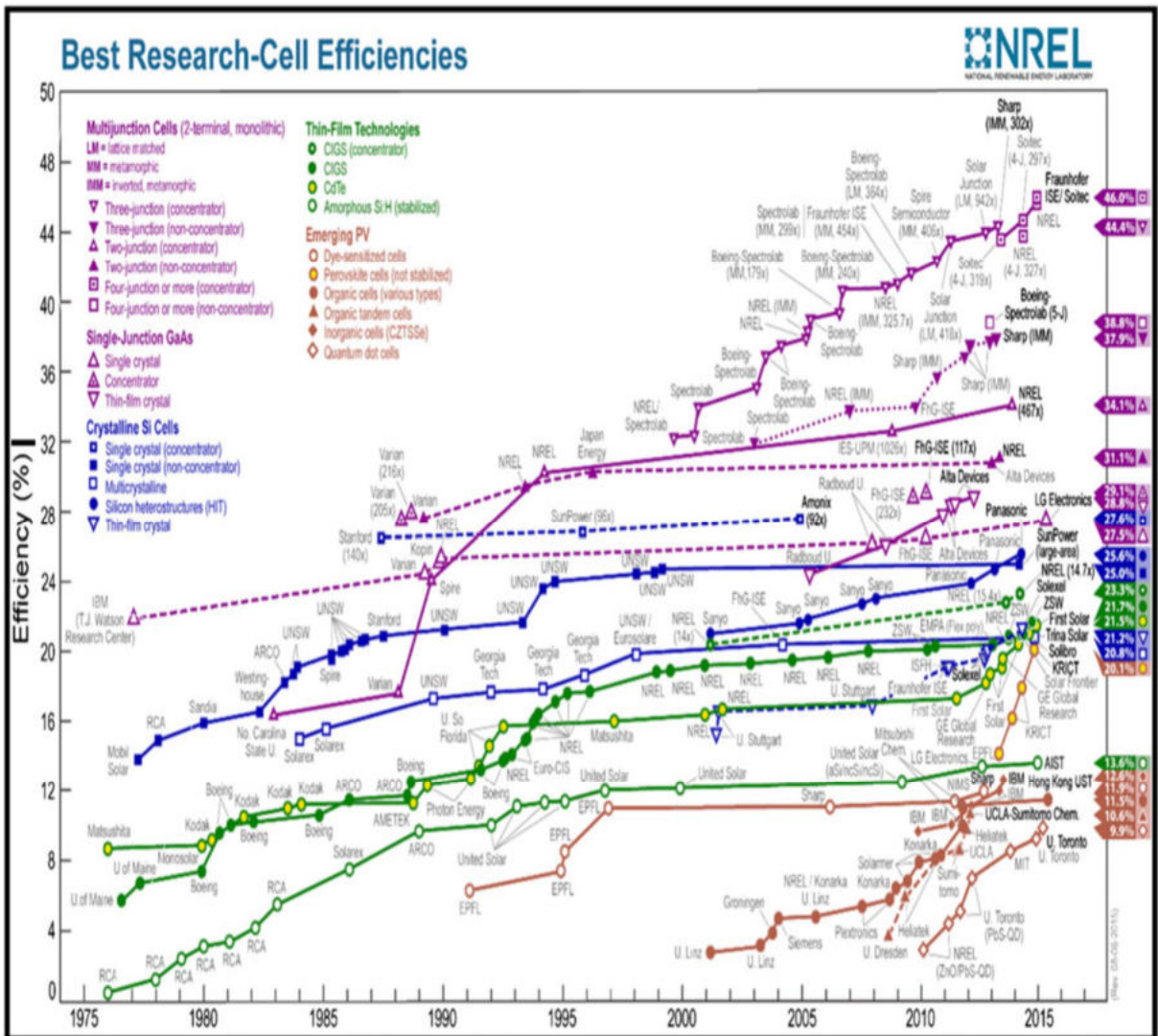


Fig 1.4: evolution of the efficiencies of different solar cell types [7]

From the figure 1.4, it is evident how efficient the multijunction solar cells are if compared with the others: the record of efficiency has been reached by the Fraunhofer four junctions solar cells with the help of a solar concentrator: the efficiency is of 46% [7].

The single junction GaAs solar cells have an efficiency that overcome by some percentual points the one of the crystalline silicon solar cells, confirming what discussed before about the Shockley-Queisser efficiency. The crystalline silicon solar cells have an average efficiency of about 23%, although an higher result (27.6%) can be obtained with a monocrystalline solar cell with the help of a solar concentrator. Since the slope of the various curves indicates the rapidity of the technological advancements in that sector, it can also be observed that silicon solar cells have already reached the full technological maturity, while the progresses in the multijunctions solar cells are rapidly advancing.

The thin films solar cells have also reached somehow the maturity, with different classes and types of materials already explored, although their efficiency is lower compared to the types of solar cells analysed before, their use can be justified with the easy going deposition technique, a thinning of the absorption layer and consequently of the structure, and lower production costs. However, with the use of a concentrator, a CIGS thin film solar cell has reached an efficiency of 23.3% [7], which is seen as an extraordinary result for this kind of technology.

What about the latest available techs in the market? The third generation solar cells has the highest slope of all the curves, which underlines that these devices are still in the starting phase of their lifetime. From fig 1.5 we can observe that there are no data available for the majority of that technologies before 2008, with the only exception of dye sensitized solar cells, which started to be studied at lab scale in 1990. The average efficiency of that systems varies from 10% for the dye solar cells to 12% [7] for the organic solar cells.

A huge exception in this field are the perovskite solar cells, which were discovered just in 2013, but they are already arrived to an efficiency of 20.1% [7], which makes them the most promising solar tech of the future, once their problems will be faced and solved, as will be discussed in the following paragraphs.

As a final conclusion of the analysis of the graph, it is interesting to underline how different results can be achieved by different companies or institutes starting with the same active material, just changing the design of the device and the process used to manufacture the sample: the know-how of building a more performant device starting with the same raw materials is one of the hearth skills of materials engineering.

Now that a complete panoramic of the different technologies has been done, it is time to explore the pros and cons of the different solar cells, considering also the production processes available, the costs and the environmental impact. After that, an overview on the currently available recycling process will be given, to have a complete idea of what is the current state of art.

1.1)First generation solar cells

To this class belong the crystalline silicon technologies, divided in polycrystalline solar cells and monocrystalline solar cells [16], [17]. Although the difference might seem not so big, the manufacturing process of the cells is different in some aspects: in particular, building a monocrystalline solar cell requires some further attentions [16], that will later be discussed and that bring a slight increase of efficiency. With a market share swinging between 80 and 90% [18], the silicon solar cells are actually the most dominating technology. The reason behind that, as mentioned before relies on silicon itself: it's an abundant, non toxic material, which is also stable for a long time, meaning that the lifetime of a silicon solar cell is usually

higher compared to other technologies, and its bandgap approaches the maximum efficiency, being very efficient in harvesting photons [18]. The manufacturing process of the solar cell starts from a silicon wafer [16]: this wafer can be mainly doped p with an n zone doped, or mainly doped n with a p zone doped, in order to create the junction [19], with a junction depth that usually is about 0,2 or 0,3 micrometers [16]. Despite the evidence for n-type wafers to be superior in many different electronic properties [19], nowadays p-type wafers represent almost the totality of the wafers produced, mainly for two reasons:

- Historically, the first wafers produced were p-type, because the discovery of solar devices in the early 50s, was simultaneous with the interest of various companies and industries for the space industry: despite a lot of other characteristics were superior in the n-type wafers, when approaching the end of life p-type wafers had better performances, due to the fact that they degrade less when exposed to massive radiation [19], which is fundamental for space applications
- The other reason relies in the higher mobility of electrons if compared to the holes mobility, by a factor of three [19]. This impacts especially the mobility of the minority carriers, that in p-type wafers are the electrons, increasing their lifetime and, thus, the diffusion length [19].

Although these arguments are indeed valid, the majority of solar panels are used for terrestrial applications, which make radiations less dangerous, and thanks to modern processes the wafer is very thin (approximately 150 micrometers) [20], without considering the thin film technologies that are maximum 100 micrometers of thickness [21], making other characteristics more relevant compared to the diffusion length.

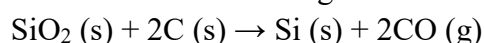
For example, in n-type wafers it's easier to introduce engineered defects, that are essential for more functional devices [20].

In the next paragraph will be discussed the processes that permit to manufacture these wafers and the most important devices that were built starting with crystalline wafers.

1.1.1) Processes:

The first step consists in the production of silicon, starting from what? Sand [22], [23].

In particular, we are interested in the silica contained in quartz, which will be reduced in an electric arc furnace using carbon electrodes [22], according to the following reaction [23]:



Which has an environmental impact due to the emissions of carbon monoxide included in the process.

In the reactor the raw material is first heated up at the temperature of approximately 500 or 600 °C and in the center of the furnace the reaction starts, generating first SiC and SiO [22].

Later, the silicon carbide further reacts with silicon dioxide to produce melt silicon at a temperature of approximately 2000-2200 °C [22].



Fig 1.5 A zoom on the quartz powder, the raw material of the process [22]

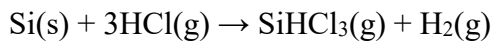
In the following table will be represented a rank of some of the main characteristics that the raw materials should have, ranked from 1 to 5 in which 1=very bad, 2=bad, 3=average, 4=good, 5=very good [22]

Silicon source	Chemical content	Size distribution	Packaging effect	Treatment	Thermostability
Quartz	4-5	5	5	5	4-5
Sand	4-5	1	1	1	1
Quartzite	1-2	4	3	1	1

Table 1.1: characteristics of silicon sources [22]

The silicon obtained is massively influenced by the raw material, as it can be seen in the table 1.1, furthermore is an MGS (metallurgical grade silicon) and must be further treated to answer the high quality requested by semiconductor applications.

The next step consists in a reaction with hydrochloric acid in order to generate trichlorosilane [23]:



The trichlorosilane is a gaseous product that can be distilled: by distilling it the remaining impurities are just a few *ppb*: in particular, other silanes molecules and some atoms of C, Al, Fe, Ca remain in the system [23].

After the purification, independently of the crystallinity of the silicon, to have high quality silicon it is needed a further process.

For monocrystalline silicon, it is needed a process that keeps the orientation of the crystal such as the Czochralski method: High-purity, fine-grained polysilicon is melted in a quartz crucible, with a seed that is inserted into the melt and slowly withdrawn [17].

During the solidification also molecules that will diffuse in the melt silicon as dopants can be added, such as for example boron and phosphorous. Recently, this method has been improved through the use of magnets, generating a magnetic confinement.

Another technique is the floating zone process, also produces crystalline silicon: A rod of fine-grained polycrystalline silicon is recrystallized by passing a molten zone from a

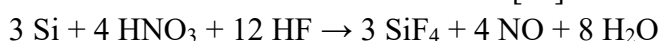
seeded end to the opposite end. This produces crystals with much lower oxygen and carbon than the CZ process and of better quality for cell fabrication [17].

For specific polycrystalline silicon also another technique has been developed, cheaper and more easy going: the silicon, molten or solid, is resolidified in a crucible, usually made of graphite, quartz, coated with silicon nitride, or silica ceramic; the way it is solidified, the material of the crucible and the starting condition of the raw materials influence the process, but the final result will always be of poorer quality if compared with the ones described above [17].

After their growth, ingots can be cut to more appropriate geometries, such as blocks, cylinders, that will later be sawn into wafers [17]. The cut can be done through a thin metal blade diamond coated to improve hardness and durability, which is kept in tension, or a wire cutting through the use of a wire in a parallel array which simultaneously cuts hundreds of wafers by grinding an abrasive slurry through the ingot [17].

The wafer is already mainly doped and it is ready for the treatments that will lead to the basic configuration of the solar cell.

- First of all, the wafers are inspected to find microcracks through the use of infrared transmission [18]
- Later, the wafers are cleaned from the saw damage through the use of a sodium hydroxide solution at 70-80 °C: In the case of monocrystalline silicon, this is also the process of texturing, which is conducted in order to form the pyramidal section of squares (1,1,1) oriented [16]
- In the case of polycrystalline silicon, the texturing is conducted through a wet chemical etching in which substances such as nitric acid and hydrofluoric acid are involved in a reaction described below [18]:



During the process attention for the nitrous oxide must be done.

After this, potassium hydroxide is used to remove the thin porous surface layer (stain) that remains after the etching process [18].

- At this point, a diffusion process must be conducted in order to build the p-n junction: usually the doping is obtained using boron for p-type doping and phosphorous for n-type doping, using molecules containing the requested atoms or directly atoms or ions of the type needed [16]. In the case of phosphorous, a lot of gases can be used, such as POCl_3 , PBr_3 , P_2O_5 carried by a carrier gas of nitrogen, without considering the recent developments for the use of phosphoric acid as a source of n-type doping [17].

As it has been shown before, the majority of the wafers are p type, which means that to build a junction usually a gas containing an n-type material is used, which is the reason why a lot of efforts are conducted in studying molecules of phosphorous to dope the material and build the junction. The temperatures used for the process usually vary from 750 to 850 °C [18], guaranteeing the diffusion of the atoms in a reasonable amount of time. The use of phosphorous has also the advantage of gettering the

impurities of the silicon, that diffuse from the bulk of the wafer to the highly doped region causing no harm to the future device [16].

- After the diffusion, the source of the dopant have also reacted with the wafer, causing an undesired thickening of the layer, usually made of isolating byproducts: In the case of phosphorous, a PSG (phosphosilicate glass) is formed, with a thickness of few tens of nanometers. Although it is through this glass that the diffusion starts to take place and in fact some oxygen is added to the mixture of dopant gases to ensure its formation, after the process it is important to remove it. To remove it, a wet chemical etching with hydrofluoric acid is used [18], the choice of this acid is due to its big selectivity, with an etching ratio of 400:1 between silicon and the glass [18].

The resistance of the layer formed varies from 30 to 100 Ω : According to the resistance a different metallization process will be used in the building of the basic solar cell structure.

- The next step is essential to enhance the future performances of the solar cell: a layer of amorphous silicon nitride is deposited as an antireflection coating: the technique involved is the PECVD (plasma enhanced chemical vapour deposition) using silanes and ammonia. The PECVD can usually be conducted in two different ways: low frequency direct plasma [18], or microwave plasma [18]. The silicon nitride provides also a very efficient passivation of the silicon [16].
- The last step involved is the screening and firing of contacts [17], [18]: usually for the screening two different pastes are used, one of silver that will be screen printed on top of the antireflection coating [16], and the rear side will be composed by a paste of silver and aluminium or pure aluminium which will dope p the rear side [17], [18]. After the screening a drying step at 200 °C is needed in order to let the solvents of the paste evaporate [16].

The firing of the contacts take place in a belt conveyor furnace [18] and is composed of two steps: The first step at 400 °C to combine the remaining organic compounds of the paste with the oxygen in the atmosphere and evaporate them [18], and the second step at more than 700 °C to generate the real contact in the rear side and the front side, that have a conductivity that is still three times worse than pure silver [17].

The aluminium also acts as a back reflector and has a solubility in silicon very low (10^{19} cm^{-3}) [16]. This parameter will also be useful in the results and discussion section because it will show how much doping from an aluminium source we can obtain in a material containing very high levels of silicon.

To keep minority electrons from reaching the rear metal/silicon interface, a thick p+ layer is used, so that the total conductance (conductivity divided by distance) for the electrons is low.

- After the contact preparation, the only step remaining is the edging of the silicon [18], that is fundamental in order to increase performance: in fact power is limited by a severe shunt path over the edge of the solar cell, where the highly doped emitter meets

the highly doped aluminium back surface field and yields high-high junctions which allow for substantial tunnelling or worse. The process which has been introduced 10 years ago is the removal of the n-conducting layer in near edge areas by laser ablation. Typically the area is ablated using an UV solid state laser featuring ns pulse duration [18].

- When all the processes are completed, some experimental setups are needed in order to verify the performances of the solar cell: although a complete characterization requires a lot of different instruments, the most important analysis is the plot of the $I-V$ curves, using a flash light [18]. The test is conducted under standard conditions, which were described in the previous paragraph.
- After manufacturing and testing, the cells are connected into modules [17]. By soldering interconnection they are assembled in their final layout [17]. The interconnected cells are then stacked through the utilization of a glass superstrate and a layer of EVA (ethylene-vinyl acetate) which was synthesized by US department of energy specifically for its use in solar cells applications [17].

To optimize the efficiency of the solar system it is important to understand (and engineer) the two most important parameters: the cell thickness and the bulk carrier lifetime [18].

From these two parameters derive the two main losses of the cell:

- The ratio of electrons that are not excited to the conduction band (optical losses) [18], usually it happens because the photons don't enter the solar cell, they enter but without being absorbed or they are absorbed but without causing an excitation [18].
- Electrons that are excited but not delivered to an outer circuit, also referred as electrical losses [18]: They are divided in losses because of the recombination between electrons and holes, and losses because of the thermal scattering of the majority carriers, which happen in all the elements of the structure [18].

1.1.2) Devices

The history of solar cells started between 1940 and 1950 [17], and since that time a lot of efforts were put in building devices that were always more performant, more efficient and more resilient in time. Violet cell, black cell, the solar modules of the space era are just some of the examples of structures built for specific applications and to try to overcome the limits of that time [17]. Although for obvious reason it is impossible to list all of the devices available in the market or ideated in the past, some of them are more performant and commonly used in the world, making more interesting their discussion. In this paragraph just

two examples of possible devices that overcome in a way or in another the limits of the basic configuration described in the previous paragraph will be described in order to understand the mechanism at the basis of the design.

The first structure is the EWT (emitter wrap through) solar cell: it is made by replacing the front metallization with a lot of densely placed vias of small diameter (approximately 50 micrometers) [18]: the rear structure and the vias feature another emitter structure which improves the current transport [18].

Since both front and rear side are collecting carriers this configuration is attractive not just for silicon but also for materials with a very short lifetime [18]: the only challenges are the large amount of surface in which a p-n junction is created, a problem that can be solved introducing passivating layers [18], and the larger series resistance of the EWT because of the interconnected grid: this problem is still an open challenge because it is impossible to remove the adding resistances introduced by the vias, although some researchers independently demonstrated that it is indeed possible to build high efficiency EWT solar cells, using for example photolithography or PVD metallization processes [18].

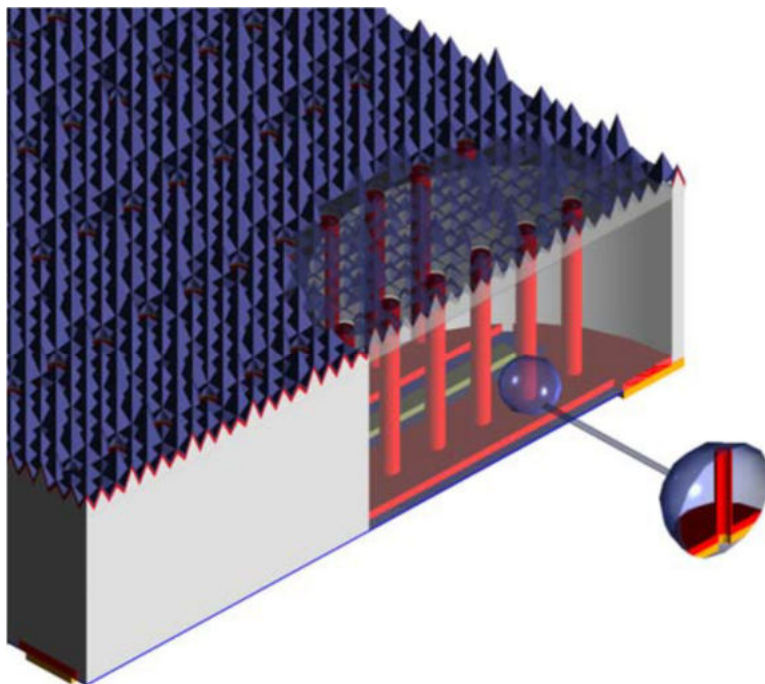


Fig 1.6: EWT structure

The other configuration is maybe the most used in the crystalline solar cells technology: the PERC (passivated emitter rear cell) [16], [17], [24]. In this configuration, a rear passivating scheme is added to the system, which involves the deposition of a passivating layer and the consequent opening to a local level in order to form a contact [16]

The optimization of the rear surface aiming at reducing recombination losses on the cell's

back side gets rid of the inherent limitations of the metallic film of aluminium in BSF solar cells, so the electrical and optical losses are reduced [24]. Furthermore, the improvement of the rear side is independent from the improving of the front side which means that further improvements can be added [24]. In general, the passivating layer is a $\text{Al}_2\text{O}_3/\text{SiN}_x$ or $\text{SiO}_2/\text{SiN}_x$, which guarantees high efficiencies [24].

The two main benefits rely on the superior control of the surface recombination achievable with insulating films (especially silica) [16], and the formation of an almost ideal back surface mirror due to the low refractive index material between silicon and metal [16]. The only problem of the configuration relies in its high precision processes, because the areas opened from the passivating layer must be of a certain dimension [16], [24]. For that reason many similar techniques more easy going were experimented during the years.

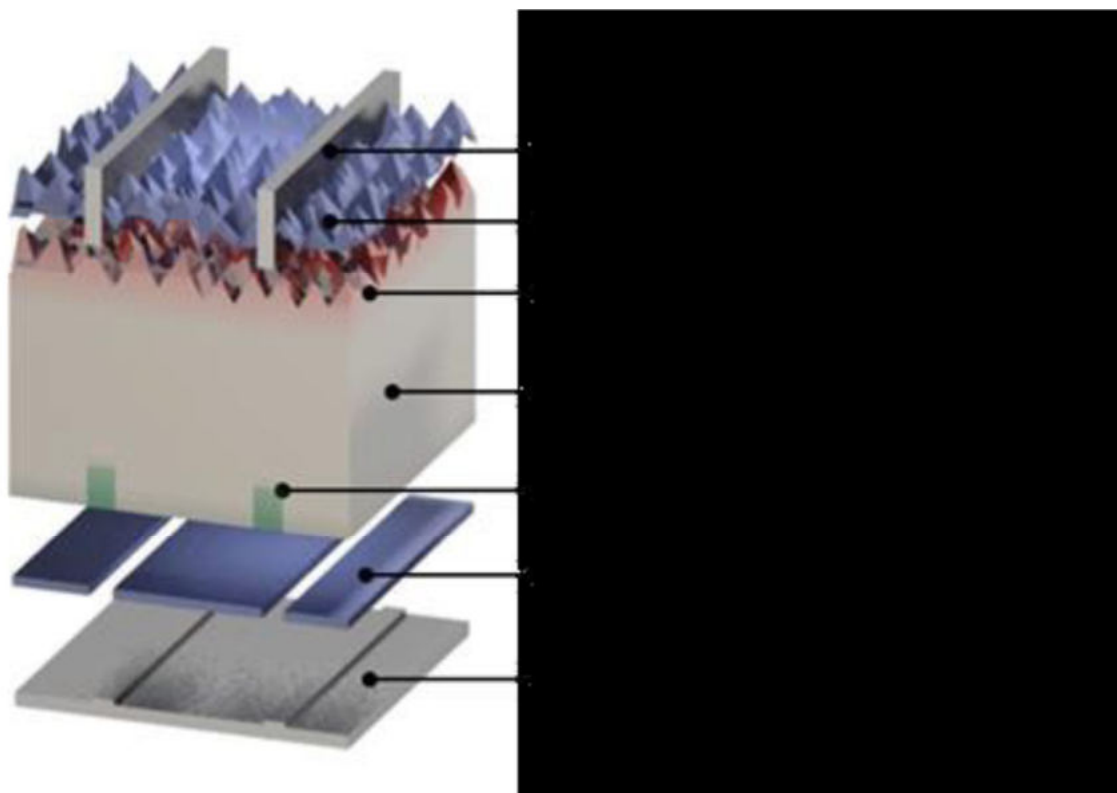


Fig 1.7 PERC structure

It is correct to at least mention other important technologies available:

- IBC (interconnected back contact) [16]

- MWT (metal wrap through) solar cells [18]
- TOPCon (tunnel oxide passivated contact) solar cell [24]
- Back-contact solar cells with boron-diffused back-junction [18]
- n-type cells with boron-diffused front emitter [18]
- Aluminium-alloyed back junction [18]
- The heterojunctions, that partially will be discussed in the forward paragraphs.

1.2) second generation solar cells

Also known as thin film solar cells, this technology had a lot of success because it could be used a film of the order of magnitude of 1 micrometer, with a deposition process on a substrate that can be made of glass or polymer at relatively low temperatures [25]. Although silicon solar cells dominate the market, the highest cost of first generation solar cells consists in the manufacturing of the wafer, which makes useful the creation of thin film technologies to build low cost devices where possible [26].

In this paragraph will be analysed not just the thin film of amorphous silicon, which is the first one compared in the 1980's to power several devices (such as watches and calculators) [27], but also the other two major technologies in the thin film market: CdTe solar cells and CIGS (copper indium gallium diselenide solar cells).

1.2.1) Amorphous silicon solar cells

Although the processes concerning the manufacturing of silicon solar cells are always improving, it is unlikely that the thickness of a classic silicon wafer reaches values below 250 micrometers [28]. To solve this problem, it is essential to rethink the way solar cells are designed: Instead of the process described in the paragraph before for crystalline silicon solar cells, it is possible to deposit through PECVD (plasma enhanced chemical vapour deposition) a layer of amorphous silicon on a substrate at low temperatures, using silane (SiH_4) as a substrate [28].

The layers have a grain size ranging from 1 to several tens of micron [28] and are formed in a range of temperature that can vary from 600 to 1000 °C according to the preference in the size of the grain [28]. Sticking to silicon technologies instead of using other types of materials that will be analysed later have several benefits listed below:

- Silicon is non toxic [28]
- Abundant and available in Earth's crust [28]
- Relatively cheap [29]
- The know how related to silicon is bigger compared to other materials [28]
- Low process temperature [30]
- Possibility to cover big areas [30]
- Material requirements are low

For this reasons the amorphous silicon was the first studied for building thin film devices although the most used in the market are cadmium telluride solar cells with a 5% of the market share [26].

To avoid the main problems of the thin film technology, apart from the efficiency that is lower as shown in figure 1.4, it is necessary to replace the glassy substrate, that is fragile, with a low specific power and more expensive, with a flexible substrate made of a polymer (PET, PEN, Polyimide) or, in the most advanced thin films, in paper (cellulosic substrate) [26].

Speaking about the performances, first of all the absorption coefficient is much higher than that of a crystalline silicon wafer, which makes it more suitable for absorber layers of smaller thicknesses [28]. Furthermore, the bulk concentration of the material spread from 10^{15} cm^{-3} to 10^{16} cm^{-3} which guarantee a good performance although some layers doped n+ can arrive to bulk concentrations of one or two orders of magnitudes higher [28].

Other parameters that can be interested because they will be analysed in the results and discussion section, are the carrier mobility of amorphous silicon which usually is lower than the crystalline one with a value of $20 \text{ cm}^2/\text{V}\cdot\text{s}$ in the best cases [28], and the conductivity value that usually in dark conditions is inferior to 10^{-10} S/cm [28].

Unfortunately, the efficiencies of common solar cells made by amorphous silicon are very low, ranging from 4 to 6% [29]. The band gap of the amorphous silicon is about 1.8 eV [30], which doesn't make it suitable for harvesting a lot of the infrared photons, because the absorption will start at 110 nm more or less [28]. Furthermore, it is a common procedure to passivate the layer of amorphous silicon using hydrogen. Why? This hydrogenation ensures the passivation of most of the defects that can be created during the deposition or the working life, improving the efficiency and the lifetime of the cell [28].

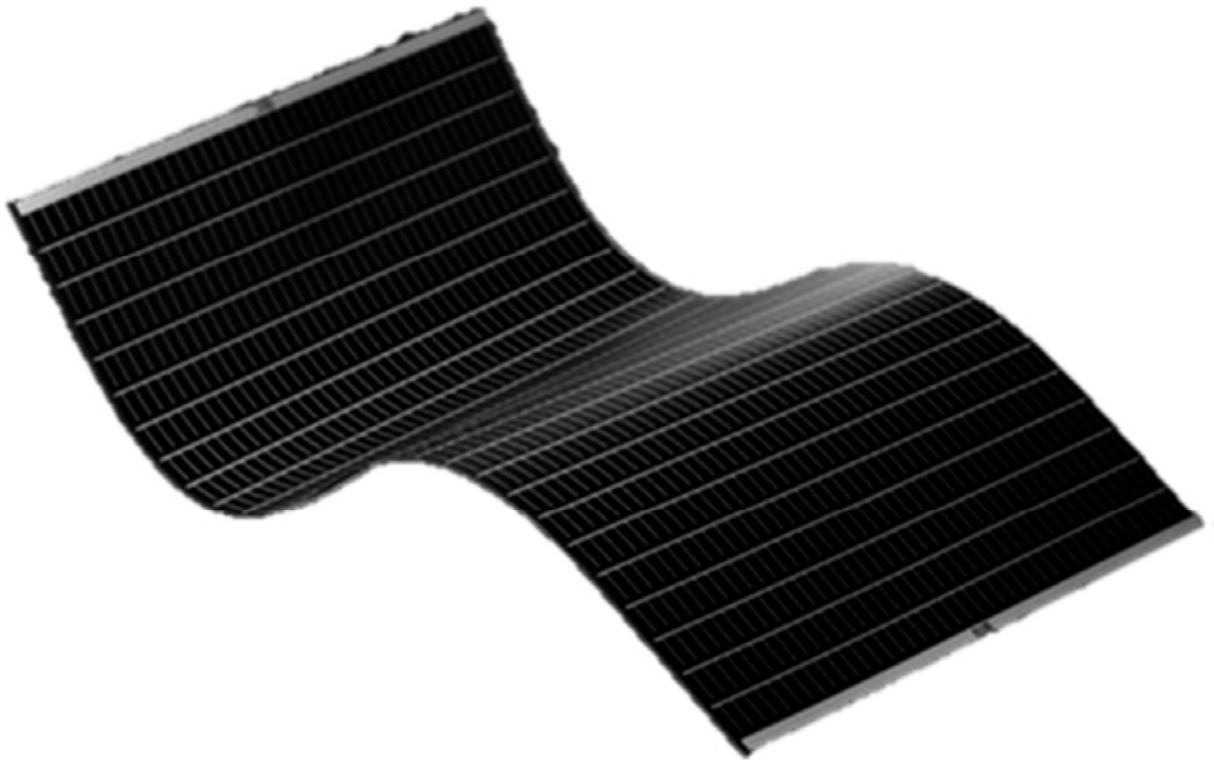


Fig 1.8: Commercially available amorphous silicon solar panel [31]

1.2.2) Cadmium telluride

Molecular formula CdTe, has shown before it has the biggest piece of the thin film market. Because of its ideal gap, very similar to the one of GaAs, of 1.45 eV [32], it has always been seen as an alternative to first generation solar cells for several applications. Furthermore, the energy gap is direct, which means that 90% of the light can be absorbed in a layer of few micrometers because of the absorption edge that is very steep [32]. Nowadays, efficiencies of around 21.5% are reached, as shown in fig 1.4. For growing good layers of this active material as an absorber, a lot of parameters should be controlled, such as stoichiometry, growth morphology, grain boundary behaviour, doping and contacting [32]. What are the weaknesses of cadmium telluride technologies? The main problem is related to the toxicity of cadmium, that has banned its use in some of the European countries, although concentrating the cadmium in solar cells utilization seems a good idea [29].

The other issue is directly linked to the performance of the cell, since it is really challenging to build low resistivity films of cadmium telluride and low resistivity contacts in cadmium telluride [27].

Last but not least, it has to be said that tellurium is quite expensive, making it really difficult to keep the stoichiometry of the module without an increase in the costs of the system, even if

theoretically the cadmium telluride technology could be cheaper than the silicon one, that has low costs just because of the mass production [26].

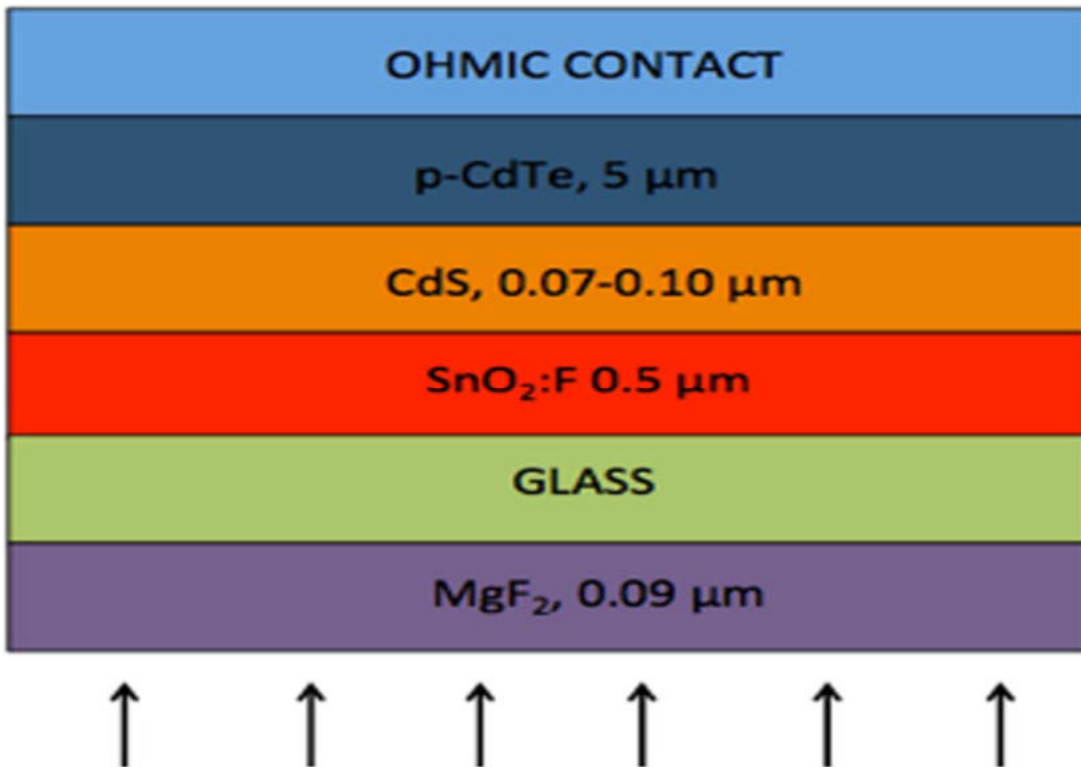


Fig 1.9: schematic of a cadmium telluride solar cell [27]

1.1.3) CIGS

The starting material has a chalcopyrite structure, and is the CIS (copper indium diselenide), that has a lot of desirable properties fundamental to build an efficient solar cell, for example a bandgap of approximately 1 eV [30]. The difficulties that must be faced during the deposition of CIS consists in controlling the sulphur during the deposition in order to keep stable the stoichiometry of the material and the relatively rapid diffusion of metals and all kind of impurities in the material, even at low temperatures, which have slowed down the development of this material [30]. Anyway, allowing a metal such as aluminium or, in most of the cases, gallium, slightly increases the band gap of the material bringing it at 1,15 eV as shown in fig 1.4. Thanks to this improvement and the enhancement of process control, it is possible to build high efficiency devices based on a single junction or a multijunction of CIGS, with the maximum efficiency that nowadays has been reached in 2015 by solar frontier and is approximately of 22% [27], has also shown in (fig 1.8). The use of expensive metals such as gallium or indium is the responsible of the increasing in manufacturing costs of CIGS [30].

The substrate used for the development of the device is a soda-lime glass, which thanks to the sodium ions contained it has been shown improving the efficiency of the system, while the window layer that also works as a front electrode contact is usually made by zinc oxide doped n, with the molybdenum as the back contact deposited above the soda lime glass [27].

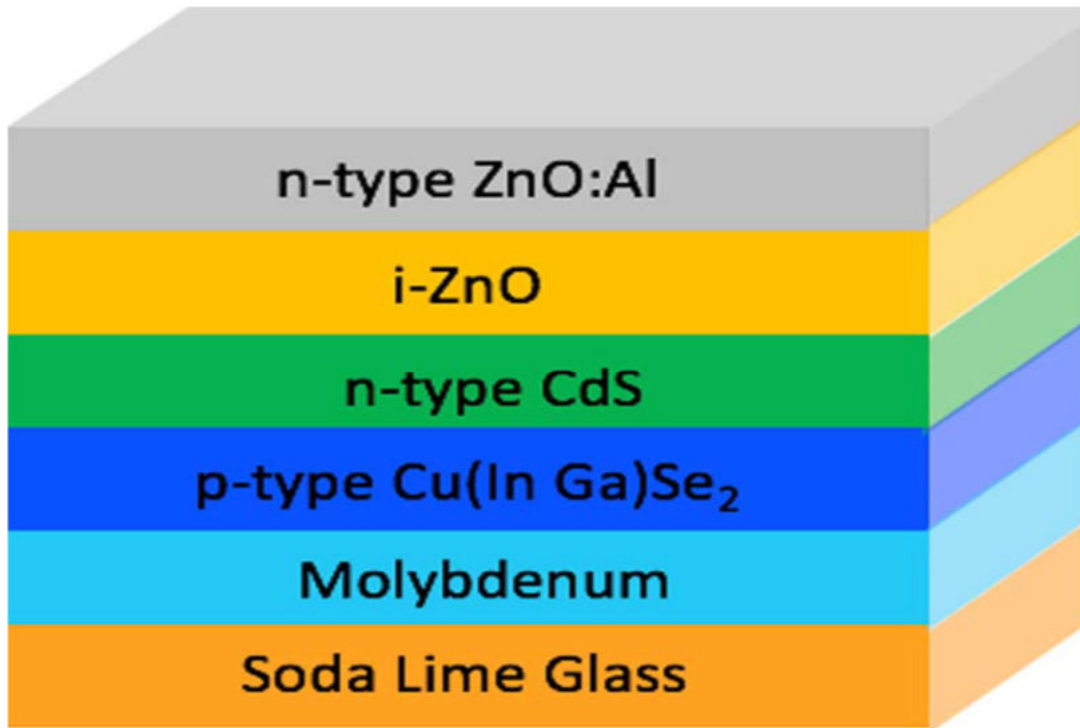


Fig 1.10: Structure of a CIGS solar cell

1.3) Third generation solar cells

From this generation of solar cells belong all the technologies that rely on a photoelectrochemical system instead of a p-n junction, single or multiple: DSSC (dye sensitized solar cells), quantum dot solar cells and organic solar cells, with the addition of the perovskite solar cells, a class of materials having the ABX_3 structure that in recent years has shown great compatibility with the solar technology [33]. Although new, they already showed the potential in several papers and commercial application to be low cost and high efficiency, guaranteeing the overcome of Shockley-Queisser limit [33]

1.3.1) Organic solar cells

Flexible, low cost, made by polymers and in some cases transparent or semi-transparent: these are the organic solar cells [33]. Their working principle is way different compared to the solar cells of first and second generation because the absorption of solar light doesn't generate free

carriers such as in inorganic semiconductor materials [34], but an exciton, which is a couple electron-hole bounded together by electrostatic forces [35], thus making essentials more steps to generate a free carrier which can be exploited to generate a current. In particular, the four steps can be summarized as the following:

- The photocurrent of excitons generated after the light absorption, that is directly linked to the matching between the solar spectrum and the spectrum and bandgap of the material [35]: most of the organic materials have a bandgap around 2 eV [34], which makes them poorly suitable for the harvesting of a great amount of solar light, with academic research that is currently focusing on synthesis and discovery of more suitable materials for this application, along with the production of great quantities of pure materials for the OSC [35].
- The diffusion of the photocurrent, made by the excitons generated in the first step of the process, is the direct consequence and is characterized by the parameter L_d , that is the diffusion length [35]. Typical distances are of 1-100 nm, and the purpose is to make L_d as big as possible: in fact, excitons with higher diffusion length have higher possibilities to reach the interface and continue the process instead of being loss [35]. The diffusion length is evidently one of the controlling parameters of the final device, because just excitons generated in the range mentioned before can hopefully manage to arrive at the interface, which means that the layer should be of a maximum of 10nm thickness. Unfortunately, that thickness doesn't allow the absorption of enough light and usually the thicknesses of the active layers are around 100 nm [36], with the majority of the photocurrent generated resulted in a loss. The solution in which universities and industries are working nowadays is the increase of L_d by doping the organic layer with a phosphorescent molecule, in order to change single excitons in long-live triplets, or decreasing the distance between the donor and the acceptor [35].
- At the interface there is a dissociation of the exciton into an electron and a hole because of the electric field that generates a V_{oc} : this potential is directly linked to the difference between the LUMO (lowest unoccupied molecular orbital) of the donor and the HOMO (highest occupied molecular orbital) of the acceptor [36], which is limited by the mobility of the excitons in organic materials, which in the best cases can arrive to $15 \text{ cm}^2/\text{V}\cdot\text{s}$ [36], which is very low if compared to the maximum possible mobility in silicon which can arrive to $450 \text{ cm}^2/\text{V}\cdot\text{s}$ [36], and the exciton binding energy that is one order of magnitude higher if compared to the one of inorganic semiconductors [36]. This is the step controlled the most by the manufacturing process: in order to have a good dissociation of charges it is needed a smooth interface, because every void or roughness can provoke short-circuits, thus reducing the efficiencies [35]. One of the ways to reduce the problem is the annealing of the device after covering it with a 100 nm thick metal electrode, which applies stress to the organic material thus increasing the smoothness.

- After that, the transport of the carriers to the electrode performed by the organic layer generate an electrical current which can be characterized by plotting an $I-V$ curve under dark and different illumination conditions [36]

Now the materials explored to build more efficient devices are silver films or grids, graphene or carbon nanotubes based solar cells and transparent conductive polymers solar cells [34], In order to build flexible and transparent devices which can be used for a great amount of applications. From an engineering perspective, the main issues of this technology regard the voltage losses, the stability issues related to the work life under illuminated conditions or the diffusion of water and oxygen in the device, and the costs related to mass production [37]. In fig 1.4, it is shown the maximum efficiency, of approximately 12%.

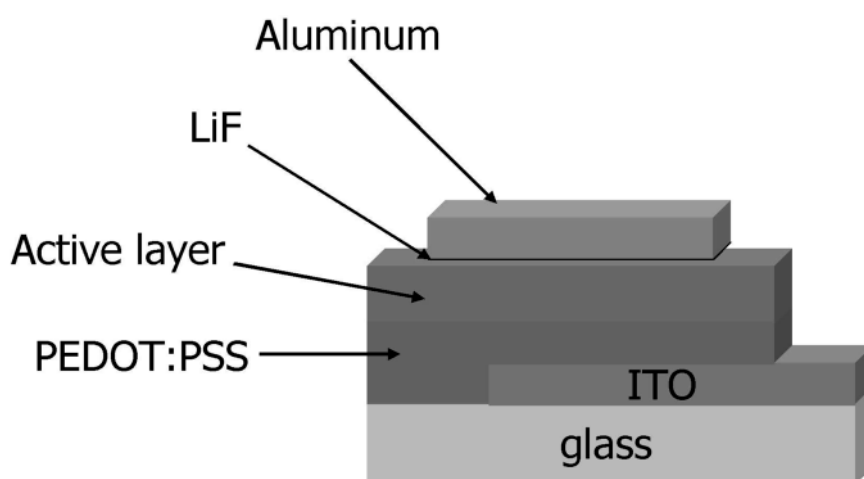


Fig 1.11 bulk heterojunction organic solar cell [35]

1.3.2) DSSC solar cells

Dye sensitized solar cells, also known as Graetzel cells [38], are considered as a new paradigm for low cost and efficient solar cells [33]. They consist of a structure composed by four elements: A photoanode made by a semiconductor, such as titania for example, a sensitizer, an electrolyte and a counter-electrode [33]. The main difference with the conventional organic solar cells relies in the structure described before, since in DSSC the sensitizer, that is a dye, is responsible for just the absorption of solar light and the consequent generation of excitons, while the electrolyte is responsible for the transport of the carriers to the electrode to close the circuit [39]. This means that the optimization of the device can be done separately by optimizing the dye in order to have a better match with the solar spectrum and consequently better absorption, and the enhancement of the performance of the semiconductor and the electrolyte to improve the transportation of the carriers generated previously to the counter electrode [39]. What is the working principle of the device? The dye, after the excitation because of the sunlight, injects an electron in the conduction band of

the semiconductor, that flows until the counter electrode passing through the external load, and later reduces the redox mediator (the electrolyte) which in turn regenerates the excited sensitizer that had a lack of carriers [39].

How can we reach a panchromatic harvesting by a single dye? In the decades, several studies have focused on the dye, that is the most innovative material of this devices. The best results have been reached with ruthenium complexes, especially with polypyridil complexes of ruthenium known under the codes N3 and N19 [40]. Other studies have been conducted on the use of hydrophobic sensitizers, in order to improve the interface between the titania and the sensitizer and prevent phenomena of desorption [40], high molar extinction sensitizers to improve the light absorption in infrared region [40], studies on cyclometallated complexes of ruthenium to improve the ligands efficiencies [40], and super-sensitizers that have intermediated properties between the hydrophobic sensitizers and the high molar extinction coefficient sensitizers, thus improving the performances and guaranteeing a reduction of the thickness. In fig 1.4 it is shown that the maximum efficiency reached is approximately 12%.

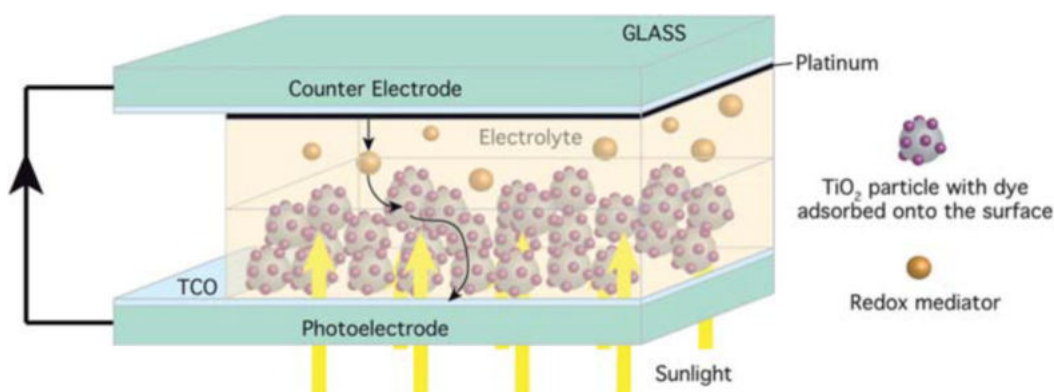


Fig 1.12 Structure of a DSSC [39]

1.3.3) Quantum dot solar cells

Quantum dot solar cells are very similar to DSSC in the working principle, but they differ in the sensitizer that is not a dye anymore but is in most of the cases an inorganic semiconductor, usually titania, with enhanced properties thanks to the dispersion of the quantum dots [41]. Although there are also self assembly structured quantum dot solar cells [41], the most interesting technology is surely the colloidal quantum dots one, which has a lot of unique benefits such as the tuneable band gap which changes according to the size of the quantum dot [41], the potential to generate multiple electron-hole pairs with the absorption of a single photon [41], and the large absorption coefficient because of the quantum confinement effect [41]. The most explored quantum dots nanoparticles are InP, CdSe, PbS, CdS, Structures core-shell with the core of CdS and the shell of CdSe are explored [42], and used to sensitize layers of metal oxides such as TiO₂ or ZnO [42]. The sensitization is made with two different processes: The chemical bath deposition, in which cationic and anionic precursors react

slowly in a bath and the rate of quantum dot's deposition is controlled by the bath's time [42], or the SILAR approach in which the electrode is dipped separately in two baths, one with the cationic precursors and the other one with the anionic precursors [42].

The quantum dot solar cells configurations can vary, giving more flexibility to this type of technology: In fact, although the sensitized nanocrystalline titania configuration is the most frequent, there is also the possibility to integrate quantum dots in a p-i-n array [43] or incorporating the nanoparticles on a polymeric matrix [43]. In a recent study it is reported also the possibility of using quantum dots nanoparticles in a device consisting just of silicon, using phosphorus-doped Si QDs in a SiO₂ matrix deposited on p-type crystalline Si substrates [44]. The most urgent problem of QD consists in their lifetime, because many degradation mechanisms occur during the work of the solar cell, especially under light conditions, which make them less suitable for industrial applications [45]. Some strategies studied to overcome these issues, such as the degradation of the active layer and the charge separation layer during lifetime and in several different working conditions, are for example the passivation of the quantum dots [45], which can be made in different steps of the process and with different molecules [45].

As shown in fig 1.4, the maximum efficiency that can be reached with the arrays exploiting quantum dots technology is 10%

1.3.4) Perovskite solar cells

Probably the most promising technology between the third generation solar cells, perovskite modules have already reached an efficiency of around 20% as shown in fig 1.4 although they are the newest technology in circulation. When referring to perovskite an entire class of molecule is addressed, with a molecular structure of ABX_3 : the properties of the resulting material strictly depend on the atoms positioned in that sites, which means that also its band gap is tuneable [46]. The A cation is not directly linked with its electronic properties, although it has been shown through simulations that its size is linked to the contortion of the layer [46]. If a little cation is used, such as methyl-ammonium in most of the cases, it can be obtained a three dimensional symmetric structure, although if it is needed an higher absorption of the solar spectrum a bigger cation can be used [46]. The B site is a metal, generally a metal of the 4 group in a +2 oxidation state such as Pb, Sn, Ge [46]. One of the problems in the use of perovskites is that the most stable and performant metal is lead, that is also toxic [46]. In the years, researchers are trying to design mixed metals perovskite cells, in which there is a ratio in the crystalline structure between Pb and other metals [46]. Finally, the X is the halide ion, and varying it is the most effective way to probe the performances of perovskite [46]. Going down the group 7 the energy harvesting shifts to higher wavelengths, which means lower energies [46]. The most used halide ion is the iodine, because its cells have the highest efficiencies, although also chlorine is studied because it enhances the carrier lifetime and the

diffusion length [46]. The most studied perovskite material is the $\text{CH}_3\text{NH}_3\text{PbI}_3$ [47], which has a band gap of 1.5 eV, very near the ideal band gap for solar applications [47].

The working principle is the same of other technologies, with light absorption, charge generation and separation, charge transport and collection [48]. The diffusion length of holes is about 1 micrometer, but it is also true that electrons diffusion length is much lower than that of holes, resulting in an additional electron transport layer to add in order to enhance the diffusion length for negative charges [48].

To manufacture them, a lot of different processes can be used: the most used for the $\text{CH}_3\text{NH}_3\text{PbI}_3$ structure is the spin coating, using two different solutions, one containing CH_3NH_3 and the other one with PbI_2 [49]. This deposition can be made in two different steps, depositing before one solution and after that the other one, or in one step mixing both solutions [49]. The most used one is the one step deposition process, with the final quality of the film strongly influenced by roughness, crystallinity, wetting and other related issues [49]. Despite the ease of fabrication with this technique, for high quality devices it is preferred the vapour deposition method that offer superior performances and better film quality. In the case of $\text{CH}_3\text{NH}_3\text{PbI}_3$, two solutions, one containing $\text{CH}_3\text{NH}_3\text{I}$ and the other one of PbCl_2 are preheated respectively at temperatures of 120 °C and 325 °C and then deposited in high vacuum in a film of TiO_2 [49]. Also vapour assisted solution process (VASP) has been used, to have a simpler and more scalable process without decreasing a lot the final quality [49]. The problem of what deposition might be more suitable for perovskites structure was also explored by Yana Vaynzof in [50].

The typical structures of the perovskite solar cells are a huge amount, with the first one which was a liquid electrolyte dye sensitized cell [51]. Later, the first solid state perovskite solar cell was discovered and had a mesoporous structure, in which properties were strictly dependent on the morphology of the layers [51]. Then the junctions structures became more studied, with planar configurations using a p-i-n structure or a n-i-p structure, with the only difference between these two configurations resulting in the position of the charge transport layer: In particular, in the first structure the HTL (hole transport layer) is on the top of the transparent conductive substrate while the ETL (electron transport layer) is on the bottom of the electrode metal, while in the second structure is the contrary [51]. In the years, many researchers have also tried to develop structures without the need of the HTL or the ETL although as it has been mentioned before creating structures without an ETL is bad for the diffusion length of the negative carriers [51]. The most advanced structures that are still in phase of studying are flexible cells, semitransparent cells and cells with carbon nanotubes electrodes that can be produced in fibers, thus giving the possibility of harvest sunlight also with clothes and other textiles [51].

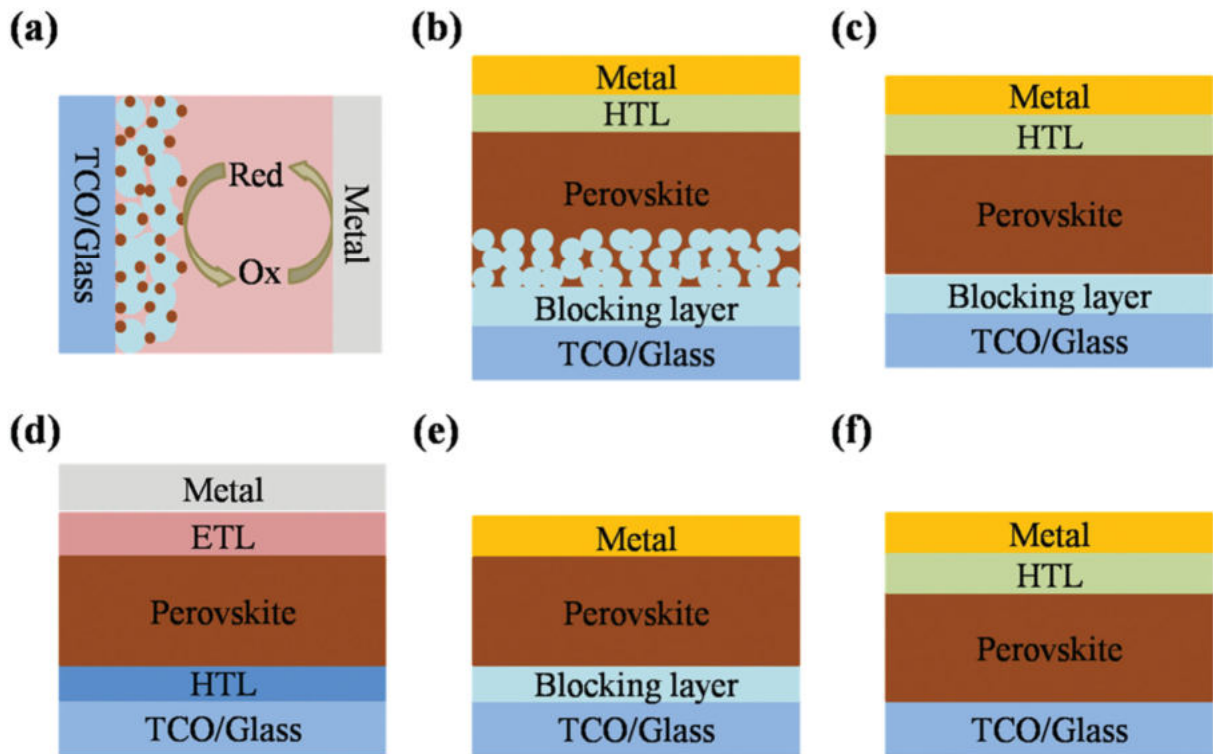


Fig 1.13 Typical structures of perovskite solar cells [51]

Along with the presence of lead in most of the cases, perovskite solar cells have also another great weakness: the stability during time. Furthermore, it is common knowledge for scientists to address “the golden triangle” when talking about perovskites, which means that cost, lifetime and performances in most of the cases are inversely proportional, so adding more to one of them decrease the value of the other [52]. The factors that influence the lifetime of a perovskite are both environmental and intrinsic: The most relevant environmental factors are the presence of moisture and oxygen which can be solved through an encapsulation of the module [52], while the intrinsic parameters can be listed as the following:

- Hygroscopicity, related to environmental factors and solved through encapsulation [52]
- Thermal stability, which can be tuned through the composition of the perovskite using for example during the deposition FA ions [52]
- Ion migration, that is unavoidable but can be decreased through the doping or partial replacement of the *A* sites with alkali, through the addition of organic molecules additives and the multiple dimensional perovskites engineering [52]

At this factors must be added the ones related to the working lifetime of the solar cell, such as chemical reactions at the interface, directly connected with the ion migration and accumulation between the contact and the perovskite layer [53], and the degradation of the top

electrode, usually made by silver or gold, due to stressful and harmful environments such as the presence of moisture, heat, light [53].

1.4) Heterojunction solar cells

Sometimes addressed as the fourth generation solar cells, heterojunction are theoretically just combinations and improvements of the materials and technologies described in the previous paragraphs. Although this is true for sure, it is important to have a glimpse in the utilization of this devices, focusing especially in silicon heterojunctions, which are the most studied, and a record triple heterojunction discovered in recent times.

1.4.1) Silicon partners

Coupling silicon with a layer of another semiconductor is a very promising strategy to overcome the limits of silicon solar cells without giving up on their numerous advantages: One of the best ways to choose the perfect partner for a tandem, triple or quadrupole junction is by looking at the spectral efficiency, which is the efficiency solved by the wavelength [54]. Although choosing a partner for silicon is recognized as a good strategy, there aren't a lot of example in which the harvesting of the energy is made by a silicon heterojunction, because in most of the cases silicon is seen as an obstacle to overcome, not as a partner for a tandem solar cell [54]. This is true, but until some extent: In fact in 2016 the best results for a tandem heterojunction were made by a stack composed of a layer of GaInP on top, which has a bandgap of 1.8 eV and a layer of crystalline silicon of usual 1.1 eV [54].

The maximum efficiency of a tandem solar cell can be calculated by summing the integrated sub-cell spectral efficiencies, each weighted by the spectra reaching that sub-cell and normalized to the incident photon power, which give birth to a junction that has no electrical losses because all the photons above a certain wavelength will be harvested and with no optical losses as well: This means that to have high increases in the efficiency we have to couple well the materials used [54]. One surprise is that a tandem between a perovskite and a layer of monocrystalline silicon results just in an increase of 4% in efficiency, valuing the thesis that in coupling it doesn't matter the performance of the single material but it's more important the skill of harvesting more efficiently different parts of the solar spectrum [54].

From the data shown in [54], is possible to see that the best results with monocrystalline and polycrystalline silicon can be obtained coupling it with a top layer of GaInP as mentioned before, but also with a layer of GaAs that has theoretical efficiency even higher than the record one of 2016, 34,9% against 34,4% although the mismatch of the bandgaps is higher with the GaInP because GaAs has a bandgap of 1.45 eV: This can be explained by the higher performances of the GaAs layer that is very near the theoretical limit [54].

Other factors must be taken into account when building an heterojunction, such as for example the temperature dependence, the irradiation quantity, and some further adjustments such as the annealing which can determine a slight increase or decrease in the performance of the junction [55]. Furthermore, coupling process must also take into account the manufacturing of the final product, especially in case of coupling with materials such as perovskites, that need a certain uniformity of the layer to perform better which usually makes essential the use of a chemical or mechanical polishing after the deposition by thermal evaporation or spin coating or blade coating [56].

To guarantee an uniform layer on top of the crystalline silicon, usually a first co-evaporation of the inorganic species such as PbI_2 and CsBr is followed by a deposition with spin coating of FAI and FABr with a further annealing at $150\text{ }^\circ\text{C}$ to obtain the best results so far [56].

1.4.2) Record heterojunction

Although the world of high tech is in constant evolution, there are some results that states some record and represent a further step in the achievement of determined results, in this case in the solar industry. Yamaguchi's studies have demonstrated how triple junction solar cells with InGaP as the top layer lead to very high efficiencies, in particular it is reported an efficiency of 31,7% for an InGaP/GaAs/Ge heterojunction [57], and a world record efficiency of 35,8% for an InGaP/GaAs/InGaAs heterojunction [58]. This result is incredible especially because of the absence of silicon or perovskite in the structure. Also, the choice of the materials lead to less lattice mismatch making easier the deposition of the various layers [58]. These types of heterojunctions are studied also under heavy radiation conditions, because they could represent a breakthrough in the harvesting of solar energy in space applications [59].

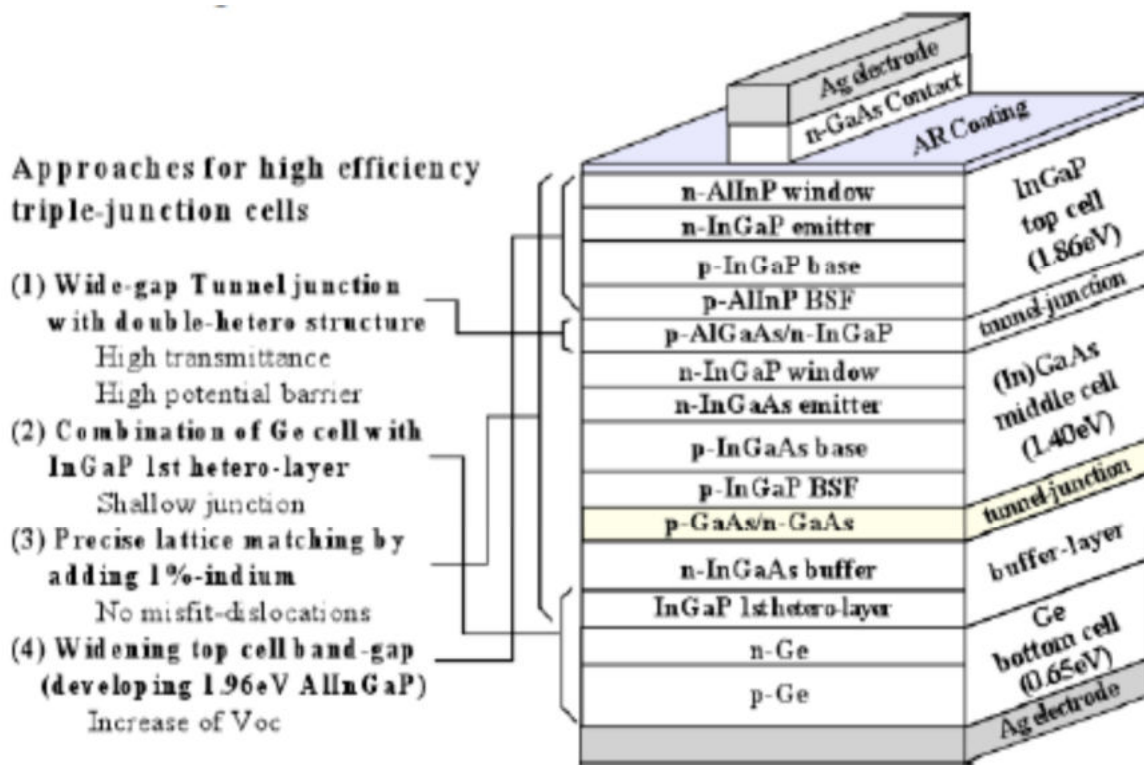


Fig 1.14 Structure of the InGaP/InGaAs/Ge HJT solar cell [58]

1.5) Recycling processes

To conclude the section, it is interesting to show a glance of the state of the art in the recycling of solar modules, focusing especially in the current ways to recycle semiconductor layers and other useful materials that are often present in the majority of the modules: For a crystalline silicon module of the first generation, the percentage of materials present are shown in table 1.2:

Materials	Percentage
Glass	70%
Aluminium frame	18%
Adhesive	5,1%
Silicon	3,65%
Other materials	3,25%

Table 1.2: Materials present in a classic crystalline silicon panel [60]

With the other materials consisting in polymers as the back sheet layer and the metals as electrodes or cables [60]. In this paragraph will be briefly mentioned before the processes to recycle silicon or perovskite from end of life modules and after that a brief glimpse on the recovery of other useful materials from a solar panel.

1.5.1) Semiconductors recycling

To recycle silicon from solar panels it is first necessary the mechanical disassembly of the module [61]: After that, the recovery of the silicon is usually maybe by a wet chemical etching, involving first the removal of EVA layer, which can be made by dissolve it in an organic solvent [61], or by a pyrolysis treatment conducted at 500 °C [62], and then the real etching: the silver electrical grid is usually removed with a saltpeter solution [61], while the aluminium electrodes with a solution concentrated of NaOH [61]. The removal of the antireflective layer of Si_xN_y is made using a solution containing 10% of HF at room temperature [63]. In [63] is also reported a different method to dissolve the electrode of aluminium, using HCl.

Finally, the etching of the p-n junction can be made with a solution of HNO_3 and HF, with the first behaving as an oxidant to produce SiO_2 from silicon and the latter creating compounds such as H_2SiF_6 with a very high rate [64].

In the case of perovskite, the recycling of the active layer is conducted after the removal of the hole transport layer and the electron transport layer through chlorobenzene [65] and the previous removal of the electrode with an adhesive tape [65]. After that, the layer is recovered dissolving the perovskite in the constituents, the solutions of PbI_2 and MAI and then extraction of MAI in water [65], with a subsequent degradation of MAI into CH_3NH_2 and HI [66].

1.5.2) Other materials recycling

It has already been shown how the EVA layer can be recovered through the organic solvent and the glass through a simple disassembly of the module. If the glass is covered by a TCO such as FTO, the coated glass can still be used for various applications, and represents the highest cost in a perovskite solar cell [67]: It is enough to ensure that the TiO_2 layer is gone by dissolving it in a solution of DMF [67].

Finally, the rare metals such as indium and gallium can be recovered by grinding or hydrometallurgy techniques while the metals dissolved in the chemicals after the wet chemical etching can be further processed to be extracted, for example with a precipitation in a solution of NaOH [68]. Before recycling the components of the solar panel it is important to understand if there is a real economic and environmental benefit in doing it, which is true in the case of rare metals such as indium or semiconductors like silicon but can be not so profitable for other materials, according to their price and the amount of material which can be recovered [68].

2) Materials and methods

This section is dedicated to the list of all materials, instruments and techniques used during the experimental part of the work. In particular, after a brief description of materials and tools that revealed themselves useful for the lab experiments, there will be a focus on the most used instruments for the deposition and characterization of the thin films. The section will be completed also with pictures to help describe better the work developed in this period.

2.1) Materials

The first list is dedicated to all the materials that had a specific purpose during the experiments and that are not shaped into a tool but used in a raw shape:

End of life polycrystalline silicon solar cell: since the work developed should apply to a great variety of wastes, it hasn't been used the documentation table to know the doping of the cell, but it was discovered during the experiments through the characterization of the materials. It is essential to underline that the part recycled consisted just in the active layer with the antireflection coating of Si_xN_y and the screen-printed electrodes of aluminium. The material has been reduced of dimension through mechanical milling since a powder of the same has been obtained.

High temperature resistant adhesive tape in order to keep the substrates stable during the various depositions. The thick one had a width of 1 mm, the thin one had a width of 0,6 mm. Aluminium wire cut with scissors and deposited on the thin films when there was the need of a contact.

Copper pellets of 99,99% purity used in the part of the experimental section related to the building of the p-n junction.

Ethanol used to clean the samples from dirt without damaging or removing the films obtained
Distilled water to clean the instruments.

Aluminium foil used in some depositions to cover some parts of the samples.

ITO used as the transparent conductive oxides in our configurations of the samples, the ITO has been sputtered in case it was used just as the TCO or a square of 10*10 mm of ITO has been used when the purpose was also to be the substrate.

Corning glass used as the substrate in the majority of the thin films: this glass can be used until the classic temperatures of annealing of a thin film, until 600 °C.

Crucibles of molybdenum used to host the powder of silicon, the pellets of copper or the wire of aluminium inside the thermal evaporator.

High vacuum grease used to lubricate the dome of the thermal evaporator to avoid losses during the working functions.

Conductive carbon ink printed in the samples as a contact if the main contact is too damaged: it can be used just when there is the possibility to modify the voltage according to the resistance, because it's more resistant than a metal contact.

Simple glass, used during the Seebeck coefficient measurement to have a reference in order to calculate the difference of temperature between the two sides of the sample.

2.2) Useful instruments

This list is dedicated to all the tools and instruments that have demonstrated useful once or several times during the experiments:

- Metallic sample holder, in order to keep the substrates stable after being attached with the tape:
- Ceramic grinder, used to pulverize the end of life active layer of the solar cell and obtain a fine powder that can be used for the depositions
- Glass cutter with a diamond probe, used to cut the initial corning glass in pieces of different shapes and dimensions, to deposit different configurations that can be used in different experimental setups
- Tweezers, used mainly to remove the adhesive tape from the samples after the depositions and in the hall effect to move the golden probes
- Scale, used to be sure that the amount of silicon deposited was always the same to create layers with approximately controlled thickness
- Beckers used to contain the powder during certain measurements
- Polymeric Pasteur pipettes used to take controlled amount of chemicals
- Polymeric masks used during the depositions to deposit metals in different configurations in function of the experimental setup required
- Voltmeter used to have a previous check of the resistance of ITO or the samples obtained after the depositions
- Solar survey 100, used to measure the intensity of the light of different lamps used in the experiments
- Led lamp of 100 W/m^2
- Halogen lamp of 200 W/m^2
- Infrared lamp of 500 W/m^2
- Tuneable halogen lamp used during the measurement of I-V curves: This lamp had six different intensities available, which are, in order of intensity: 100 W/m^2 , 170 W/m^2 , 370 W/m^2 , 550 W/m^2 , 850 W/m^2 , 1000 W/m^2
- White body, used in the spectrophotometer to standardize the reflection of the samples to a reference and reflect the light emitted when the instrument is used in transmittance mode

- Scissors used to cut metallic wires
- Electrodes that can be attached to the clamps of the setups to get in touch with the contact and measure the values required
- Metallic protection of the thermal evaporator
- Pyrex dome of the thermal evaporator
- Black drape used to perform the measurement in dark
- Infrared thermal camera to measure and detect differences of temperature
- Peltier cells
- Power supplier in case a determined amount of voltage is required
- Annealing oven in air used during steps of the p-n junctions
- Various software used in the instruments to convert the measurement in a readable value
- Sputtering used to deposit the ITO on the corning glass
- Heater to heat the samples

2.3) Jaasco spectrophotometer

The spectrophotometer is the instrument used for the optical measurements, with a very simple working system: a beam of tuneable wavelength is emitted to interact with samples of several configurations, from powders to liquids or thin films just changing the setup of the machine. In the case of this study, the thin film configuration was used, consisting in two different modes: the transmittance mode and the reflectance mode.

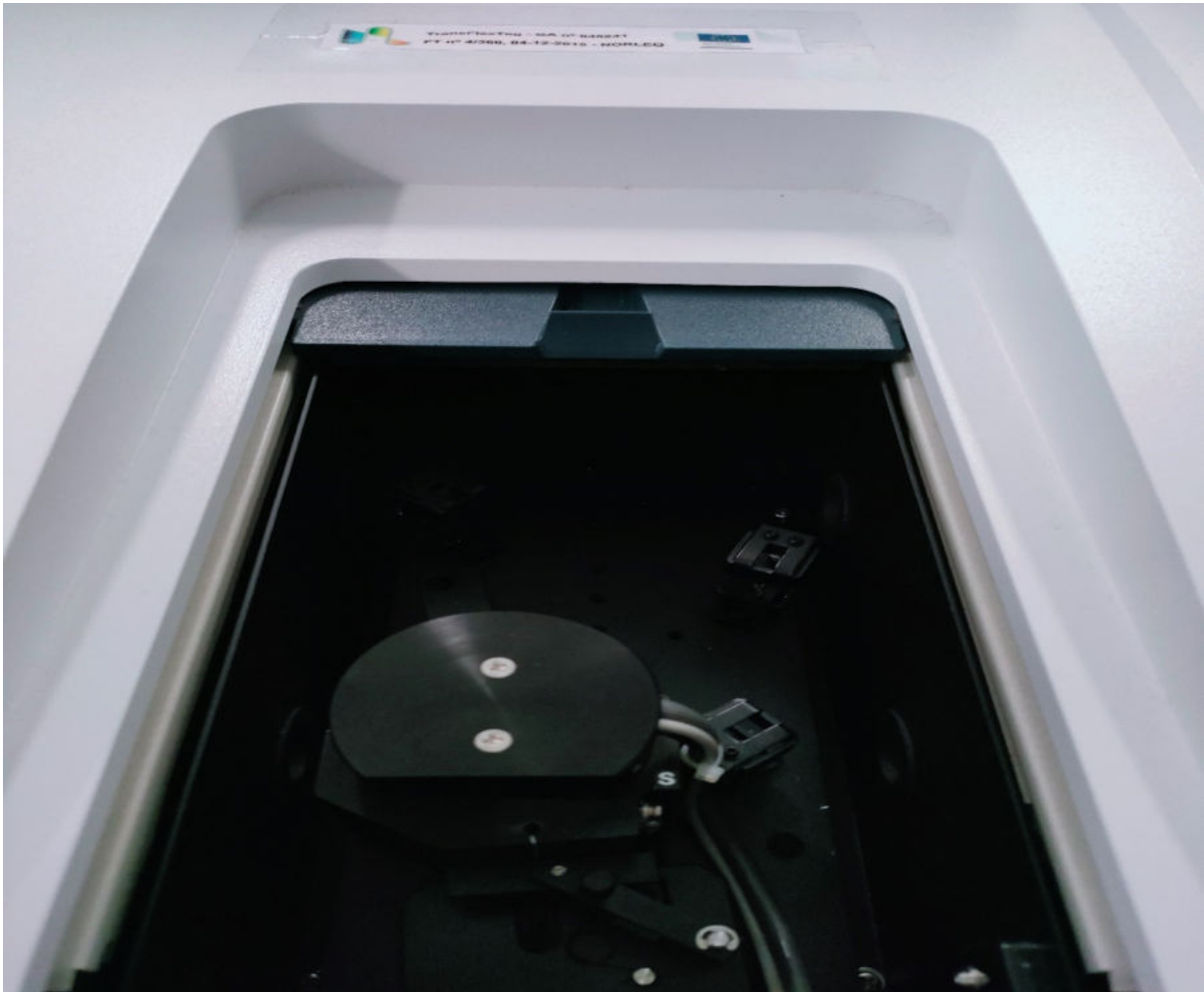


Fig 2.1 The inside of the jaasco spectrophotometer

As it can be seen in picture 2.1, in the inside the sample can be positioned down or in the upper part on the left. Since the beam arrive from the right side of the top, if the sample is positioned down it means that we are using the reflectance mode, with the beam reflected by the sample on the detector: But if we position the sample on the left side of the top, we are using the transmittance mode: we use the baseline, that is the white body mentioned before in order to reflect the beam on the sample, with the part of the photons going through it that can be detected. If the measurement is done with both the configurations, it's easy to calculate the percentage of photons absorbed plotting the two curves of reflectance and transmittance and building the third curve of absorbance, which is the complementary to 100%. The camera connected is the 60 mm integrated sphere and the range of wavelength chosen for this application varies from 250 nm to 2500 nm: This values permit to observe the optical behaviour to UV light, visible light (ranging from 400 to 750 nm) and a big part of the infrared, which is the most interesting range for the measurement of the thin films.

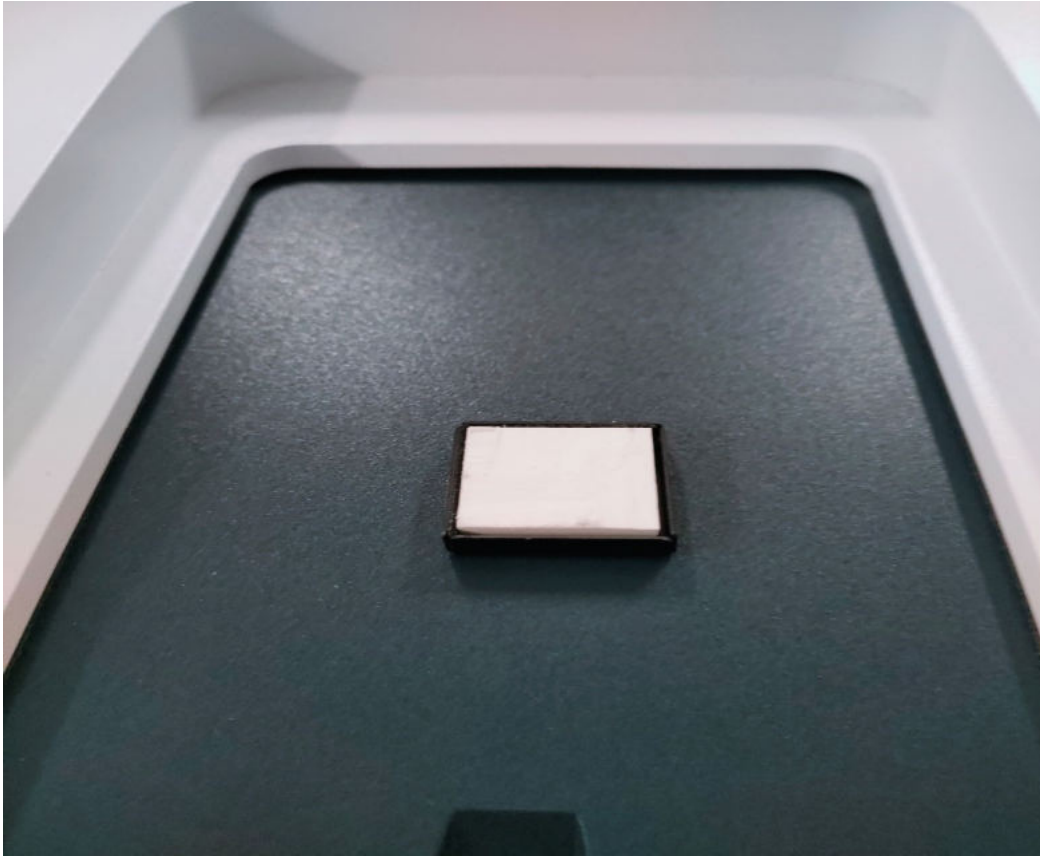


Fig 2.2 The baseline of the Jaasco spectrophotometer

2.4) Thermal evaporator

Used in the majority of the depositions, the thermal evaporator is the technology chosen for this study. Easy-going, tuneable and with the possibility to deposit a great amount of metals and semiconductors, this technique has been used in a lot of different studies to obtain several configurations: Just to give some examples, it has been used with success to build thin films of CdSe [69] or CdS [70], ring nanostructures of ZnO [71] and cupric oxide nanowires [72]. It's composed of two parts: the control panel, in which is possible to manipulate the two pumps necessary to create the high vacuum required, and the active part in which the deposition can be made. In particular, the vacuum is made using a primary pump since the pressure of $2 \cdot 10^{-1}$ mBar is obtained, that after this pressure is shut down to activate the turbomolecular pump, able to reach the pressure needed for the depositions, which is approximately $1 \cdot 10^{-6}$ mBar. A pressure measurer is inserted in the control panel to make easier to understand when the instrument is ready for the deposition and to monitor the conditions of the inside during the deposition: In fact when the chamber is saturated with the vapours of the material to deposit the pressure rise of at least one order of magnitude, arriving at $3,2 \cdot 10^{-5}$ mBar in most of the depositions effected. To keep the instrument safe, it is

important that the pressure during the operations doesn't overcome the value of $1 \cdot 10^{-4}$ mBar, which would result harmful for the instrument and for the quality of the deposition. In the panel also the current can be tuned, guaranteeing the deposition of different materials.



Fig 2.3 The control panel of the thermal evaporator

The material that has to be evaporated is put in the molybdenum crucible making sure that a high surface contact is obtained to ease the process: the crucible is sustained by two resistances, so the temperature can be increased through the increase of current passing through the resistances. The operation is conducted slowly in order to avoid thermal shock in the crucible but, especially in the case of powder of silicon, not too slowly: in fact the silicon react with the molybdenum generating a ceramic phase with variable stoichiometry. The reaction starts to take place way below the melting point of silicon, starting to a temperature of $1300\text{ }^{\circ}\text{C}$ if the operation is conducted at 10^{-4} torr [73], which is also an higher pressure to the one of the thermal evaporator. This means that the evaporation point of the silicon powder must be reached before all the melt silicon reacts with the surface of the molybdenum crucible. In the thicker crucible, used to conduct almost all the depositions, the ampere needed to evaporate the silicon where 235 A, but there is also the possibility to use the thinner

crucible that needs just 120 A to obtain the same deposition, fastening the operations and reducing the problem of the diffusional reactions.



Fig 2.4 The deposition chamber

As shown in the fig 1.4, the deposition chamber is covered with a pyrex dome for the safety of the operator. Between the pyrex dome and the crucible there is also a metallic cage that is used as a further protection but also to have the possibility of watching the material during the deposition through the use of a magnet, which can lift the moving part of the cage exposing the incandescent crucible. This and the pressure control system both ensure that the deposition goes as predicted and are direct ways to control the deposition during time. To avoid problems to the system, a deposition shouldn't last more than two minutes.

2.5) Hall effect measurement

The hall effect is an useful instrument to characterize some fundamental properties of the semiconductor, such as conductivity, mobility and bulk concentration of the carriers. In this case Van der Pauw configuration is used, with four squared metallic contacts that touch the four golden probes of the instrument. During the measurements, the voltage of the four contacts should be kept between 50 and 100 mV in order to not overestimate or underestimate the conductivity of the sample. The probes must be in the centre of the metallic contacts and before starting the measurement it's essential to check through the I - V curves of the four contacts if the four curves are aligned, because otherwise the measurement wouldn't be accurate. The working principle behind the system consists in the combination of a magnetic field through the sample and a current flowing in the length of the sample: the carriers are deviated by the Lorentz force because of the presence of the magnetic field until the carriers accumulated emit a field opposite to the first one: the presence of this field can be detected by the voltage of Hall V_h [74]. The equation that links the Hall voltage with the parameters that can be measured mentioned before is described in [74]:

$$I = \frac{q * V * A * n * \eta}{L} = \frac{V}{R} = \frac{V}{\rho * L/A}$$

In which I is the current in (A), V is the hall voltage in (V), q the elementary charge in (C/cm²), n the carrier concentration in (cm⁻³), η the mobility of the carriers in (cm²/V*s), L the length of the sample in (cm), A the cross section of the sample in (cm²), R the resistance of the sample in (Ω), ρ the resistivity of the sample in (Ω *cm). The sign of the mobility and bulk concentration gives also information on the type of the carriers: if positive, p-type if negative n-type.

For some samples used in the experiments, it is also useful to distinguish between the bulk concentration and the sheet concentration, which can be really different in case of a p-n junction for example.

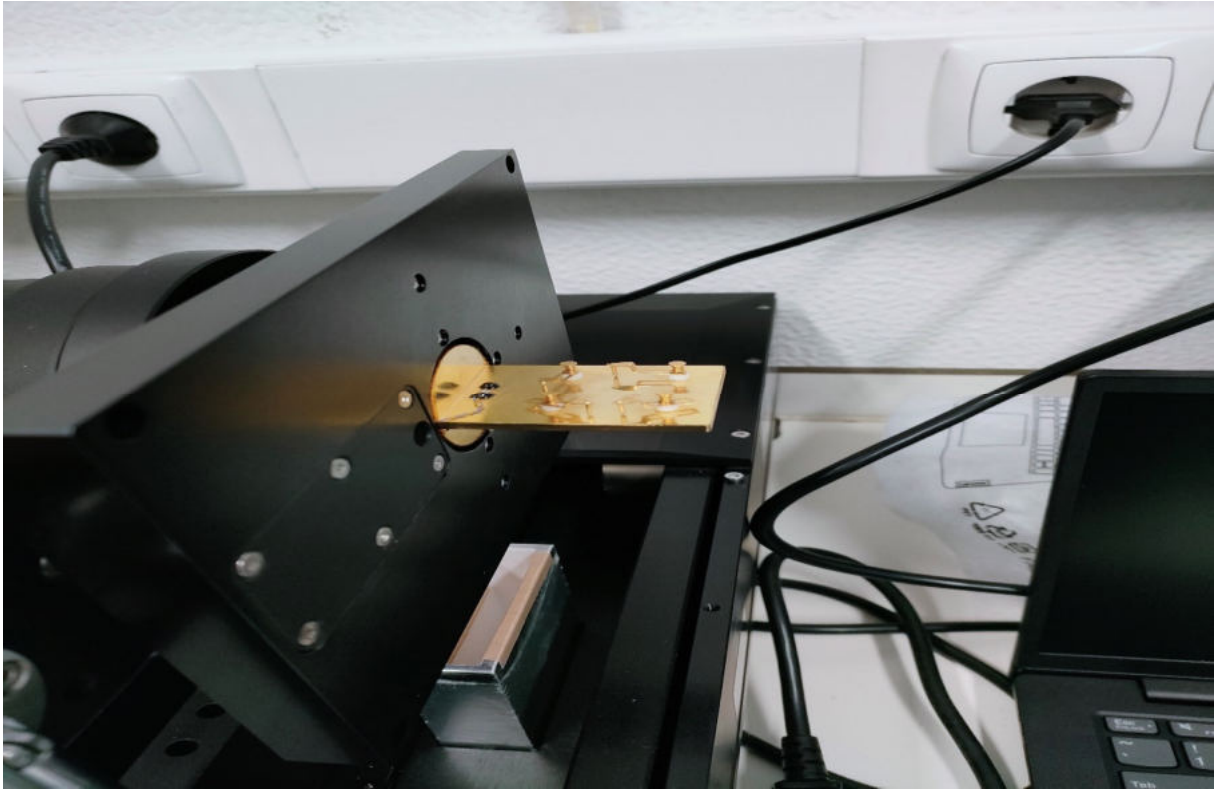


Fig 2.5 the inside of the hall effect measurement system

2.6) Seebeck and voltage measurement

The setup of the measurement for the Seebeck coefficient can be done in two configurations: The planar one and the vertical one. For the planar configuration, the probes of the electrodes will touch two metallic contacts deposited in the sample, giving information on the seebeck coefficient of the surface of the material. The sample is put between two Peltier cells, one hot and one cold. The temperature is regulated through two power suppliers that allow a change of the current, while an IR camera measures the difference of temperature between the hot side and the cold side of the sample, using also a piece of glass as reference. A voltmeter connected to the electrodes completes the setup, measuring the voltage related to the change of temperature or, in case of $V-t$ curves, to the irradiation of a lamp. To have more measurements and consequently a more accurate calculation of the Seebeck coefficient the current is changed 5 times, increasing also the difference of temperature: 300 mA, 450 mA, 600 mA, 750 mA, 900 mA. In the vertical gradient configuration, one electrode touches a metallic contact and the other the TCO that works both as the substrate of the sample and the other contact or is just the contact if sputtered to a corning glass. The sample is put in vertical in the hot cell and now the IR camera measures just the temperature in the metallic contact, making the difference with the room temperature. The current is changed also 5 times and the voltmeter still measures the resulting voltage. Now the Seebeck coefficient is not a measure of

the last layer of the material, but the result of the carrier flow through all the layers of the material. The sign of the voltage is also a way to understand if the semiconductor is n-type or p-type, usually more accurate than the Hall effect measurement. In the $V-t$ curves measurement, the planar configuration is used, but instead of tuning the temperature of the Peltier cells, the voltmeter measures the voltage resulting of the irradiation with an IR lamp, an halogen lamp or a Led lamp, while the $V-t$ software plot the results in function of time.

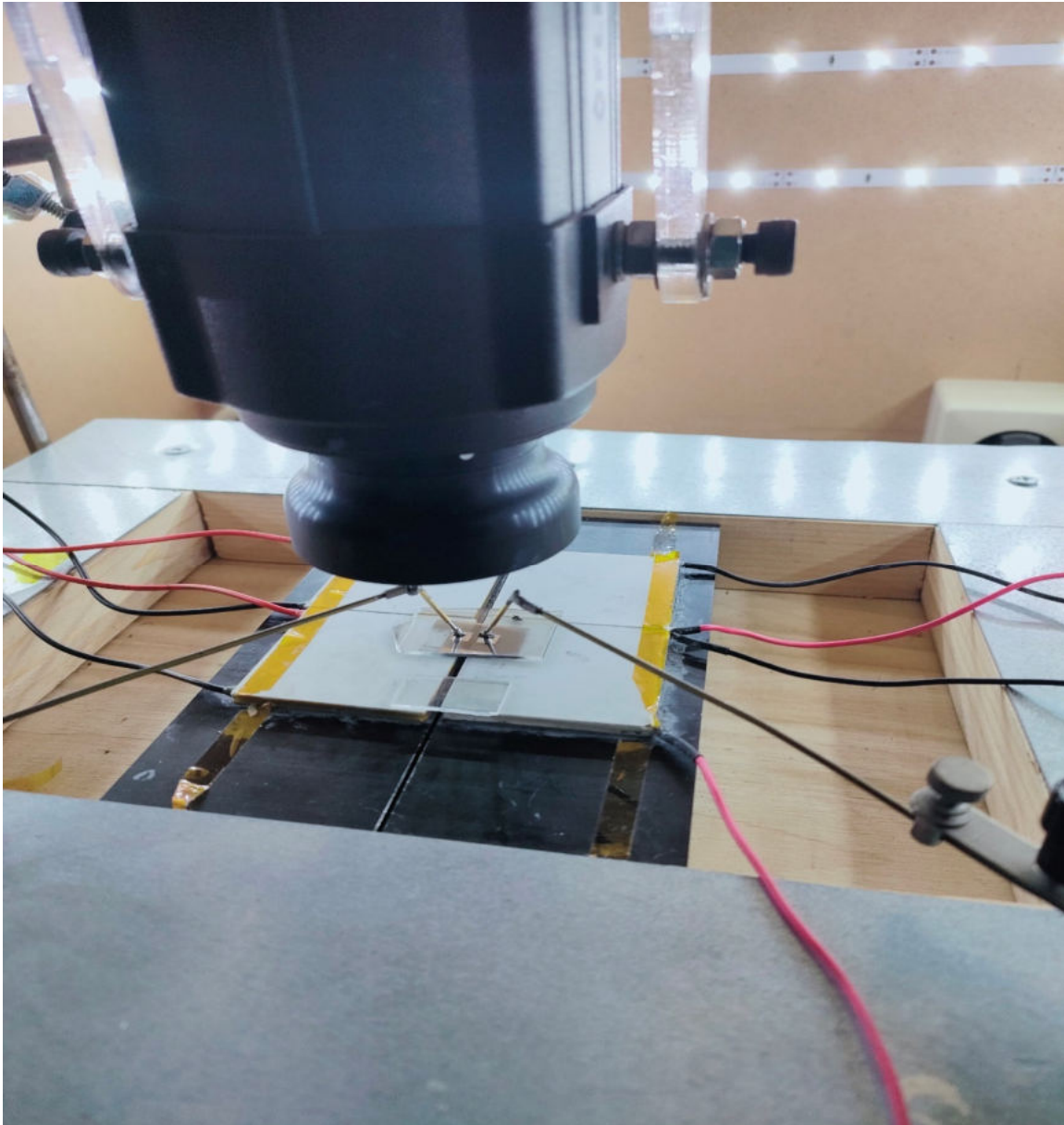


Fig 2.6 Planar configuration

2.7) I - V curves measurement

To plot the I - V curves of the samples, the experimental setup used is composed by a glass support in which the samples are positioned, with an halogen lamp of tuneable intensity put below. The electrodes touch two metallic contacts deposited in the sample with the same polymeric masks used for the Seebeck measurement deposition, while a voltage supplier change the voltage from -1V to 1V, which is directly linked to a change in the current crossing the sample. The software converts the measurement effected in the plot of an I - V curve with a shape different according to the sample or the device that is measured. Sometimes, it can be useful to measure also the I - V curve of the sample in dark: to do so, a black cap is used, that covers the sample hiding it from the environmental lights.

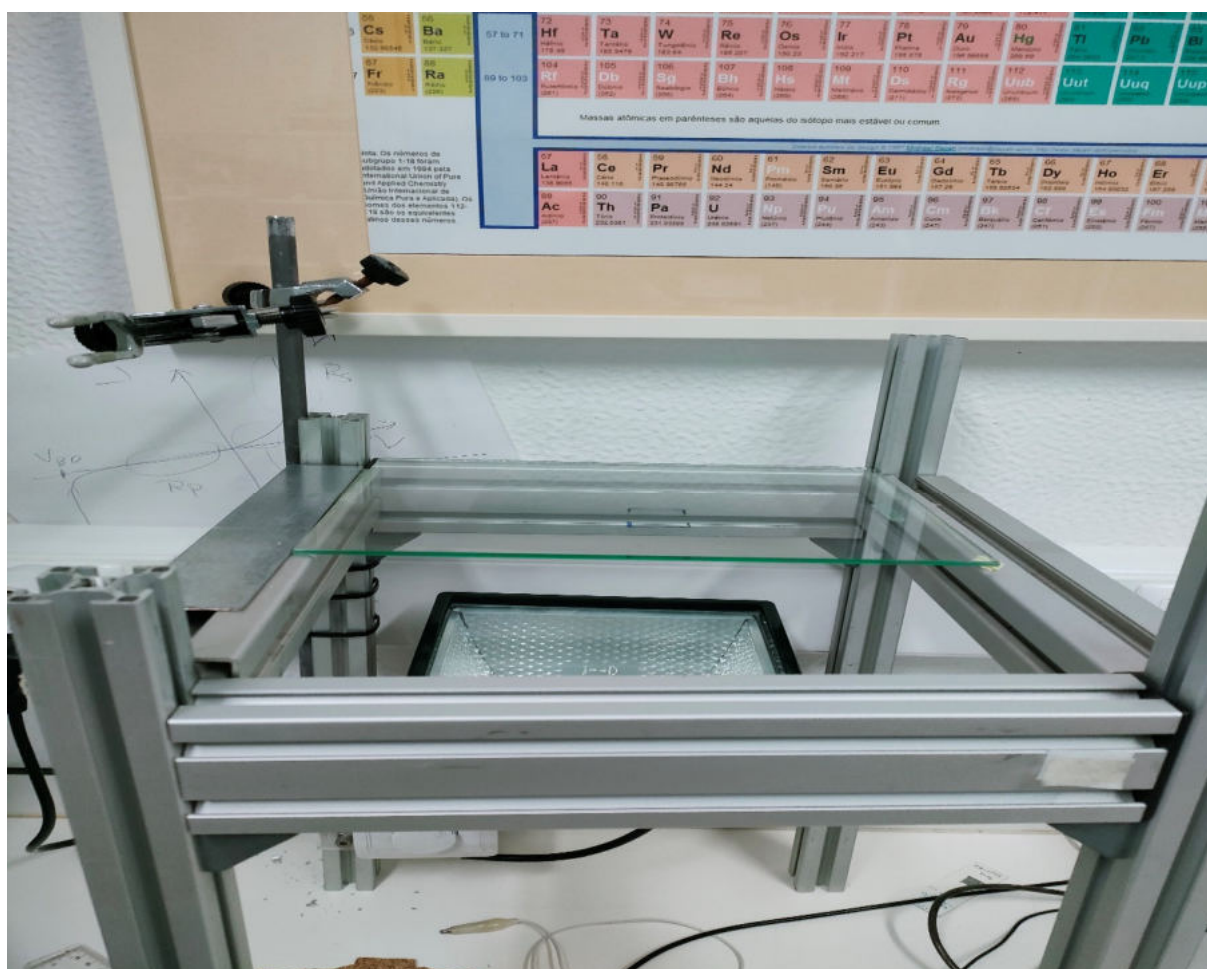


Fig 2.7 The I - V curve experimental setup

3) Results and discussion

This section is dedicated to show the results obtained through the experimental methods described in the previous chapter. After showing the results of the characterization there will be a paragraph dedicated to the discussion of the results obtained with the help of the literature review.

The results obtained were different in many ways from the characterization of an intrinsic or doped silicon sample, which is due to the presence of the other materials needed in the active layer that were not purified using previous leaching: as described in [60], in order of mass percentage in the active layer there are:

- Silicon, which is the 4% of the total panel
- Aluminium back contact, the 4% of the panel
- Silver for the front electrode, present in very little concentrations (0,053%)
- The antireflection layer of uncertain composition SiN_x

All these elements will have an influence in the development and characterization of samples and can be exploited or purified in other ways in order to obtain the best results from the material. The critical analysis of the instruments' results will be essential in order to understand the mechanisms of doping, trapping, thermal dissipations at the base of a certain behaviour.

The solubility of the metals and molecules present in this complex system, such as aluminium, silver, nitrogen are not high in silicon, which is the main constituent of the recycled powder: by the way, their presence will influence the final behaviour in certain ways which will be understood through experimental measures.

3.1) Influence of thickness

The first experiments conducted to the active layer of polycrystalline silicon reduced to powder were made to demonstrate that the performance of the future device that can be built reusing this powder (giving a second life to it) are strictly dependent on the thickness of the film deposited with the thermal evaporator.

3.1.1) Deposition

To ensure that the same quantity was deposited every time, the powder was weighted before being put into the molybdenum crucible. More specifically, 0,05 g of powder were used: in the first samples, just a layer was deposited while in the second samples three layers were deposited with the same technique. After several attempts, it has been demonstrated that the current needed to evaporate the recycled powder is 235 A, while for the deposition of

aluminium it is enough to use a current of 180-190 A. After that, the polymeric masks were used when necessary with different configurations according to the instrument that had to perform the analysis: for example for the I - V curves and Seebeck measurement were used masks with two openings of known geometry (Length of 0,4 cm with distance of 0,2 cm or length of 1 cm with distance of 0,5 cm) while for the hall effect were used masks with four openings in Van der Pauw configuration. The metal used for the contacts is aluminium, cut from a wire with pieces of 1 cm length. Although there wasn't an analysis with the profilometer, from previous works it has been estimated that the thickness of 1 layer of such amount of powder should be 150 nm, which means that the samples with three depositions have a thickness of 450 nm. After the depositions the sample were pretty similar apart from some additional scratches and tensions in the samples of three layers, caused by the depositions of single layers one on top of the other. Nonetheless, due to the size of the crucible it couldn't be deposited the triple of the amount of the powder in just one deposition. The defects created with these depositions massively affected the performance of the sample of three layers as it will be shown in the further paragraphs. Some solutions to solve this problem can be:

- Change the technique used, maybe shifting to sputtering
- Use a bigger crucible, although the current that must be used will increase
- Use a thinner crucible, making depositions with really low currents (120 A) decreasing in this way the damage caused by interfacial tensions between different layers
- Change the material of the crucible, using for example tungsten: without reactions between the powder and the crucible it is possible to increase the current slower, having more control of the deposition and thus damaging less the samples.

One attempt which has been made in order to limit the presence of the defects in the systems is to deposit the powder, the metal and all the other depositions required after the cutting of the glass substrate, instead of depositing on a big tile of glass and proceeding with the cut after the deposition: After have tried with both techniques it is indeed better to cut the glass first, although it must be clear from the beginning what kind of sample we need for the following deposition and characterization, which is not easy to choose.

For example, the samples for the hall effect must be little pieces of a squared dimension, while the samples for the measurement of the V - t curves and the Seebeck coefficient must be elongated in order to make the planar gradient configuration easier to measure: in fact, the thermal infrared camera must be positioned between the two contacts, of which one will be on the hot side and the other one on the cold side. If the sample is not long enough, it is difficult to position the two contacts in two different Peltier cells without touching the other cell.

Furthermore, in order to measure the gradient of temperature between the two contacts, which is fundamental to calculate the Seebeck coefficient as it will be explained later, the software linked to the infrared camera need the tracking of three straight lines in the planar

configuration: the first one is traced along the border on the left of the cold metal contact, the second one on the right of the hot side of the metal contact and the third one is the straight line that link the two other line and must pass from the reference sample made of simple corning glass. To simplify the tracking of the lines without interferences within the two metal contacts it is common knowledge that the sample to analyse must have an elongated form.

The samples for the spectrophotometer don't need metal contacts and can be of any size, the only important thing is that they should cover all the detecting area to avoid white spots.

The samples for the I - V curves can be of several shapes and with a non accurate number of metal contacts, as long as there are at least two where to put the electrodes for the measurement: to simplify the operations and avoid further depositions the samples for the Seebeck coefficient measurement are used also for this purpose.

The resistance of the samples was first checked with a resistometer: The resistance of the samples of 1 layer was $R=180\ \Omega$, while the resistance of the samples with 3 layers is $R=580\ \Omega$, confirming the hypothesis and the empirical evidence of the presence of more defects in the samples of three layers.



Fig 3.1 Sample of three layers for Hall effect

From the figure 3.1 it can be seen that the three layers samples have some mini scratches and defects generated because of the deposition.

3.1.2) Spectrophotometer

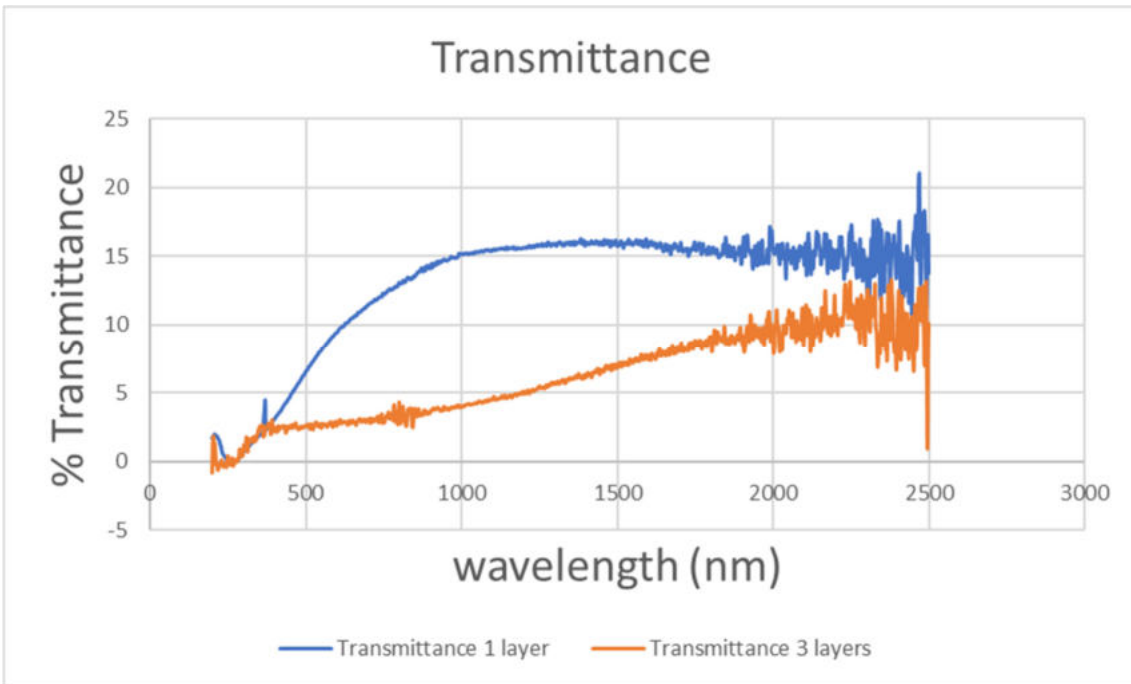


Fig 3.2 comparison transmittance

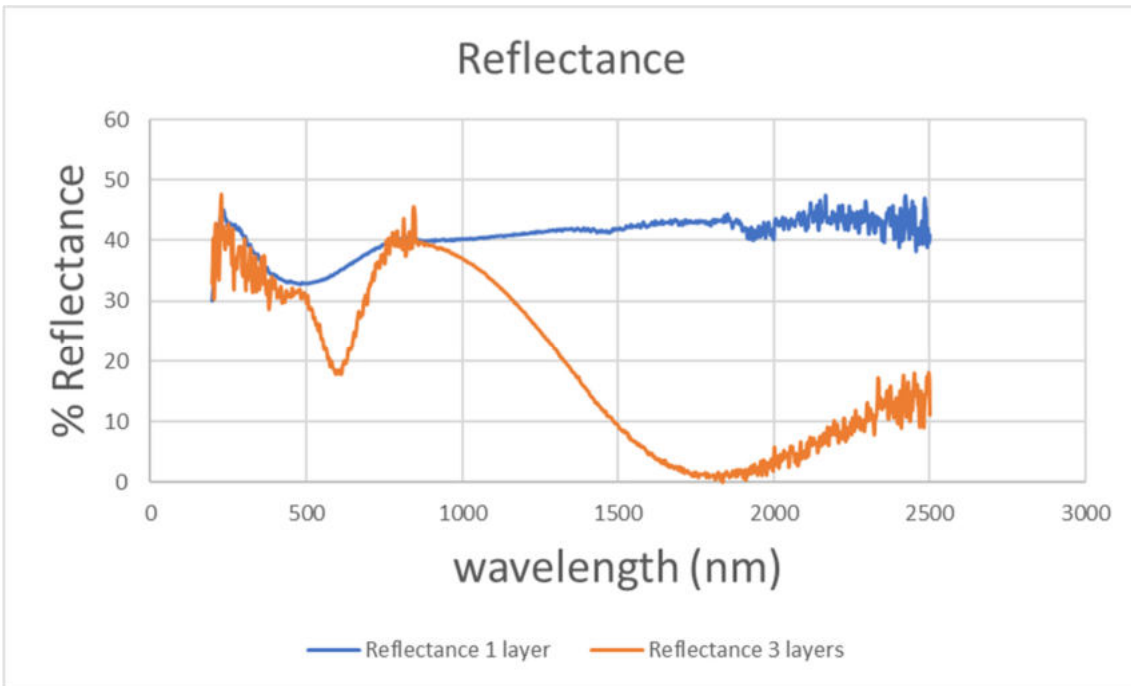


Fig 3.3 comparison reflectance

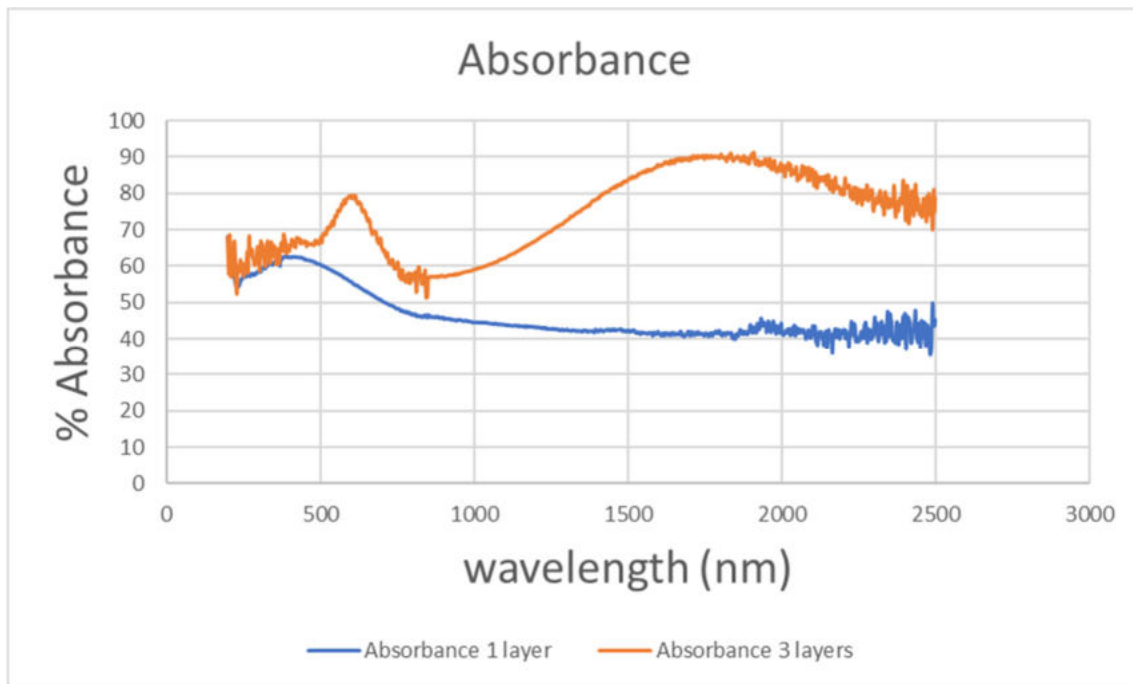


Fig 3.4 comparison absorbance

As it can be seen from the fig 3.4, the absorbance of the sample with three layers is bigger, although if the biggest difference is just in the range of the infrared, until 1000 nm with a gap of 20%. From the graphs of reflectance and transmittance it can be understood where are the biggest optical losses of the sample with 1 layer: both have a very similar curve of transmittance with the biggest losses in the infrared section, but in the reflectance curve the gap is at its maximum: one of the possible explanations for this consists in the amount of aluminium in the samples that dope the silicon and the amount that is simply included as a different phase in the system. With a thicker layer of silicon, it is of course easier for the aluminium to enter in the crystalline structure of the silicon, considering also that it has a limited solubility of 0,035% at the most favourable temperature [75]. All the aluminium that is not included in the crystalline structure of the silicon but is still present in the system contribute to the high reflection of the sample, considering that aluminium is a high reflective metal. It is also evident how the sample with three layers is more defective than the other: There is more instability in the curve with some areas, especially the ones with lower values and in the last areas of infrared. When the value goes below the zero, it means that the percentage is so small that the system cannot calculate it precisely, so it can be assumed that the value at this point is effectively zero. It is also important to underline that the absorption peak is slightly different: The peak of the sample with three layers is at 500 nm, so in the visible range, while in the sample with one layer the peak of absorption is at approximately 300 nm, which is less similar to the wavelength associated with the highest photon energy in silicon samples, 2,8 eV, which is the energy corresponding to wavelength of 443 nm [76]. It is not considered the tail of absorption of 90% in the spectrum of the three layers because it can

be considered as an overestimation of the spectrophotometer. According to other optical studies referring to several semiconductors, with the transmittance of the samples analysed in this study that is way lower than the transmittance of CIGS thin film [77], enhancing the quantity of photons absorbed. Compared to the absorbance of thin films of CdTe, the absorbance of the samples made with recycled silicon is higher in the IR part of the spectra, but only the sample of three layers can reach the 80% of absorbance gained by the CdTe film [78].

3.1.3) Seebeck and voltage measurement

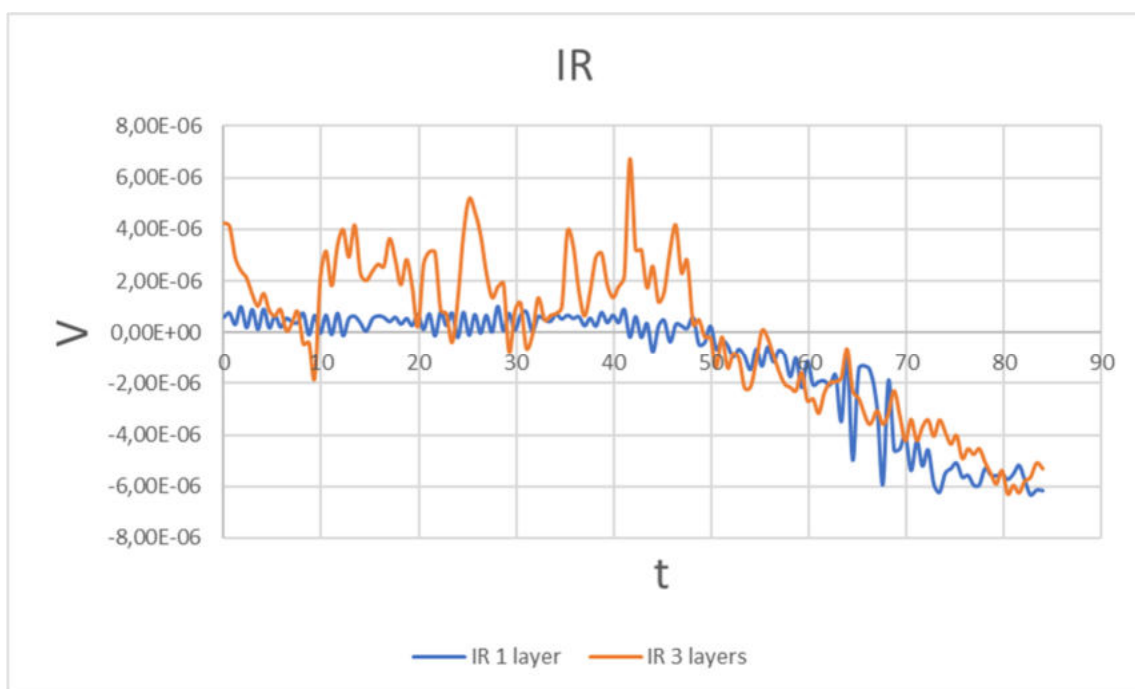


Fig 3.5 Comparison $V-t$ curves IR

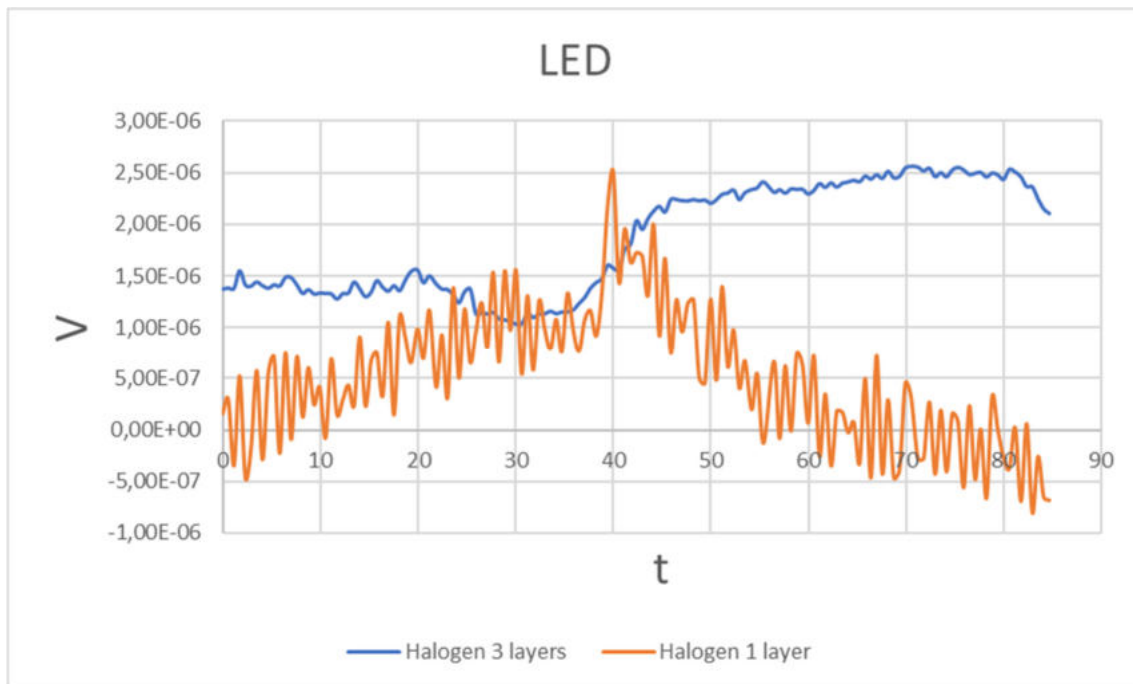


Fig 3.6 comparison V - t curves LED

This curves show the response of the samples if irradiated with a light bulb emitting in infrared or in LED. The analysis has been conducted in planar configuration and the graph must be read without considering the sign of the voltage, that depends just on the polarity of the electrodes. It is more important to focus on the difference of the signal compared to the zero level, which represents the response of the sample to the light. The behaviour of the two samples is very similar and the voltage obtained, between 10^{-6} and 10^{-7} V, is too low to justify the building of a photo-responsive device made with this material, such as a sensor. It absolutely make sense, since no external electric field is applied to the material which is not a p-n junction, but a semiconductor with some free metal nanoparticles in it. Although this is true, it is interesting to observe that the fluctuations of carriers generation provoked by the illumination with the different lamps generate a voltage which is slightly different from zero, also with some differences according to the thickness of the layer. Apart from the graphs, it is also difficult to find in the bibliography a performant sensor made with silicon, recycled or not and doped or not, with the research that is focusing more on semiconducting oxides and carbon nanotubes for several applications, photo-sensing or not: for example, the voltage required to build an H₂S sensor made of carbon nanotubes and silicon junction cannot be lower than 0,18 V [79]. Independently from the application, in the bibliography the value of voltage reported for good sensing properties shouldn't be lower than a value of 10^{-1} V. The Seebeck coefficient was measured using the planar gradient configuration with values reported of $S=-4 \cdot 10^{-4}$ mV/K for the sample with one layer and $S=1,5 \cdot 10^{-3}$ mV/K for the sample with three layers. The critical reading of the results makes easy to understand how the influence of the aluminium doping works in this case: there is an increase in the

thermoelectric properties of the silicon, although the thermoelectric properties strongly depends on the temperature of the system: the Seebeck value reported in an average of all the results calculated with the formula:

$$S = dV/dT$$

In which the coefficient calculated is not constant but slightly changes according to temperature, usually increasing when the temperature decreases [80]. It is also reported in [80] how the Seebeck coefficient for silicon can reach values of 1,4 mV/K for samples of polycrystalline silicon at 400 K, showing how the thermoelectric properties of the samples are not good enough to think about some applications. The other evidence that is possible to understand from the Seebeck coefficient regards the sign of the carriers: in the sample with one layer the sign is negative, probably because of a previous doping of n-type on the solar cell that is huge compared to the counter doping of the aluminium. In the sample of 450 nm thick the greater quantity of aluminium added with the silicon in the three depositions overcome the counter-doping of n-type making the sign of the carrier positive. This is an important evidence of the fact that a doping effect is indeed reached during the thermal deposition of the powder.

3.1.4) I-V curves measurement

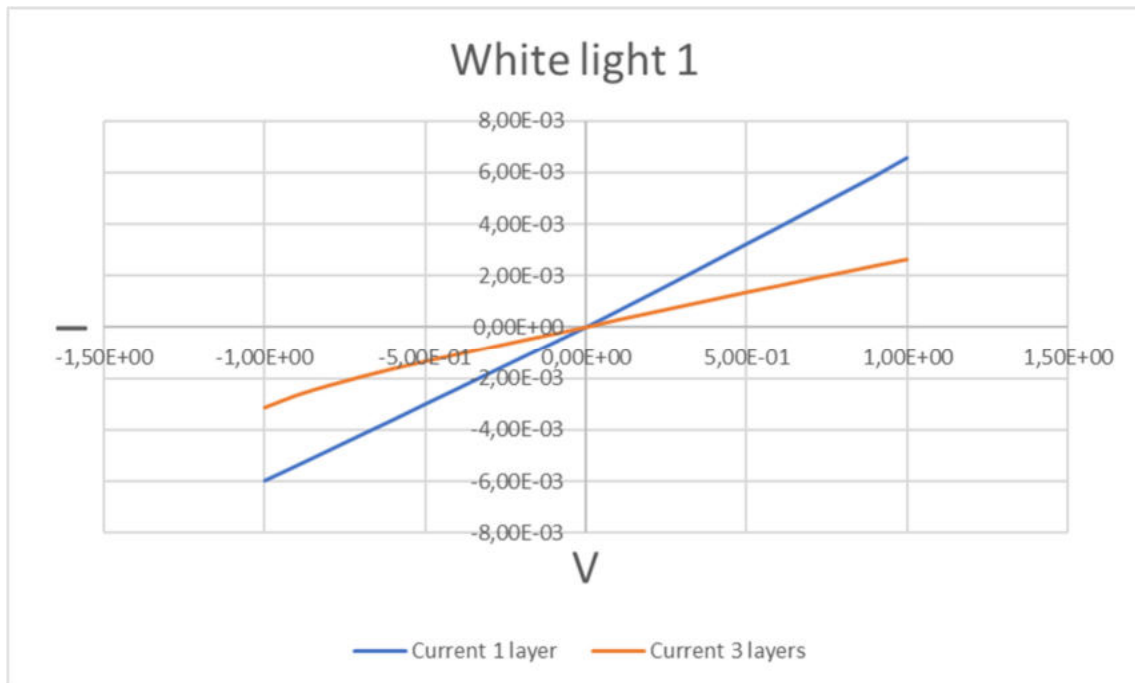


Fig 3.7 comparison I-V curves white light 1



Fig 3.8 comparison *I-V* curves white light 3

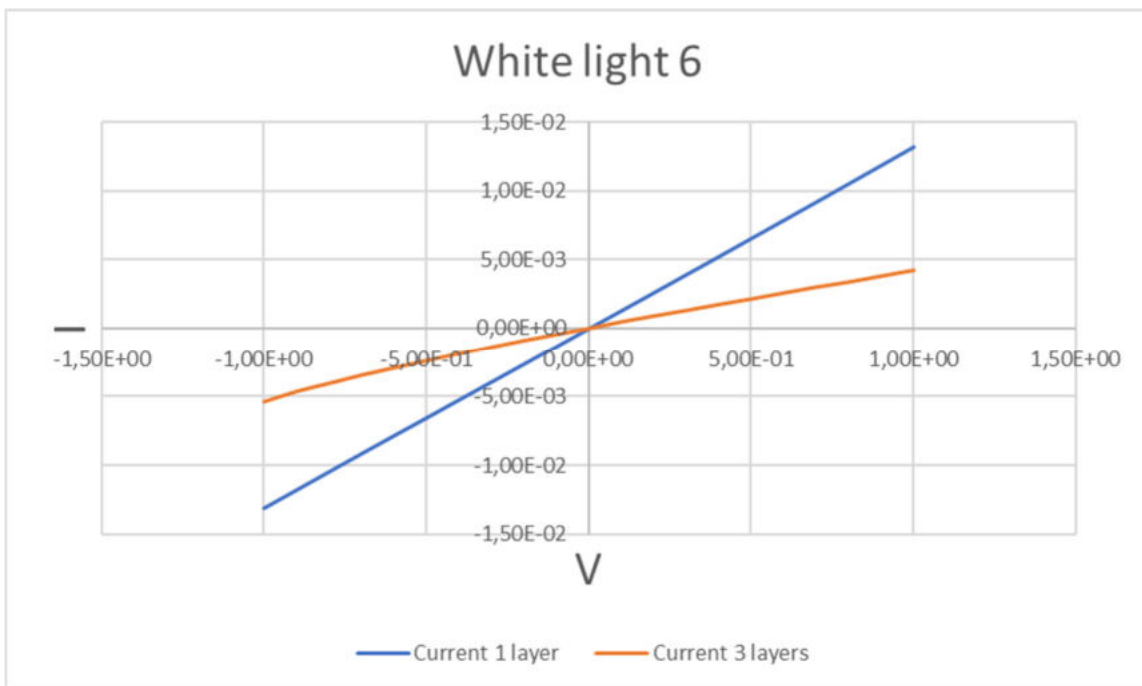


Fig 3.8 comparison *I-V* curves white light 6

The *I-V* curves measurement is one of the greatest evidence of the defects present in the samples of three layers: the maximum current measured in that samples is $4,23 \cdot 10^{-3}$ A, corresponding to the measurement of 1 V while exposing the material to a source of light of 1000 W/m^2 . The difference between the different light exposures is not evident at all, with

just slight increases happening while changing the irradiance. In the samples of 150 nm thickness the situation is way different: a value of $1,3 \cdot 10^{-2}$ A is reached for the white light 6, which is the highest value registered for the samples containing just the layer of recycled silicon without further building of the structure. How is the performance of these samples if compared to solar cells of silicon of commercial purity? It is reported that the maximum current reached for a polycrystalline solar cell is $10 \cdot 10^{-2}$ A, while for a monocrystalline is $15 \cdot 10^{-2}$ A and for an amorphous solar cell the value estimated is about $2 \cdot 10^{-2}$ A [81]. Further considerations must be done in order to take this comparison in the right way: First of all, in this paragraph it has been characterized the I-V curve of a material, and not of a device such as a solar cell which is a p-n junction. Furthermore, although it is considered the dependence on the irradiance it has not been measured the dependence on the temperature, which can decrease the performance of a semiconductor device. The value of current reached by the samples of 1 layer is very similar to the one of an amorphous solar cell, although it has been demonstrated by several studies that the aluminium doping induces the crystallization of the silicon [82], [83]. It is indeed true that aluminium induces the crystallization of silicon but just at temperatures not lower than the annealing: 475 °C is the minimum temperature used in these studies [82].

3.1.5) Hall effect measurement

1 Layer	Bulk concentration (cm⁻³)	Mobility (cm²/V*s)	Conductivity (S/ cm)	Sign of the main carriers
1	6.61E+18	1.50E-02	9.12E+2	-
2	5.15E+17	1.93E-01	7.41E+2	-
3	1.05E+19	9.42E-03	4.68E+2	+
4	1.47E+18	6.78E-02	5.25E+2	-
5	1.58E+19	6.28E-03	5.62E+2	-

Tab 3.1 Hall effect of a sample of 1 layer

3 Layers	Bulk concentration (cm⁻³)	Mobility (cm²/V*s)	Conductivity (S/ cm)	Sign of the main carriers
1	3.80E+17	5.36E-02	1.29E+2	+
2	8.59E+16	2.37E-01	9.20E+2	+
3	2.32E+17	8.79E-02	9.74E+2	-
4	2.26E+17	9.00E-02	2.15E+2	+
5	2.51E+17	8.12E-02	2.87E+2	-

Tab 3.2 Hall effect of a sample of 3 layers

The hall effect measurement was repeated five times in order to have more observations of the same sample. As mentioned before, it is really important that the voltage is kept between 50 and 100 mV to have accurate measurements of the conductivity. The comparison between table 3.1 and 3.2 shows that the doping highly changes, with the sample of 1 layer n-doped because of the previous doping during the lifetime of the silicon solar cell and the sample of 3 layers p-doped because of the high amount of aluminium. If we compare with other studies the conductivity of the samples, it is clear that some aluminium didn't enter the crystalline structure and contributed to generate a free second phase in the samples: In fact, the conductivity of silicon is between 10^{-10} S/cm and 10^{-8} S/cm for phosphorous doping [84] and between 10^{-7} S/cm and 10^{-6} S/cm for doping with rare earth elements [85]. The conductivity is higher in the sample with three layers because of the higher amount of aluminium in the system but the bulk concentration is also lower of one or two orders of magnitude: this is probably due to the defects introduced in the samples during the various depositions, which affects also the mobility of the carriers in terms of carrier lifetime and obstacles for the flux of the carriers. Furthermore, all the interfaces between the free metal of the sample and the semiconductor generate losses of mobility in the sample. Comparing the bulk concentration with other studies, the doping of 10^{18} cm⁻³ or 10^{19} cm⁻³ of the samples with 1 layer is very similar to other doping effected, in fact a p+ doping of aluminium is approximately $3 \cdot 10^{18}$ cm⁻³ [86], [87] while the mobility reported is 0,1 cm²/V*s [88]. The bulk concentration is therefore also strongly dependent from the quality of the deposition, making the choice of a single layer deposition most effective even if less doped by the aluminium and the nitrogen contained in the antireflective layer. By the way, it is also correct to add that the results of the bulk concentration have an high dispersion, with the numbers varying by two orders of magnitude in the worst cases for the single layer, while with the three layers the concentration stabilizes: the conclusion is that the percentage of free metals is the responsible for the dispersion of results, with the samples of three layers containing more aluminium in the crystalline structure and less under the shape of free particles.

3.1.6) Discussion of results

To conclude this section, it is essential to discuss the influence of defects in the system, because as mentioned several times is the main responsible for the difference of quality between the sample of 1 layer and the sample of 3 layers. In effect, it has already been demonstrated that the device performance of thin films of polycrystalline silicon is influenced by deep defects, such as dislocations or grain boundaries [89]. Other defects that must be mentioned, and that are more important for our system, include the mechanical damage of the surface (that can comprehend risks, cracks and interfacial tensions between the layers that cause a real peeling of the sample), inhomogeneity of the sample and holes in the surface, that have big influence on the performance and the characterization [90]. The most influenced

parameters are the tension of open circuit and the $I-V$ curve, [90] with the $I-V$ curve that can also change shape due to the high presence of defects [91]. Some attention must be paid also to the precipitates that can form during a deposition, with particular attention to some atoms like oxygen and carbon, but also some metals such as iron and chromium [92]. The presence of some atoms or precipitates introduces some deep energy levels in the bulk, that is linked to the reduction of carriers in the semiconductor [93]. How do they affect the bulk concentration of the samples? Acting as recombination centres for electrons and holes, thus reducing their lifetime and the concentration [93]: the recombination can be radiative if associated with the emission of a photon or non radiative if there is just an interaction with phonons [93], without forgetting that in the construction of a device the lifetime of the device itself can massively influence the presence of defects in the bulk and in the surface, further reducing the performances [93]. Some of the impurities mentioned before (oxygen and carbon for example) are more present in the surface of the material, which means that their concentration and thus the performance of the device can be plotted as a function of the depth of the material [92].

3.2) Shutter and Al-Bottom configurations

The next step of the research consists in finding new configurations in order to exploit differently the material, without using leaching or other steps involving chemicals: To do so, two different configurations have been used, the first one consists in the attempt of purifying in the thermal evaporator the powder from the silicon in order to have a thin film without the aluminium doping: To do so, it has been used a shutter, that can be seen as a metallic shield in which is possible to do an intermediate step of evaporation to get rid of impurities and other materials not desired in the system. The second attempt is trying to evaporate just the aluminium in an intermediate evaporation step without using the shutter: This means that the structure created is a back aluminium contact on the bottom and a purified silicon powder on the top. The characterization of the new structures will be made with the same techniques described before.

3.2.1) Deposition

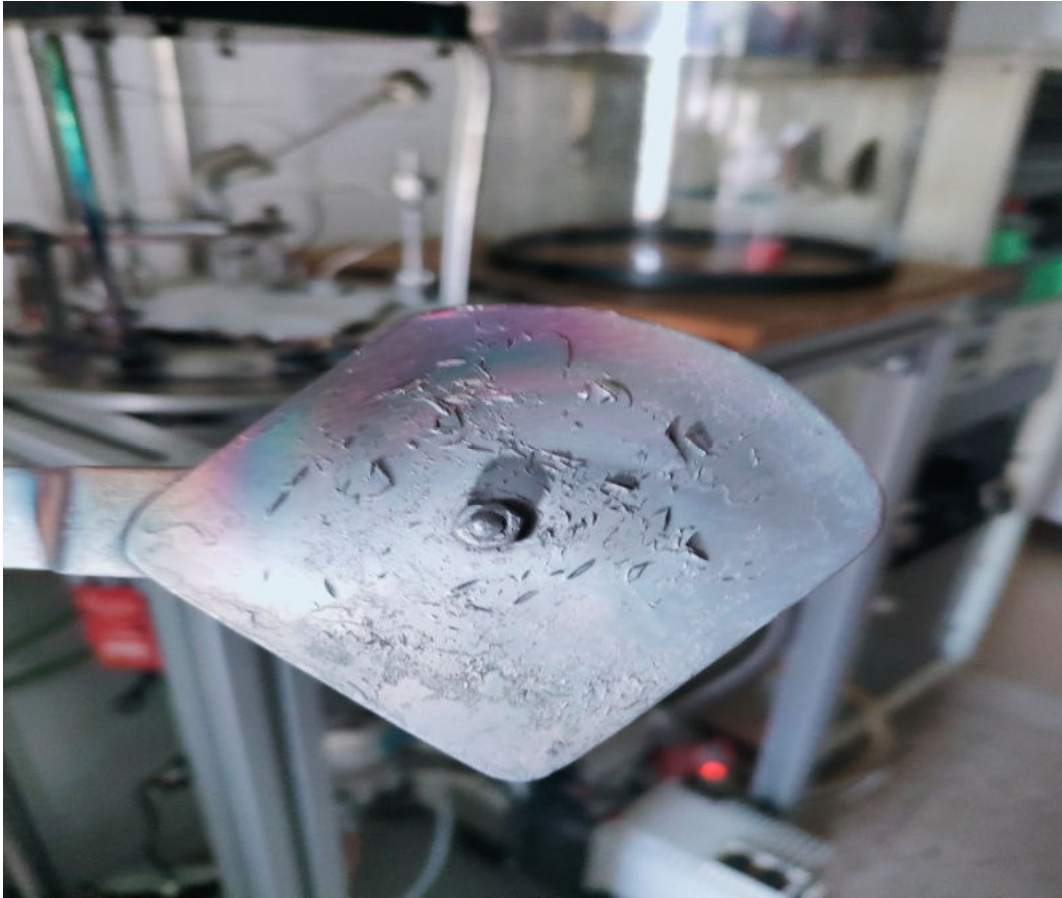


Fig 3.9 shutter after the aluminium deposition

The deposition has been made at the same current described for the deposition of aluminium contact, keeping the shutter for 90 seconds in order to ensure a complete purification from the metal, confirmed also by the pressure control system that started to lower the pressure after the initial increase due to the presence of aluminium vapour in the chamber. Same procedure for the second configuration, but without using the shutter in order to let the aluminium evaporate in the corning glass. While the samples with the shutter are different from the ones of 1 layer in the aspect (in particular a higher transparency is reached), there are not a lot of differences between the samples Al-bottom and the samples characterized in the previous chapter of this section. Makes sense anyway, because the visible properties depend on the materials present in the sample, although the different structure will reveal some changes in the spectrophotometer. It is also important to underline that the deposition has been made all at once, without opening the chamber after the intermediate step and introducing the purified powder again, mainly for two reasons:

- In order to create the high vacuum in the chamber at least six hours are needed, resulting in a great waste of time if after the intermediate step the chamber must be opened for another deposition in the same sample

- Doing the depositions in the same step results in less external impurities and lower presence of defects, as shown in the previous chapter

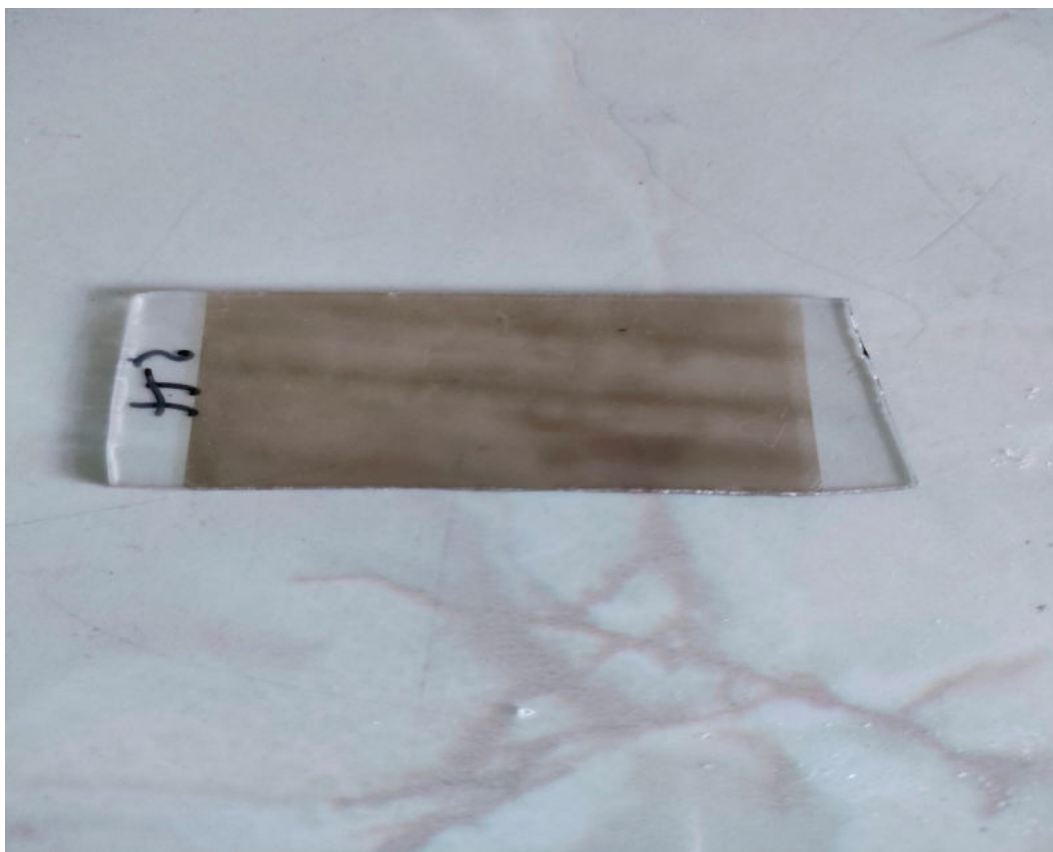


Fig 3.10 sample after use of the shutter

3.2.2) Spectrophotometer

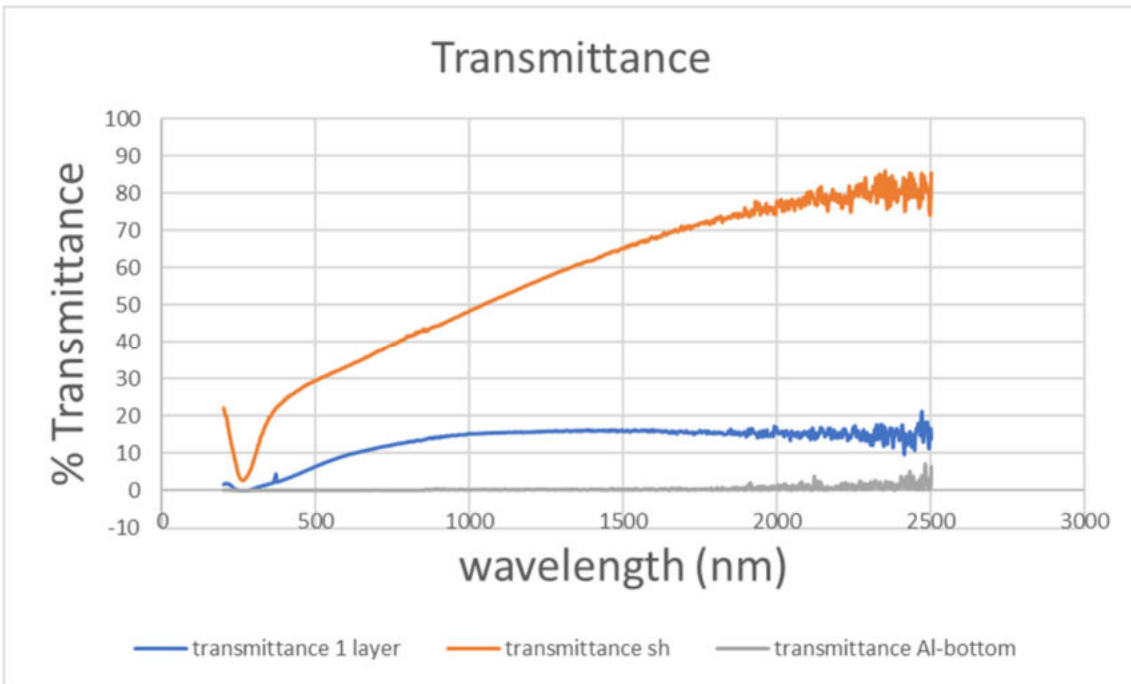


Fig 3.11 comparison transmittance

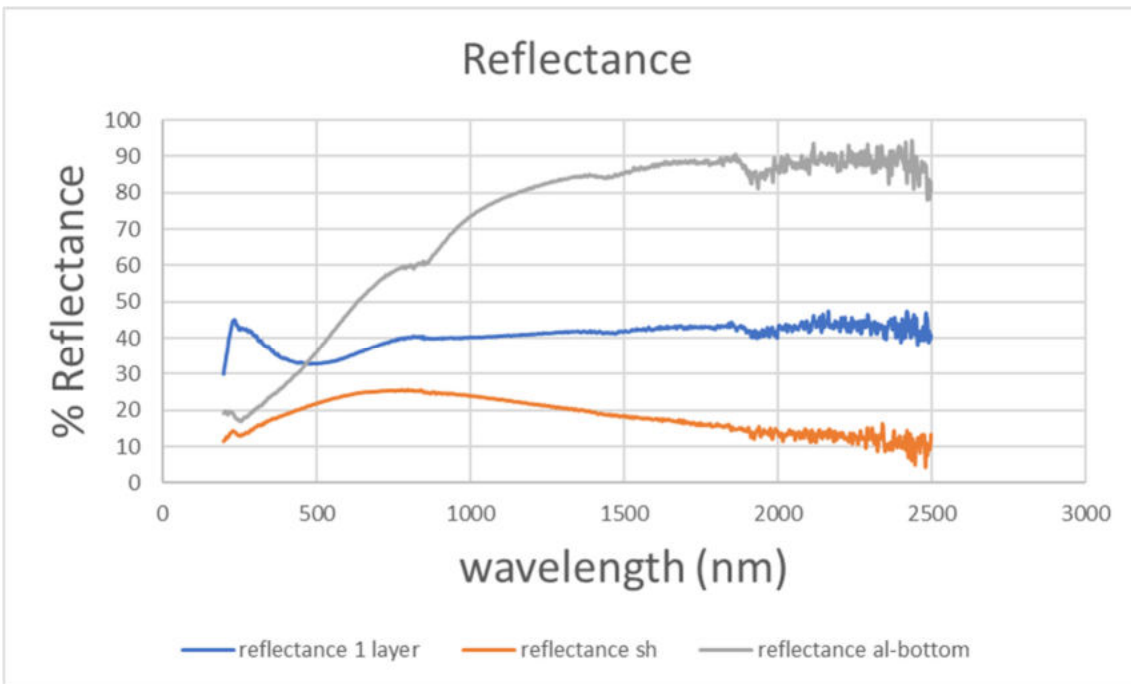


Fig 3.12 comparison reflectance

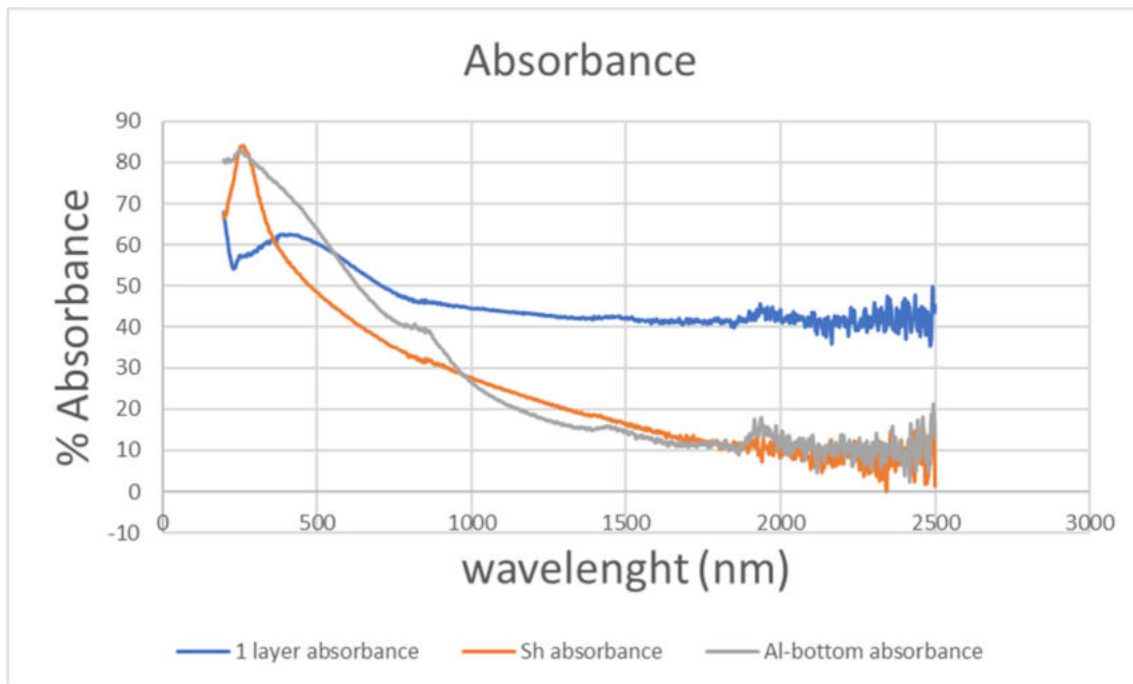


Fig 3.13 comparison absorbance

The analysis of the spectrophotometer reveals some data that could have been foreseen simply by understanding the building of the structure: the samples with the shutter have a massive transmittance because of the lack of metal which participated both in the reflection of the photons and its thermal dissipation, resulting in an interaction and thus in a resulting absorption or reflection increase. As a consequence, the percentage of reflectance in the Al-bottom configuration is the greatest, because now there is a coherent layer of metal which enhance the reflection of the photons, especially in the infrared range. The absorption curves show that for optical absorption the normal sample of one layer is the more effective until the UV range, in which the peak of both the new structures can reach values of 82%. The shape of the absorbance curves in the two new structures is really similar, but for completely different reasons: The low level of absorbance of the infrared range is due to the almost complete reflection of the photons in the Al-bottom, while in the shutter configuration all the photons are transmitted throughout all the sample and detected, without interacting in any ways with the system. The absorption tail is present in all the samples, and it is still the range of the analysis with the highest uncertainties: the curve is not stable in that range, meaning that the instrument is less accurate in registering the percentage, which is however theoretically correct to be lower than in the range of visible and UV. The only big difference with classic samples of polycrystalline silicon still continue to be the peak, that is near the visible range but in the near UV: even in the shutter configuration, some impurities are still present and acting as modifiers of the optical properties of the silicon. The last peak of the silicon at 250 nm is considered as an overestimation of the instrument, with the highest peak still considered at 300 nm.

3.2.3) Seebeck and voltage measurement

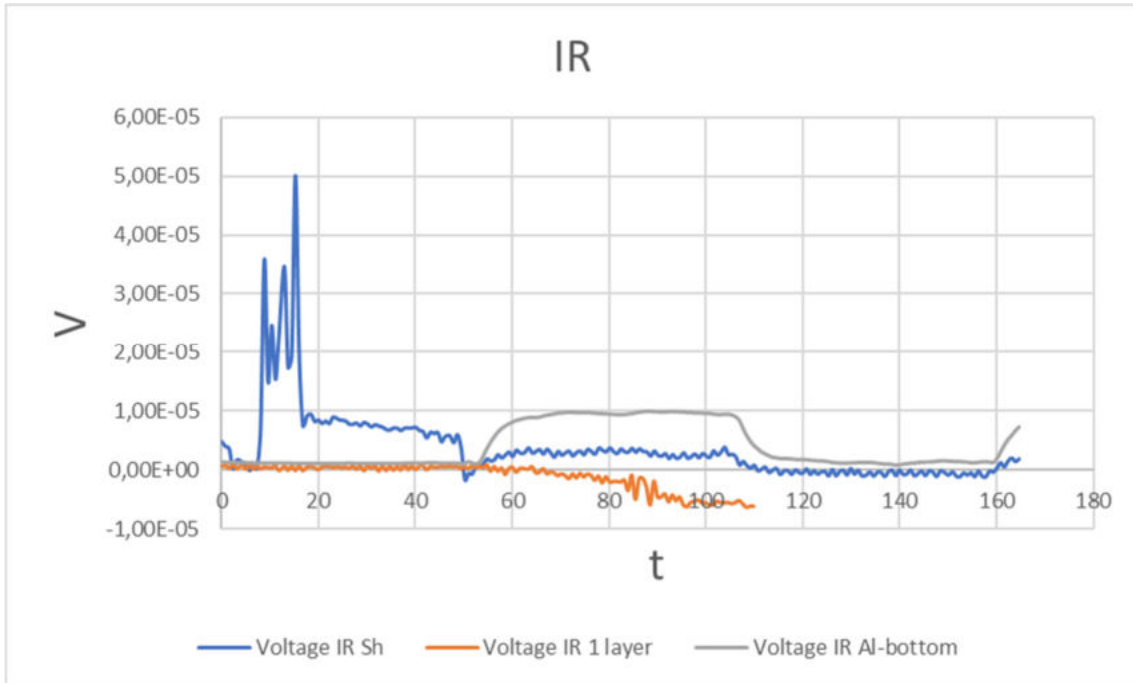


Fig 3.14 comparison $V-t$ curves IR

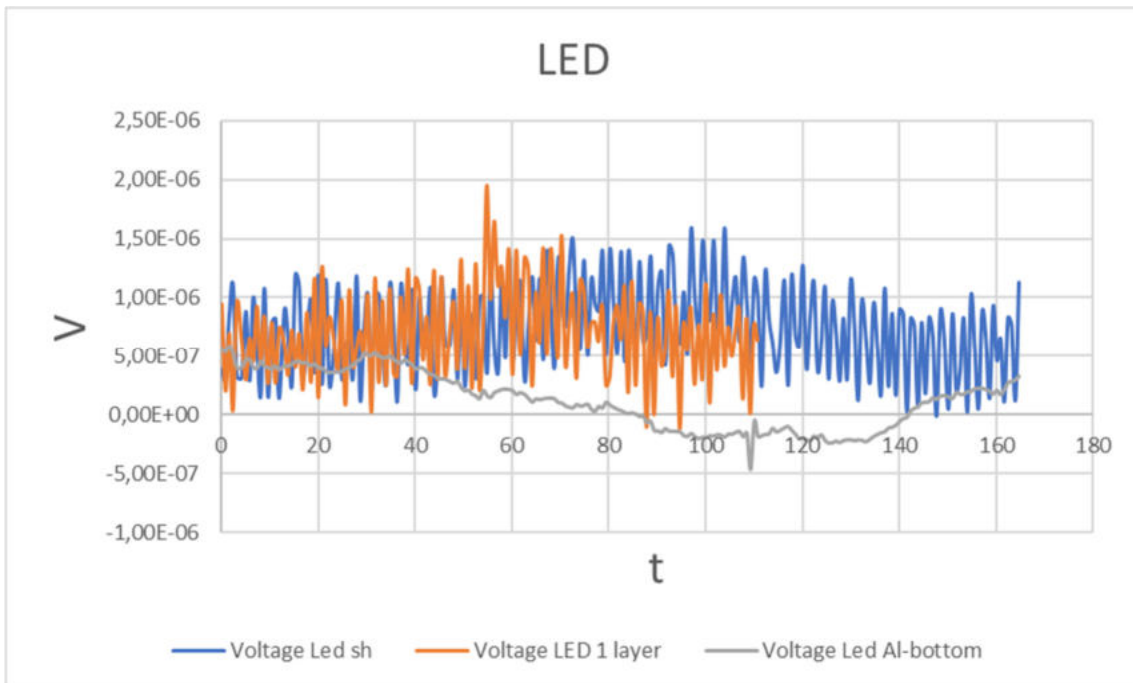


Fig 3.15 comparison $V-t$ curves LED

From the plotting of the $V-t$ curves in planar configuration, it is possible to see how the change of the structure didn't change a lot the photo-sensing properties of the samples: the order of magnitude of the voltage is still between 10^{-6} V and 10^{-7} V, which is not sufficient in order to think about the construction of a photosensor. To explain this, the same considerations made before about the absence of an electric field can be done: there is not external force able to extract the carriers generated within the sample after the irradiation with the lamps, neither there is an electric field generated by the p-n junction, which is not used in these samples. The presence of an anomalous peak in the IR curve for the shutter configuration is probably due to an instability during the measurement: in effect, for the shutter configuration has been challenging to provide stable data, due to the high lack of conduction of the sample: the resistance, measured with the voltmeter, was higher than 1000 Ω . The Seebeck coefficient was measured in the planar configuration, but there weren't big differences with the vertical configuration: without building a more complex device such as a p-n junction it is not necessary to measure both the values. $S = -1,5 \cdot 10^{-3}$ mV/K for the shutter configuration and $2,2 \cdot 10^{-3}$ mV/K for the Al-bottom configuration. In another study is reported an higher value for the sample doped with aluminium, with a Seebeck coefficient that can arrive to $397 \cdot 10^{-3}$ mV/K, although if it has also been shown how the electrode used for the measurement of the coefficient influence the final parameter obtained [93]. It is interesting to notice that in the Al-bottom configuration the change of the structure didn't affect of orders of magnitude the Seebeck coefficient if compared to the sample with one layer, even if the coefficient obtained now is the same of the pure aluminium, which underlines how the coherent layer of the aluminium makes the structure more similar to the one of two layers of different materials instead of a material resulting on the mix of two different species. In conclusion, the thermoelectric properties of the samples didn't improve with the change of the structure, with the shutter configuration that is the worse and needs further improvements. It is anyway useful to purify the powder from the aluminium if the final destination of use is different and needs a different raw material. Finally, it is important to focus on the sign of the Seebeck that is an evidence that the initial doping of the solar cell was n-type: in fact, without the aluminium that acts as a counter-doping the sign of the carriers measured is n-type. In the Al-bottom configuration the layer of aluminium is predominant, showing a positive sign of the main carriers even if the layer n-doped of silicon is always present.

The possibility of modifying the purified powder of silicon will be further discussed in the next chapters, because it is seen as a possibility to exploit in every possible way the recycled solar cell at its end of life.

3.2.4) I - V curves measurement

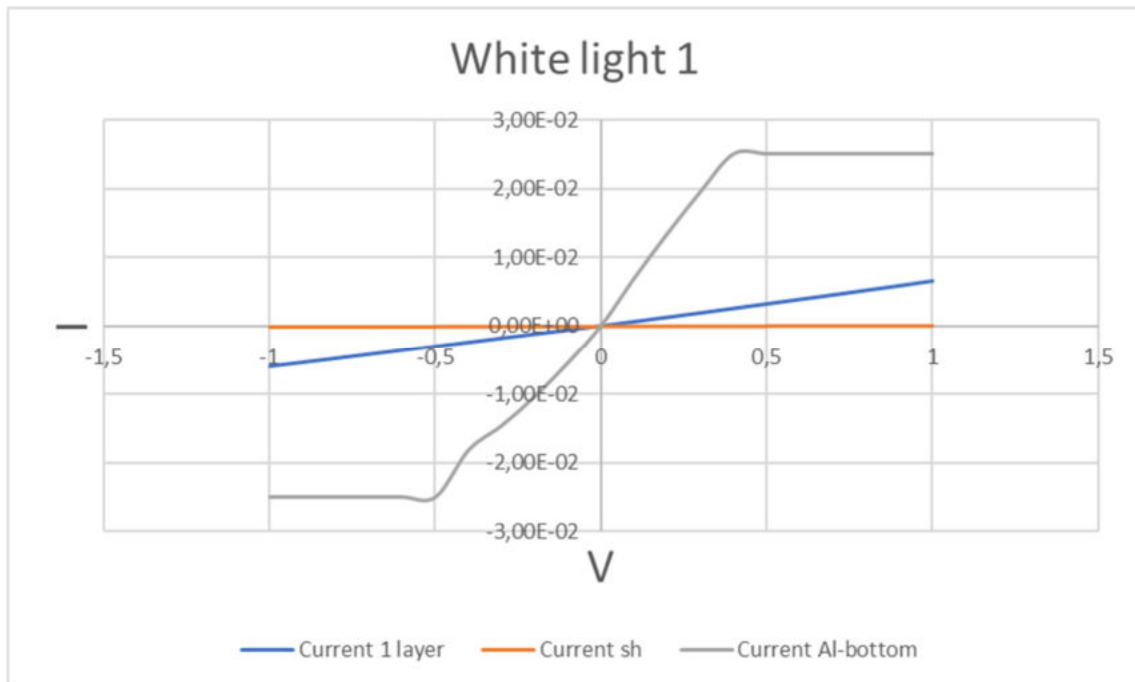


Fig 3.16 comparison I - V curves white light 1

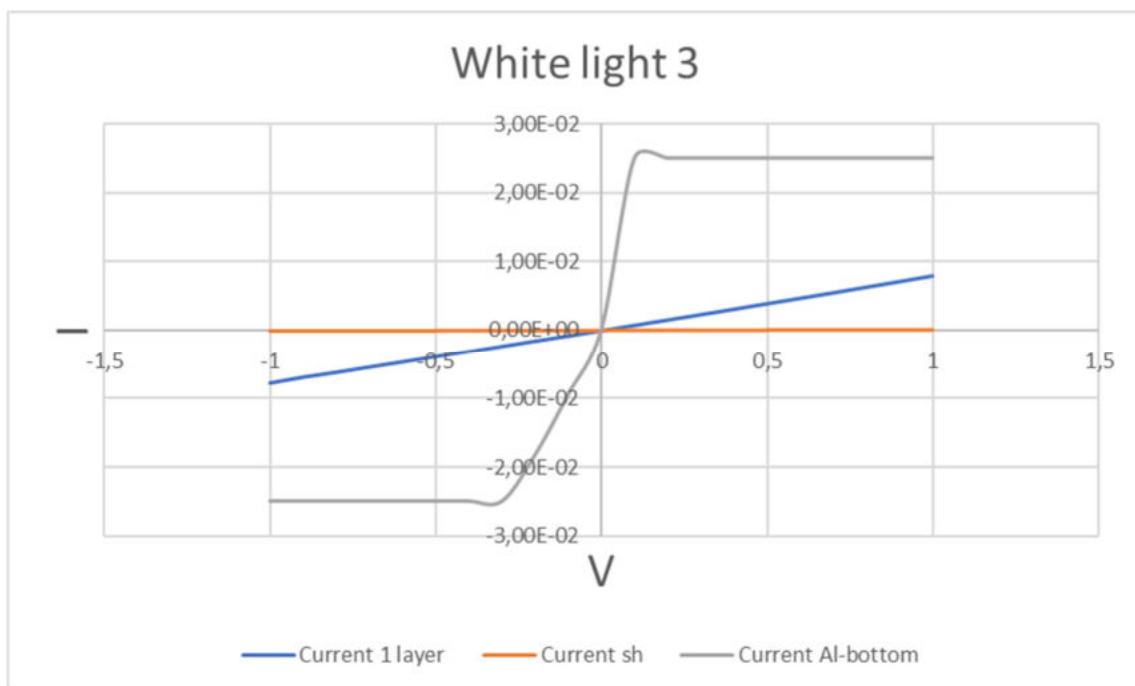


Fig 3.17 comparison I - V curves white light 3

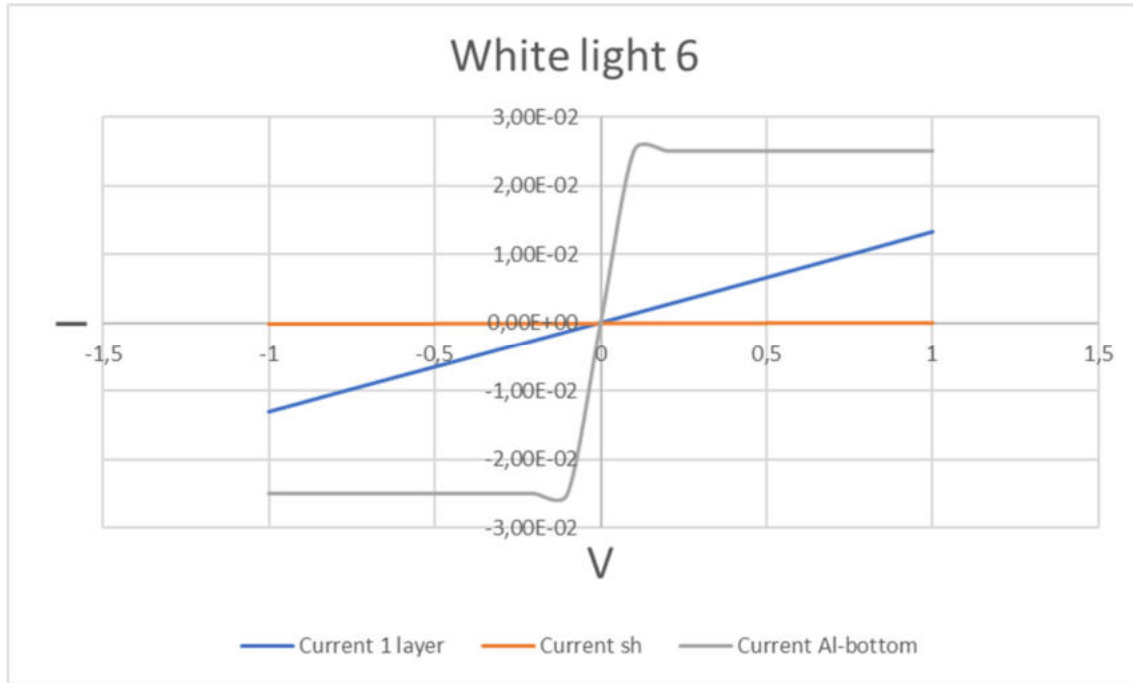


Fig 3.18 comparison I - V curves white light 6

In the I - V curves measurement is evident the presence of a metal contact on the bottom in the Al-bottom configuration. The current flowing in the sample is so high that reaches the limit of sensibility of the instrument, stated at $2,5 \times 10^{-2}$ A. The plateau of the curves is due to the limitation and not to a change of the shape of the curve, which should always be a line since is the characterization of a material and not of a more complex structure. The shutter curve seems flat, but it's just because the current detected is way lower compared to the others: In fact its order of magnitude is 10^{-7} A for all the lamps used, meaning that the doping effect of the aluminium is if not totally partially disappeared.

To understand if there is still some dopant in the crystalline structure the analysis on the hall effect will be essential, especially the bulk concentration detected.

The Al-bottom structure can definitely be used in some devices that needs a back electrode, maybe adding some raw metal to the deposition made with the recycled powder: it is indeed interesting to exploit even the metal present at the moment of the deposition in order to lower the environmental impact of the process.

3.2.5) Hall effect measurement

Shutter	Bulk concentration (cm ⁻³)	Mobility (cm ² /V*s)	Conductivity (S/cm)	Sign of the main carriers
1	5.31E+13	5.91E+00	1.68E+00	+
2	9.60E+13	1.03E+01	5.31E+00	-
3	2.89E+14	5.43E+00	8.41E+00	+
4	2.69E+14	7.81E+00	1.12E+01	+
5	3.72E+14	6.93E+00	1.37E+01	+

Table 3.3 Hall effect of the shutter sample

Al-bottom	Bulk concentration (cm ⁻³)	Mobility (cm ² /V*s)	Conductivity (S/cm)	Sign of the main carriers
1	1.98E+18	1.29E+01	4.12E+05	-
2	1.70E+18	1.51E+01	4.13E+05	-
3	1.63E+18	1.58E+01	4.13E+05	-
4	3.01E+18	8.58E+00	4.13E+05	+
5	2.54E+18	1.01E+01	4.13E+05	-

Table 3.4 Hall effect of the Al-bottom sample

The hall effect reveals that almost all the doping effect of the aluminium disappears in the shutter sample, with a bulk concentration between 10^{13} cm⁻³ and 10^{14} cm⁻³. Anyway, the intrinsic concentration of carriers at room temperature in silicon is of $1,08 \cdot 10^{10}$ cm⁻³ [94]. This is mainly due to the previous doping of the powder, although the sign of the carriers this time is opposite as the expected, with the concentration of the acceptors predominant on the concentration of the donors. This can be due to the nitrogen doping of the antireflection layer present in the initial powder, but if compared with the other elements present in the system the nitrogen is less relevant, although after the purification from the metal electrode its concentration in the sample is surely more significative, but another explanation is preferred to find a reason for the sign of the carriers which is opposite from the one expected. As mentioned before, the hall effect is not always accurate with the sign of the carriers, especially in less conductive samples such as the shutter sample. In effect, it was impossible to characterize the sample keeping the voltage between 50 and 100 mV, which results in an overestimation of the value of conductivity.

To have a more accurate measurement of the conductivity, the I - V curves were consulted: In particular, if the slope of the curve is constant such as in the case of the line, the ratio dI/dV is

the conductance of the sample, which means that the opposite is the resistance. It is possible to calculate the resistivity exploiting the geometry of the contacts used for the measurement of the I - V curves, which is possible to know from the geometry of the masks. It is therefore possible to use the second law of Ohm:

$$R = \rho * L/S$$

In which the length is the distance between the two contacts and the section can be calculated considering a rectangular section in which the side of the contact is the base and the height of the section is the thickness, estimated of approximately 200 nm (to consider the deposition of the contact but also the loss of aluminium in the powder).

The conductivity calculated is of $7,4*10^{-6}$ S/cm if exposed to the white light 6. The difference between this parameter and the one calculated with the hall effect is considerable, with the value calculated with the second method that is for sure more correct considering the system and the bulk concentration detected. In the Al-bottom sample, the bulk concentration is not higher than the sample of 1 layer with a value stable on 10^{18} cm⁻³ but the conductivity is way higher: this is due to the fact that the aluminium now is all in the back, creating a preferential lane for the carriers that can more freely flow in the sample through the coherent layer of the aluminium. The mobility of the carriers is higher in the shutter configuration, which is normal because the bulk concentration and the mobility are inversely proportional in semiconductors: the less carriers there are in the system, the more freedom of movement they have, until some extent: If it is certainly true that the mobility of the shutter sample and the Al-bottom sample is way higher if compared to the samples analysed in the previous chapter of the section, the gap between them is not high if considering the difference of carriers: there is a limit on the increase of the mobility due to the decrease of the carriers concentration [95].

3.2.6) Discussion of results

Although it cannot be used without further improvements, also the studies on the shutter sample are interesting: it is indeed possible to dope the silicon in order to regain the properties desired. However, one of the purpose of this study is to recycle the active layer of the solar cells in order to make them more environmentally friendly. Without forgetting the goal, the doping methods used for the recycled silicon must not involve the use of polluting or harmful chemicals, in order to keep the footprint low.

To do this, some other studies on possible alternatives to dope the samples can be used, focusing on two aspects: lowering the thermal budget and using the correct chemicals. For example, a spray coating using phosphoric acid can be used in order to obtain a doping of n-type without the using of dangerous chemicals, with the firing temperature that can vary from 880 °C to 940 °C according to the depth of the doping that we want to obtain [96].

The same spray system can be used with boric acid if the doping that we want to obtain is of p-type, keeping an eye open on some particularities such as the absence of oxygen that is

detrimental to the performance of the device [97]. For this doping, the firing temperature is a bit higher, between 900 °C and 1100 °C which is harmful for the thermal budget and can damage the environment in an indirect way [97].

Another easy going technique that can be used is the dipping method using phosphoric acid or boric acid [98], which would obtain a similar result as the one obtained with the spray coating method. Lastly, there is also the possibility to dope the silicon at temperatures of annealing, saving thus time because one of the steps is deleted and using way less energy, using temperatures of 560 °C in a furnace [99], or a low temperature CVD process at 550 °C to dope for example with boron [100].

3.3) P-N junction

In the last chapter of the section, the discussion about the performance and the characteristics of a simple device constituted by a p-n junction will be done. It has already been established that our monolayer of recycled powder from the active layer of the solar cell is a semiconductor of n-type, although the system is really complex and a lot of doping and counter-doping happens in the crystalline structure of the main component (the silicon) during the deposition. To be sure about the doping of the layer, other two measurement on the sign of the Seebeck coefficient were performed: the first sample had a result of $-7,7 \cdot 10^{-4}$ mV/K while the second one had a Seebeck coefficient of $-2 \cdot 10^{-3}$ mV/K, which is a bit higher, showing that the depositions are not completely uniform due to the technique used and the raw material used which can have slight changes in the composition from time to time. Anyway, all the samples showed a negative sign in the coefficient, which is a direct proof of the n-type doping in the samples.

The need of a material p-type to couple with the recycled layer in order to form a junction let us explore many possibilities: theoretically it is possible to use as a p-type layer the sample with three layers of recycled powder, since it has been shown how the bigger influence of the p-type doping due to the electrode made of aluminium created an inversion on the sign of the carriers: although it is indeed possible in a theoretical way, the final result is not given for granted: furthermore, the total of four different depositions just to have one sample to characterize is seen as a waste of time, also considering that the characterization need other depositions such as the metal contacts at the end.

The other factor to watch in order to choose the correct material for the coupling is the performance obtained in the previous chapters of the section: in order to build an effective p-n junction, it is better to strengthen the weakest points of the material that are known to be its thermoelectric properties (it has been shown how the Seebeck coefficient of the samples make not them suitable for thermoelectric applications) and the photo-sensing properties (for the same reason of before, the order of magnitude of the voltage fulfilled is not high enough). The materials that guarantee all these properties are the copper oxides, which are divided in three

types: The Cu_4O_3 , also known as paramelaconite, that has a body centred tetragonal crystalline structure but unfortunately is too difficult to synthesize in a stable way [101]. The other two oxides are the ones used in the building of the p-n junctions of this study, with the cuprous oxide (Cu_2O), also known as cuprite [101], which is composed of a body centred cubic crystalline structure for the oxygen ions and a face centred crystalline structure for the copper ions, with a direct band gap of 2,17 eV [102]. The other one is the cupric oxide (CuO), also known as tenorite [101], which has a monoclinic crystalline structure and an indirect band gap of approximately 1,35 eV [102].

Both the cuprous and the cupric oxides are naturally p-type semiconductors, with the carriers mobility due to the impurities of the lattice: in fact, the cation vacancies are the ones exploited for the carriers diffusion in both the materials [101].

The various applications of the oxides have been studied since the 20's, and nowadays comprehend solar cells [102], rectifiers [102], thin film transistors [101] and photosensors [101] with many others. Some solar cell devices have already been studied in other papers, such as the coupling of the oxides with GaN and ZnO [101], in which it has been shown that both performances were satisfying although the coupling with GaN gave better results, other studies comprehended the coupling of the CuO with the fullerene (C_{60}) with an electrode made of ITO [103], which provided a short circuit current density of 0,18 mA/cm^2 and an open circuit voltage of 0,04 V [103]. With the cuprous oxides is reported also an use with the cadmium oxide [104], along with the ZnO mentioned before. The advantages of copper oxides devices rely on their multiple ways of being synthesized, which vary from thermal oxidation to anodic oxidation, sputtering, CVD and electrodeposition [104].

Because of these several studies, and because of the full characterization and synthesis completed by [105], the choice to build the p-n junction using copper oxides is now clear: however before describing the deposition and characterization of the junction it is fundamental to understand the working principle hidden behind it.

The semiconductor doped p has more positive carriers, named holes while the semiconductor doped n has more negative carriers, named electrons [106]. When they are coupled, because of diffusional flow negative carriers go on the positive side and positive carriers go on the negative side: while they flow, the charge accumulated in both sides start to generate an electric field until the electric force generated through this field stop the motion due to diffusion mechanisms [106]. In the depletion region generated because of the electric field the mobility of both electrons and holes is very low, but it is possible to modify the resistance of the region applying an external electric field, thus generating again a flow of carriers (current): if a positive voltage is applied to the p side and a negative voltage to the n side we are in the forward biased configuration and the current can flow until it reaches a maximum value, which will depend on the voltage: the depletion region starts to become thinner and thinner until a value of voltage for which it becomes neglectable, with the current that can flow virtually free: this value is 0,6 V for silicon [106].

In the reverse bias configuration the passage of the current is obstructed by applying a negative voltage on the p side and a positive voltage on the n side: this is true until the reaching of the breakdown voltage, which is the negative voltage for which the current start to flow again [106]. This phenomena give rise to the typical $I-V$ curve of the p-n junction, shown in [106]: in the characterization the building of a curve of similar shape will be crucial.

3.3.1) Deposition

The need for more steps make the preparation of the samples longer if compared to the ones of the previous sections: furthermore, not just the thermal evaporator or the sputtering have been used because for the synthesis of the copper oxides the technique used was the thermal oxidation through the use of an annealing oven in air, after the initial deposition of metallic copper on a substrate made by corning glass with ITO sputtered as the back electrode. After covering with the high temperature resistive tape enough ITO in order to use it as a contact in the measurements that would have followed the deposition, the current reached in the thermal evaporator in order to deposit the copper is approximately 205 A, which is intermediate between the aluminium and the recycled powder: in effect, the boiling temperature of copper is between the one of aluminium and the one of silicon, which is the main constituent of the powder. Furthermore, it has already been studied that in order to obtain thin films of pure cupric oxide or cuprous oxide, the temperature to be used is 375 °C for the first one and 225 °C for the second one [104], for at least one hour [104]. The molecular structures have already been identified in the same study through the use of an XRD measurement, for samples of thickness of 50 nm and 110 nm [104]. As mentioned in [101], the technique used to synthesize the samples, thermal oxidation, will give rise to samples that are rougher on a nanometric level, and a part of the light in the optical measurements will be scattered due to this [101]. The thinner samples were less conductive, with the conductivity decreasing from $2,9 \cdot 10^{-2}$ S/cm to $2 \cdot 10^{-4}$ S/cm. For this reason and to have a junction with both n layer and p layer of the same thickness the copper deposited formed a layer of round 150 nm.

The Seebeck coefficient of both the copper oxides is very high, with values higher than 1 mV/K [104], while the bulk concentration arrived up to 10^{16} cm⁻³ [104] with the mobility stable around 4,1 cm²/V*s [104].

After the deposition of the copper and the transformation into copper oxides in the annealing oven, a monolayer of recycled powder is added through thermal evaporation and then aluminium contacts are added using the polymeric masks in order to be used as front contacts, with the back contact made of ITO.

In fig 3.19 is demonstrated how the difference between the samples made by cuprous oxide as the p-layer and the samples made by cupric oxide as the p-layer is visible also with empirical evidence: the first ones assume a greener colour while the latter ones are darker, assuming a blue tonality.



Fig 3.19 a p-n junction made using CuO (on the left) and using Cu₂O (on the right)

3.3.2) Spectrophotometer

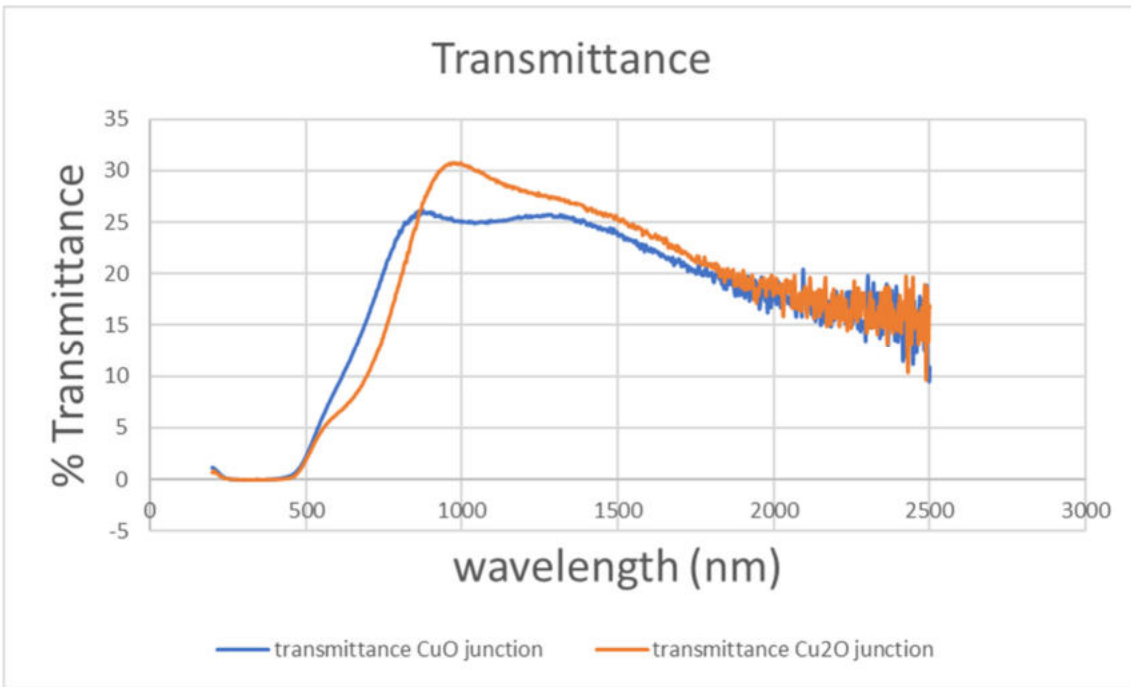


Fig 3.20 transmittance of the junctions

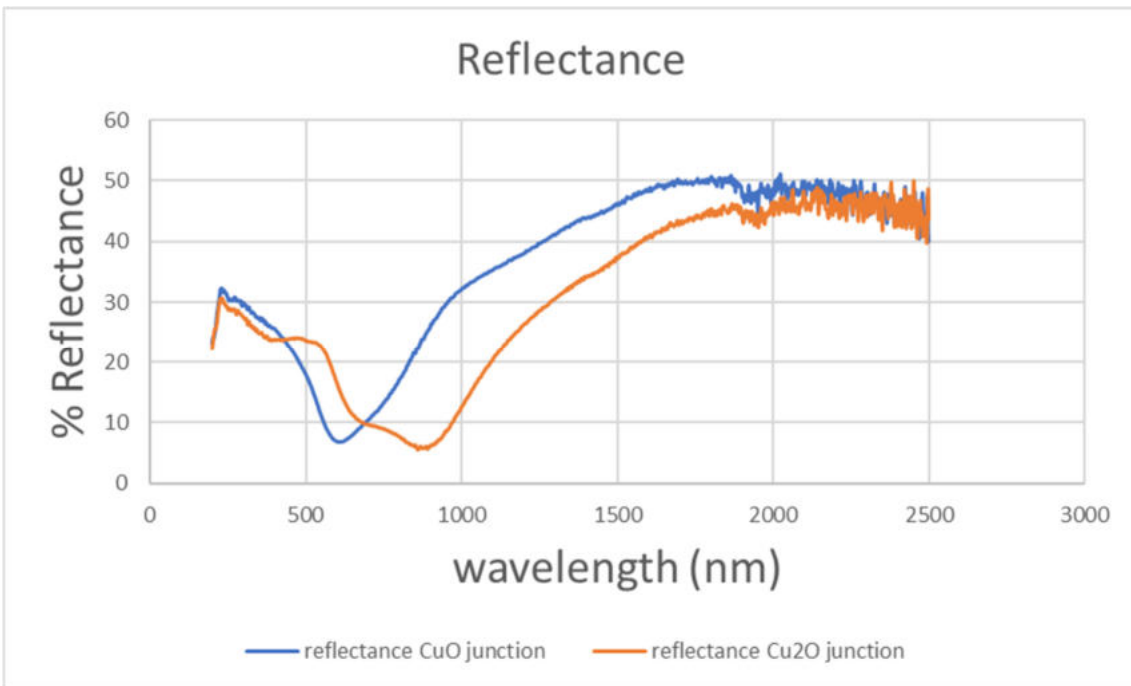


Fig 3.21 reflectance of the junctions

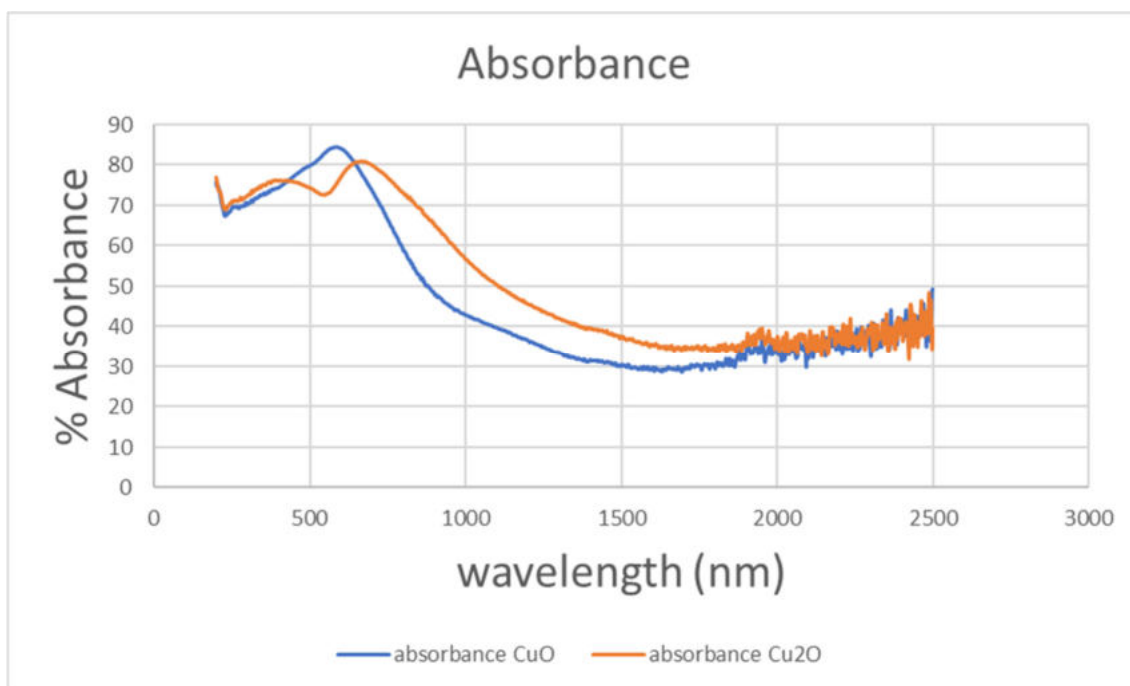


Fig 3.22 absorbance of the junctions

The analysis of the spectrophotometer shows that the optical spectra of the junction are different compared from the ones of the samples studied before, because of the presence of the copper oxide: the first thing to notice is that the peak of absorption is at 600 nm for the junction with CuO and at 680 nm for the junction with Cu₂O, which are both in the range of visible light unlike the samples of simple recycled powder, which had a peak in the near UV.

The curves are really similar with some exceptions: the cuprous oxide absorbs a bit more in the infrared, because of its lower bandgap, while the cupric oxide absorbs more in the visible range: for photovoltaic applications should be better to exploit the cupric oxide, since the majority of the light flux is in the visible range. All this data have to be read keeping in mind that this is a junction, so also the monolayer of recycled powder is present in the system.

The other peculiarity of the curves can be read analysing the transmittance and the reflectance curves of both the junctions: the transmittance of the cuprous oxide is higher, while the reflectance of the cupric oxide is higher: this is due to the different stoichiometry of oxygen and copper present in the materials: where more copper, which is a shining metal, is present, the reflection of light must be higher, like in the samples which had a coherent layer of aluminium on the bottom. In the samples which have more oxygen in the crystalline structure on the contrary, the quantity of light transmitted to the detector is higher. These effects are balanced in percentage, which means that the final optical performance in terms of absorbed light is pretty much the same, but at this point is not known if the light absorbed will result in a generation of carriers or would be just dissipated in the system through several mechanisms: this will be confirmed with the next step of the characterization.

3.3.3) Seebeck and voltage measurement

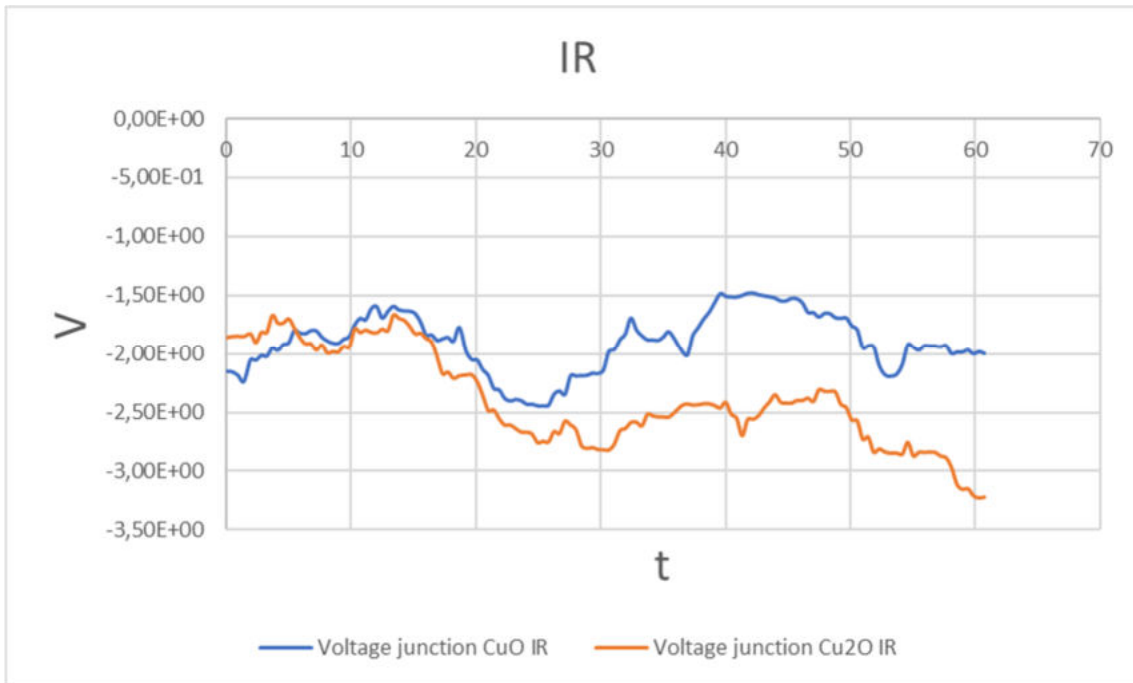


Fig 3.23 $V-t$ curves of the junctions for IR light

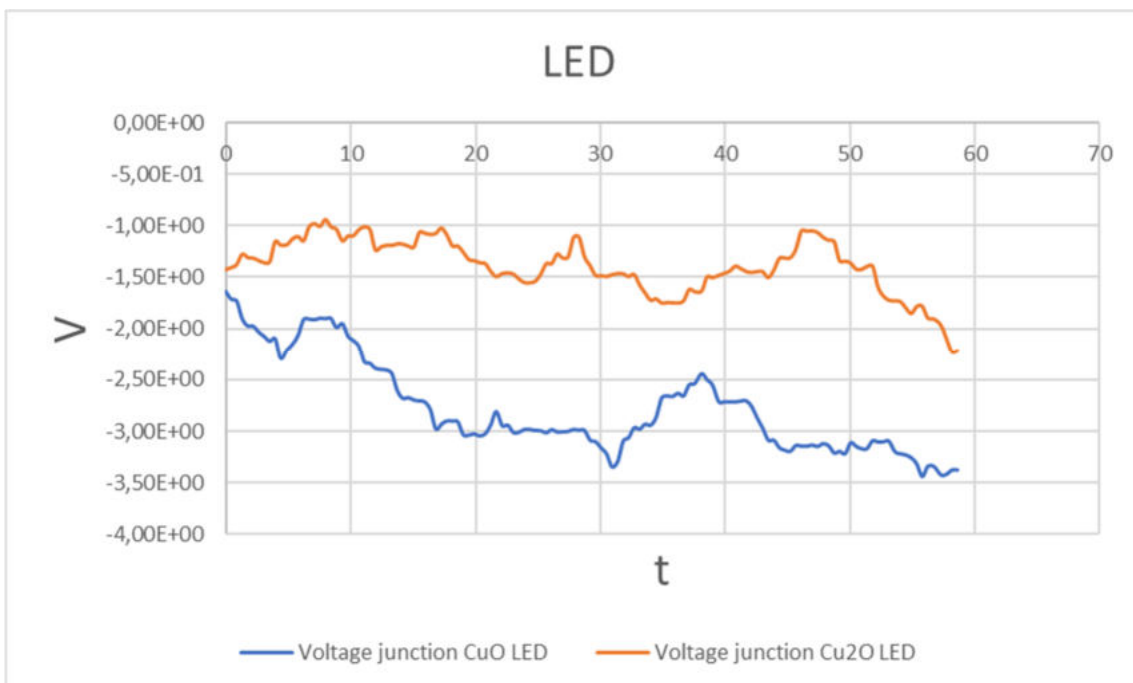


Fig 3.24 $V-t$ curves of the junctions for LED light

The voltage-time curves are the next step of the characterization of the junctions, showing good results: this time the voltage is between 1 and 2,5 V, and thus can be used for photo-sensing applications as it was mentioned before and it will be further discussed later.

In particular, the response was higher when the samples were exposed to the infrared light if compared to the LED light, with a peak of -3 V.

It has to be underlined that the sign of the curve doesn't have a specific purpose also in the case of the p-n junctions: the parameter to see is the gap with the zero, that gives information about the photo-sensing capabilities of the samples.

Since now the contacts are one in the back and the other one on top of the sample's surface, for the measurement of the Seebeck coefficient is now essential to take the measurements in both planar configuration and vertical configuration, which can be slightly different because of the different flows of the carriers in the setups: in the planar configuration it is highlighted the influence of the surface layer, which is made with the monolayer of recycled silicon powder, while in the vertical configuration the carriers flow from the bottom electrode to the top one, making easier to understand the behaviour of the junction in the complex.

The Seebeck coefficient of the samples for the planar configuration is -0,019 mV/K for the junction made with cupric oxide and -0,009 mV/K for the junction made with cuprous oxide, meaning that for thermoelectric applications the first junction would be more adapt, although the values are not high enough for commercial applications and necessitate further improvements.

For the vertical gradient configuration, the values registered are 0,025 mV/K for the junction made with cupric oxide and 0,02 mV/K for the junction made with cuprous oxide.

The results are higher than the ones obtained for the planar configuration, which means that the thermoelectric materials in these p-n junctions are the copper oxides: not a surprise, since the coupling with n-doped silicon has been chosen for this purpose along with other reasons.

The resistance of the junctions has been also measured before proceeding with further analysis, exploiting the voltmeter of the experimental setup of the Seebeck measurement: The ITO alone provides a resistance of 400 Ω , meaning that the back electrode used for the building of the junctions is high resistive, conditioning the results obtained. The junction with CuO has a resistance of 700 Ω , while the junction with Cu₂O has a resistance of 750 Ω .

The sign of the Seebeck coefficient show that the copper oxides are the main source of carriers in the vertical configuration, while the n-type carriers are predominant in the planar configuration, which is as expected.

3.3.4) I - V curves measurement



Fig 3.25 I - V curves of the junctions white light 1

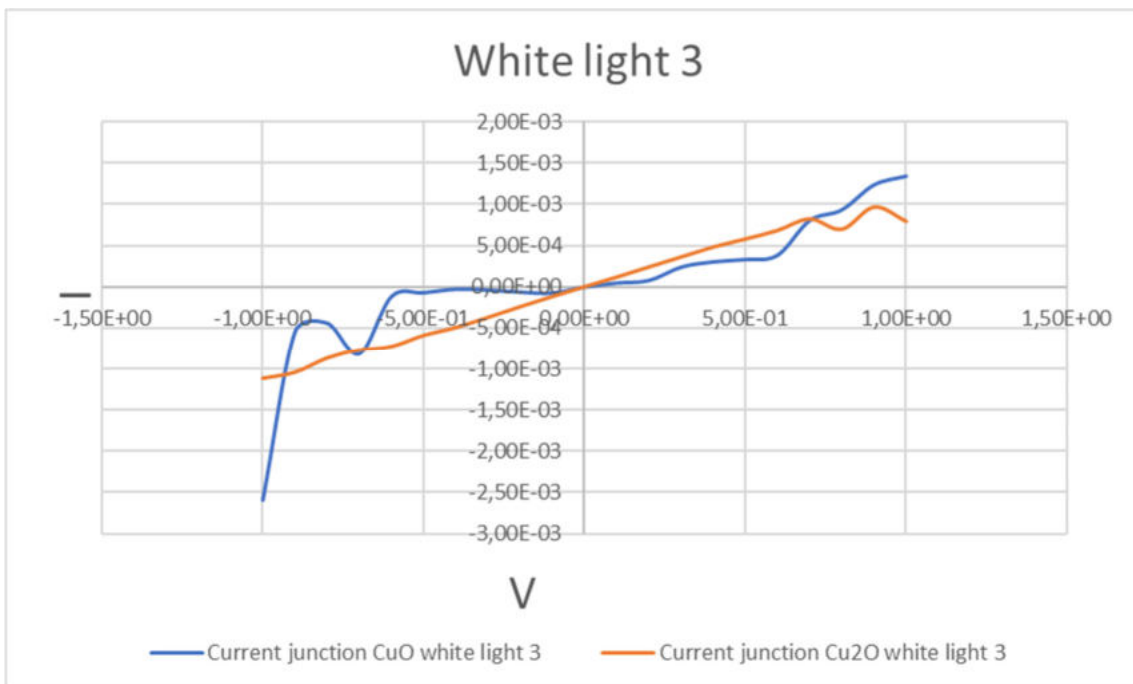


Fig 3.26 I - V curves of the junctions white light 3



Fig 3.27 I - V curves of the junctions white light 6

The I - V curves of the junctions for several intensities of the LED lamp show a shape that is similar to the one described before when talking about the understanding of the p-n junctions: the positive tract of the graph has a linear shape, while in the reverse bias the current is prevented from flowing partially or totally: it has to be said that the most accurate results are obtained for the junction with CuO that in the reverse bias mode stop the current totally from flowing: although this is true, it is not known if it's just because of the performance of the cell or because of the deposition effected with the thermal evaporator that were performed better, giving birth to samples with less defects.

The maximum current registered is very similar even if the light changes of intensity, meaning that the samples are not so sensitive to the change of irradiance or they already registered the maximum value of current allowable for 1 V applied, which is $1,25 \cdot 10^{-3}$ A for the junction with CuO and $1 \cdot 10^{-3}$ A for the junction made with Cu₂O, although in the second case the maximum current is reached in correspondence of white light 3, of 370 W/m^2 .

Although these values are a bit lower if compared to the ones of various silicon solar cells described in the first chapter of this section, it is impossible to forget that this junction is made with a recycled material and one of the cheapest and most easy going oxides present in circulation: with these premises, the values presented are more than competitive. In the chapter about the discussion of results there will be some other examples regarding other I - V curves of p-n junctions studied in other studies.

3.3.5) Hall effect measurement

Cuo junction	Bulk concentration (cm ⁻³)	Mobility (cm ² /V*s)	Conductivity (S/cm)	Sign of the main carriers
1	3.02E+16	4.12E+0	6.84E+2	-
2	1.04E+16	1.19E+1	2.18E+2	-
3	1.72E+17	7.22E+0	1.82E+2	+
4	3.60E+16	3.46E+0	1.21E+2	-
5	2.97E+16	4.20E+1	2.15E+2	-

Table 3.5 Hall effect of junction with CuO

Cu ₂ O junction	Bulk concentration (cm ⁻³)	Mobility (cm ² /V*s)	Conductivity (S/cm)	Sign of the main carriers
1	6.02E+16	2.07E+0	6.09E+2	-
2	1.44E+16	8.63E+1	1.56E+2	-
3	2.03E+16	6.12E+1	2.36E+2	+
4	2.03E+16	6.14E+0	4.29E+2	-
5	1.20E+17	1.03E+1	1.08E+2	-

Table 3.6 Hall effect of junction with Cu₂O

The tables 3.5 and 3.6 show little dispersion of results, with values that are not just similar within the same table but also if the two samples are compared. The bulk concentration is lower than the one of the monolayer of recycled powder just because of the recombination happening in the depletion zone of the p-n junction, while the mobility is lower than the one described in analysing the copper oxides samples in [105] probably because of interfacial tensions between the layer of copper oxide and the layer of silicon, which reduce indeed the mobility of the carriers, but not a lot: in fact, the presence of a depletion region that reduce the concentration of the carriers positively impacts the mobility of the carriers itself, which usually has an inverse relation with it. The sign of the carriers is mostly negative, meaning that also this time the n-type nature of the recycled powder wins over the p-type conduction of the oxides, probably because of the higher concentration of the carriers that are present in the silicon layer and make a statement on the predominant sign of the junction, although is also relevant the presence of free metals in the n layer which strongly influence the predominance of electrons carriers over hole carriers. The conductivity is very similar for both the junction with CuO and the junction with the cuprous oxide, which means that this parameter wasn't influenced by the efficiency and the final outcome of the deposition, guaranteeing an

agreement with the literature review: apparently, as reported in [105], there shouldn't be this big difference between the conductivity of cuprous oxide and conductivity of cupric oxide, with similar results that can be obtained with the characterization of other samples. Considering the bulk concentration of both samples, the junctions can be suitable for a solar cell device if it is considered that a concentration of 10^{18} cm^{-3} carriers is seen as a p+ or n+ doping [86], [87]. Anyway, further improvements such as another dopant source for the layer of the recycled powder or an annealing process in a vacuum oven can indeed be useful in order to improve the parameters of the device and guarantee an optimum of the performance. Also the partner of the studied layer can change, with a huge variety of p-type materials existing under the shape of thin films that can be adapted in order to build more performant junctions.

Finally, it is important that when the source is a waste that has to be recycled, the final outcome can be different from time to time and an hypothetic industrial scale up must always be coupled with a lab that characterize the raw material with the instruments used in this work and with others, such as XRD and SEM images. It is indeed possible to find a layer of p-type after the deposition of recycled powder which comes from other end of life silicon panels, and in that case it would be necessary to couple the material with an n-type semiconductor such as ZnO if the final purpose is to build a p-n junction.

3.3.6) Discussion of results

This discussion of results will be exploited to compare the junction with other junctions and materials analysed and characterized in other works. In fact, to understand properly the p-n junction built in this work and if recycled silicon from solar cells can effectively be used in the construction of some devices, it can be useful to compare it with other innovative papers related to the same field. The comparison will be done with other semiconductors and not with silicon, which has already been analysed in the first paragraphs of this section. The mobility is indeed the weakest point of this work: carbon nanotubes synthesized for transistor applications have an intrinsic mobility of $10^5 \text{ cm}^2/\text{V}\cdot\text{s}$ [107], although this is a record also for the world of semiconductors used for transistors application: furthermore, it was stated from the beginning that the purity and the efficiency of the recycled semiconductors from solar cells was indeed not enough to think about transistor applications (even the virgin material cannot guarantee these results). Analysing the world of semiconductors for solar cells and photosensitive applications the recycled material and the junction built with it are more interesting: the electron mobility of some 2-6 semiconductors is very near to the one of the p-n junctions analysed in this work, with the mobility of CdS and CdSe which is, respectively, $5 \cdot 10^2 \text{ cm}^2/\text{V}\cdot\text{s}$ [108] and $7 \cdot 10^2 \text{ cm}^2/\text{V}\cdot\text{s}$ [108], with the data read for room temperature (never forget that electron and hole mobility are inversely proportional by a strong factor from the temperature), while the electron mobility of CdTe is around $10^3 \text{ cm}^2/\text{V}\cdot\text{s}$ [108]. For other

semiconductors, the trend is similar: from $400 \text{ cm}^2/\text{V}\cdot\text{s}$ for the hole mobility in GaAs [109] to $1600 \text{ cm}^2/\text{V}\cdot\text{s}$ for germanium [109] and $200 \text{ cm}^2/\text{V}\cdot\text{s}$ for InP [109], just an order of magnitude more than the junctions built with copper oxides. Regarding the conductivity, the results are higher compared to other semiconductors of different kinds because of the percentage of free metals present in the samples: the intrinsic germanium has a conductivity very similar to the intrinsic silicon, with a value around $1,67 \cdot 10^{-2} \text{ S/cm}$ [110].

What about the organic semiconductors for the third generation solar cells? In this case is really difficult to find a stable value even in the same class of organic molecules: for example, the conductivity of phtalocyanine metal-free or containing metals of various nature varies from 10^{-2} S/cm to 10^2 S/cm [111], while other specimens like pyrene or anthracene exhibited a conductivity which way lower than the conductivity of the junctions with copper oxides, with values which are orders of magnitude lower than 10^{-10} S/cm [111].

The devices built in other works show values which are in line with the values of this work: a ZnO homojunction photovoltaic device which can be suitable for diodes and UV sensing applications, shows in the I - V curves values of 10^{-5} A [112], lower than the maximum current of the copper oxides junctions: furthermore, the V - t curves demonstrate that to have sensing skills it is enough to exhibit a voltage of $0,2 \text{ V}$ [112] under illumination conditions.

Also a CdS/Se heterojunction, considered an high performance photodetector for UV and visible light shows values of I - V curve and V - t curve which are in trend with the value of the junction, with the current of the I - V curve around 10^{-4} A [113] and voltage of $0,8 \text{ V}$ [113].

The absorption spectra in the same work shows peak of 80% of absorbance in the visible range [113], which is similar to the one of the junctions with copper oxides.

A junction with p-CuO/n-Si manufactured on glass was studied in another work, showing an I - V curve in which the current of the diode has the same trend of this study [114], which means that the recycled material behaves not differently if compared to the virgin silicon: this ensures the quality of the junction with a greener approach. Although the free metals present in the junction enhance the conductivity, their presence also damage the performance of the device in some ways: in fact, the absorption spectra of a p-GaN/n-SnO₂ junction is reported in [115], showing a gap of around 10% of absorption in visible and near UV range: since the other performances of I - V and V - t curves are superior in the copper oxides and recycled silicon junctions, the lack of absorption is certainly due to the reflection caused by the metals of the samples, which can also be seen in the curves of reflectance itself: in effect, the shape of the reflectance curve is similar to the shape of a thin film of simple aluminium made for comparison in the lab, with aluminium being the most present free metal of the system.

This section can be concluded stating that the overall performances of both the junctions are satisfying if compared to other experimental studies independent: the work which can be done to improve the junctions must effect the absorbance and the semiconductor mobility.

4) Conclusions

The final section is related to some conclusive considerations which can help the reader to focus on the importance of this work from the point of view of sustainability: although renewable energies are one of the best alternatives available on the market, they bring with them some issues related not just to their manufacturing phases but also if the end of life footprint is considered: to analyse properly these aspects it is essential to define some important parameters regarding the economic and environmental aspects of renewables, photovoltaic panels in this specific case. Following this, some final considerations about the state of art and the future of this work will be made, in order to make the future devices designed with recycled material from the active silicon layer of the panel more and more efficient and sustainable, trying always to set the bar for the overall energetic, economic and carbon footprint lower and lower.

4.1) Energetic and economic considerations

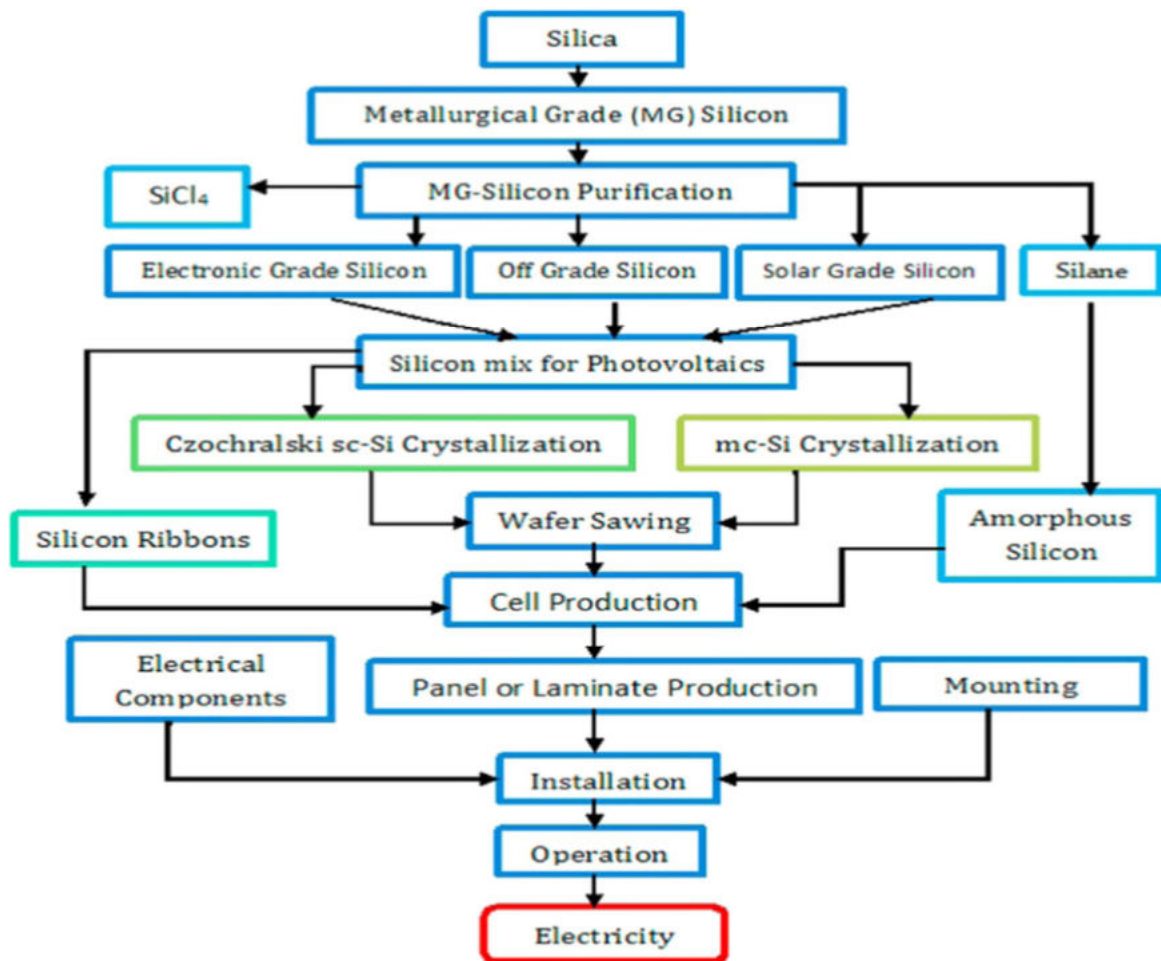


Fig 4.1 Life stages of a silicon PV module [115]

As shown in fig 4.1 the steps that involve an energetic, economic and environmental footprint in the life of a silicon PV are quite a lot: from the manufacturing steps involving the transformation of silica into silicon of a certain purity, to the Czochralski crystallization process, not to mention the manufacturing processes for the electrical components and the laminate production: after that, the installation of the system is required with a certain maintenance to ensure the quality [115].

The cumulative energy demand for the solar panel is the sum of five contributes [115]:

- Energy required for the production of the raw materials
- Energy required for the manufacturing processes
- Energy required for the transportation of materials
- Energy required for installing the system
- Energy required for the end of life management

Although many of them are fixed energy costs the end of life costs are the most flexible ones, with the improvement of silicon recycling processes making the EoL management always more efficient.

Totally, the energy requirement varies from 1034 MJ/m² to 5150 MJ/m² for multicrystalline solar panels [115] and from 1123 MJ/m² to 8050 MJ/m² for monocrystalline solar panels [115], while for amorphous silicon solar panels the energy requirement is way lower, varying from 862 to 1731 MJ/m² [115], without forgetting that also their efficiency is lower, which means that the energy payback time can be higher. Their EPBT are shown in [115], varying from 1 to 3 years. If we consider that a silicon PV panel has a lifetime varying from 20 to 30 years, the investment is for sure convenient from an energetic point of view although the energetic footprint is not low.

The economic payback time is analysed in [116], through a study involving several solar panels technologies used in Greece, with results shown in table 4.1:

Material of PV	Annual revenue (€/year)	Payback time (years)
Sc-Si	542	10
Mc-Si	542	9,3
CIS	531	9,6
a-Si	572	8,8

Table 4.1 Comparison of economic payback time for common PV materials [116]

For the same considerations about the lifetime of solar panels done before, also from an economic point of view is profitable the installation of photovoltaic systems, with the recycling processes that can be done to lower the cost of manufacturing processes an increase the revenue for both the producer and the user.

The fact that the systems were installed in Greece is relevant because the electricity that can be produced for both personal use and to be sold in the national grid strongly varies from the place of the world where the installation is made: The availability of the sun is indeed not the same in every place of the world [116].

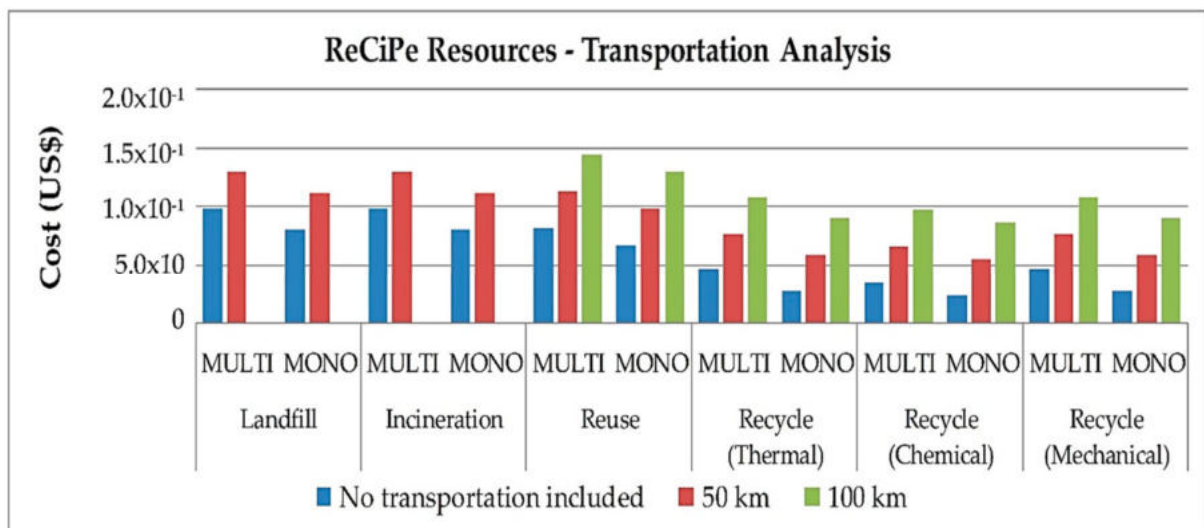


Fig 4.2 Comparison of costs for different EoL scenarios [117]

To conclude the paragraph, the analysis of the costs of different end of life management is reported: the data are analysed for six different scenarios: the simple landfill of the waste, the incineration of the waste in order to recover some of the energetic content, the reuse of the wastes contained in the wastes for several applications, the thermal recycle of the wastes, the chemical recycle of the wastes and the mechanical recycle of the wastes.

The analysis was conducted considering no transportation, 50 km of transportation and 100 km of transportation: indeed, the energy consumption related to the means of transportation increases the economic footprint of every waste management scenario.

By the way, indeed the most efficient processes from an economic perspective are the ones which include the recycling of the materials used during the lifetime of the solar system: the most efficient one is the chemical recycling, but the thermal and the mechanical recycling have an environmental benefit because no leaching processes are involved for the accomplishment of the final result. It is important to underline that not just the kilometers impact the final cost, but also the mean of transportation (land, air, water) [117].

4.2) Environmental considerations

Although solar panels are surely one of the possible paths to follow in order to decarbonize several industries and produce clean electricity, there is indeed an environmental impact to understand and limit during the production of the photovoltaic panel itself.

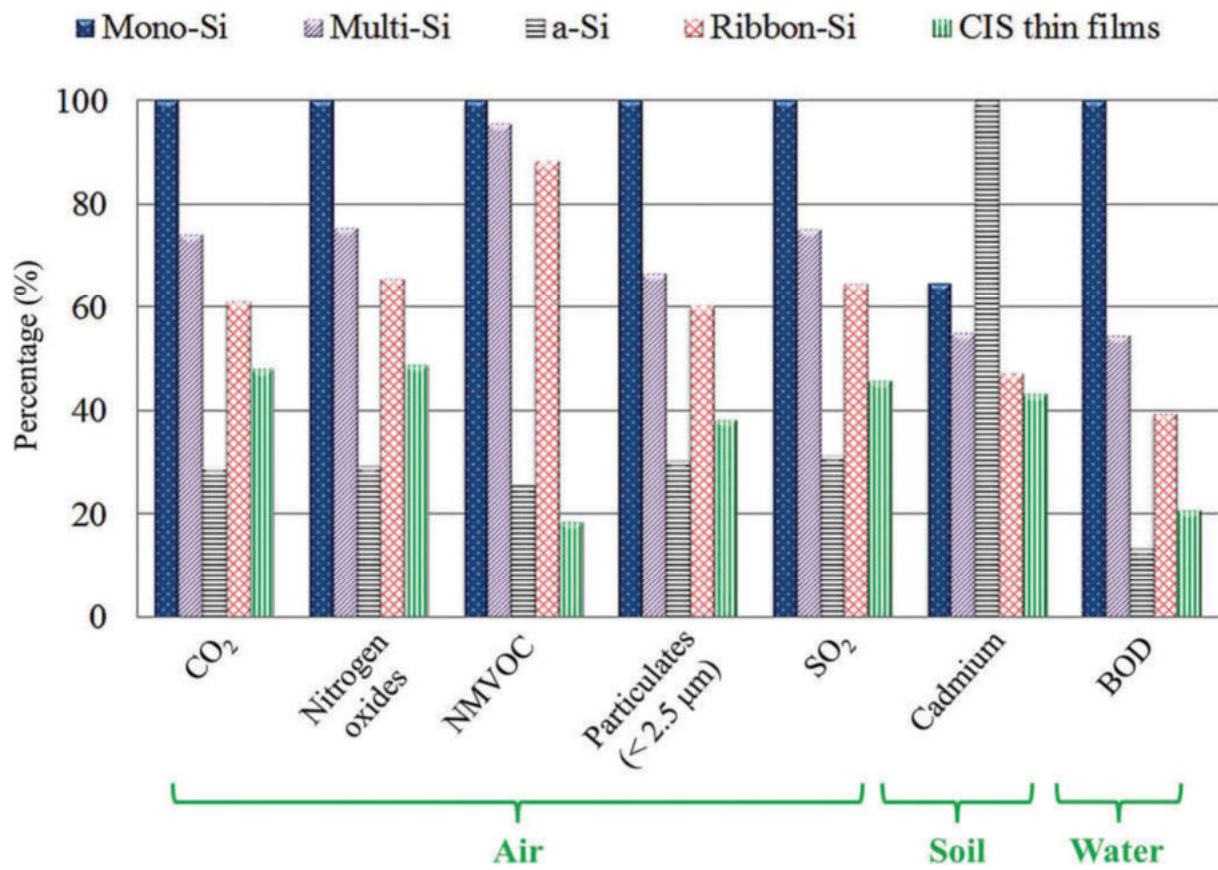


Fig 4.3 by-products of the manufacturing of several PV devices [118]

In fig 4.3 is shown the comparison between several materials for photovoltaic applications using percentage indicators: 100% is the maximum emission that is made during the manufacturing process. The monocrystalline silicon is the worst in terms of emissions, with the highest percentage of all the greenhouse and toxic gases such as SO₂, NO_x, CO₂ and even solid particulates [118]. The amorphous silicon is the worst just in terms of cadmium, which is a toxic metal: by the way, is the most performant in terms of greenhouse gases. Overall, the thin film technology is the most convenient from an environmental point of view, confirming the advantages of using easy-going technologies sacrificing the efficiency of the crystalline silicon.

The overall impact score of the various generations of solar panels is shown in fig 4.4, which strongly varies moving from the first generation to the third generation.

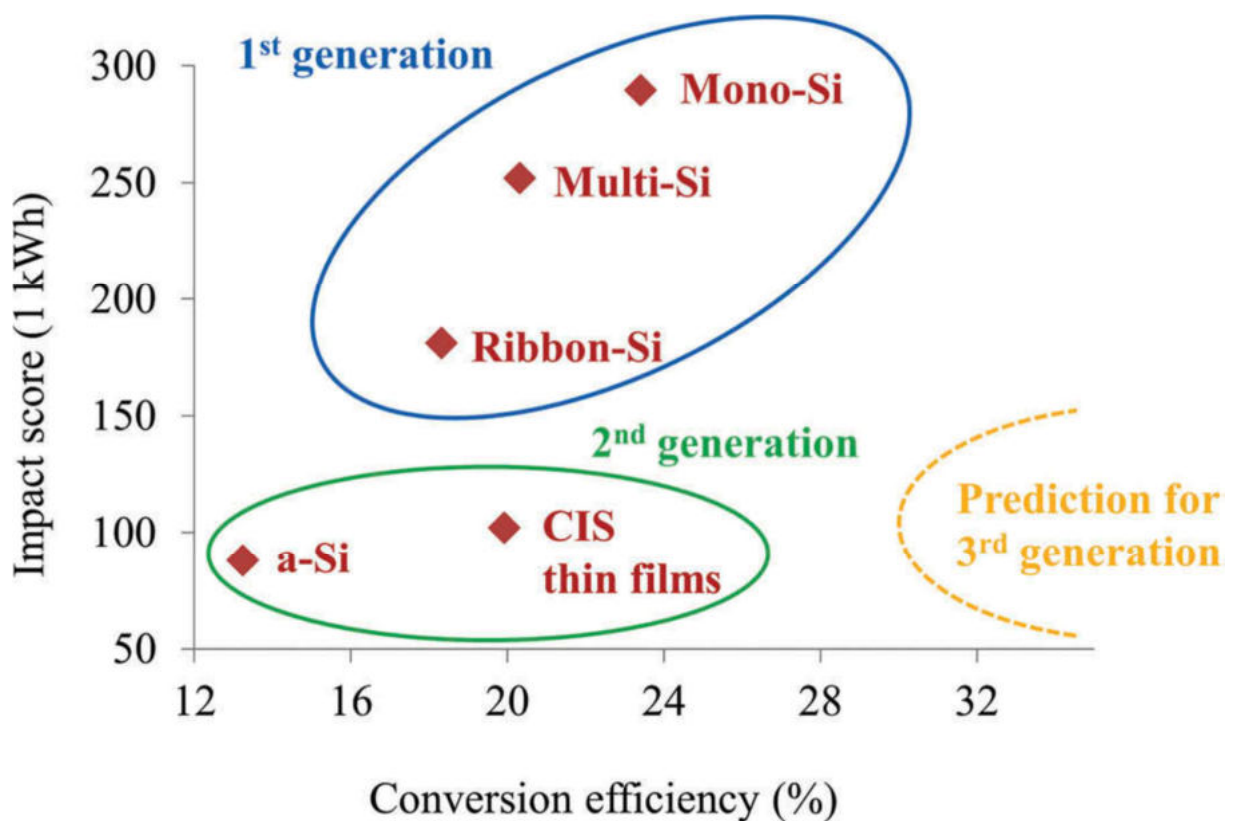


Fig 4.4 Impact score of the generations compared with the conversion efficiencies [118]

The impact score of the second generation solar panels is lower compared to the first generation solar cells, but the conversion efficiency will never reach the efficiencies of the best crystalline silicon solar cells, which is the main reason below the development of third generation technologies: with the best perspectives a conversion efficiency of 32% will be granted through the use of perovskite solar panels or improving the efficiency of the other technologies described in the introduction section, guaranteeing still a lower impact score if compared with the first generation solar cells [118].

Finally, after the analysis of the impact of the active layer, which is the core of the photovoltaic technology, the last thing to understand is the environmental impact of the whole system: in effect, apart from the solar panel other constituents are needed in order to ensure the energetic performance of the photovoltaic system, such as the converter, the battery, the cables, the breaker, the power-meter and the inverter [119].

The graph reporting the greenhouse impact of the various devices that compose the photovoltaic system is shown in fig 4.5:

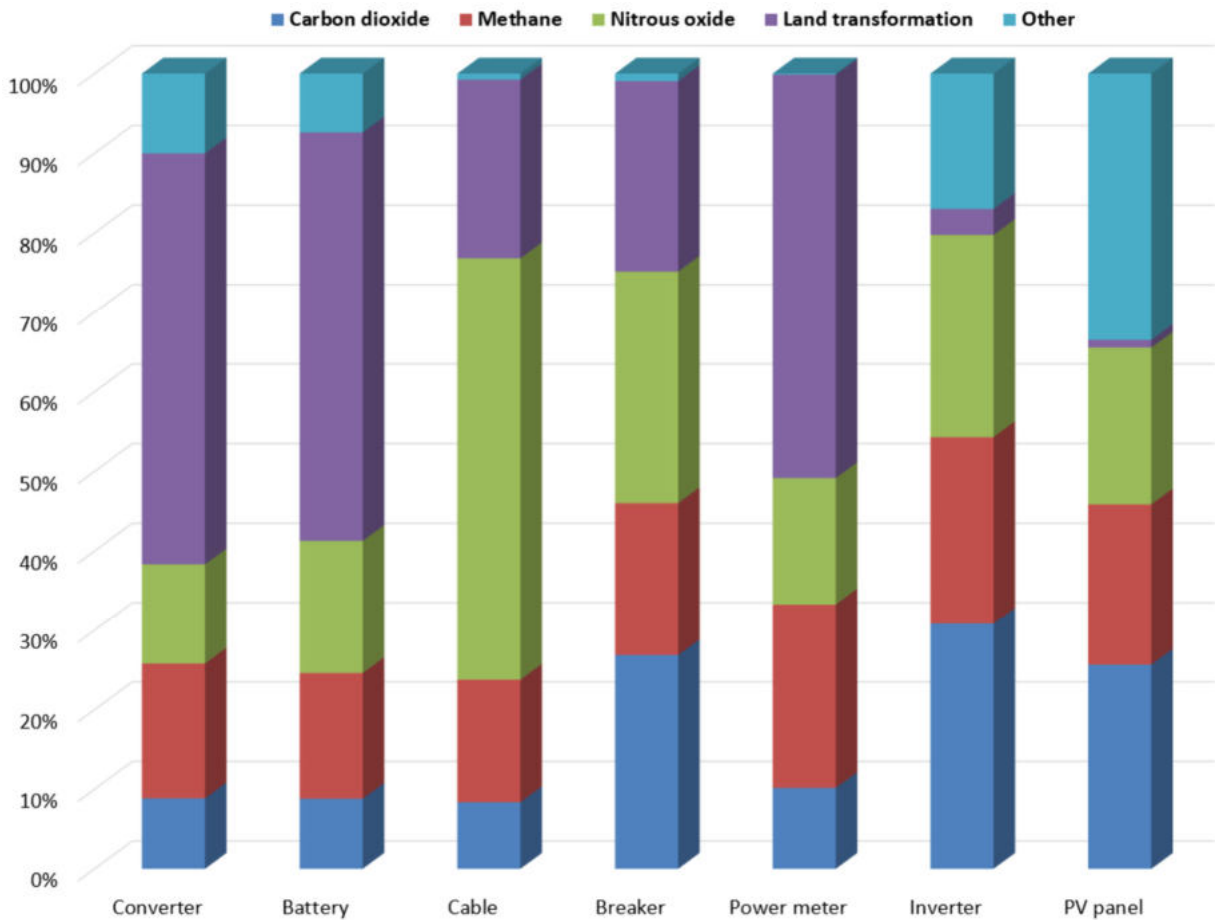


Fig 4.5 Greenhouse impact of PV constituents [119]

The biggest impact on the land transformation is made by the battery and the converter, big instruments that strongly impact the landscape. The maximum amount of dangerous nitrous oxide and carbon dioxide emission were the responsibility of the cable and inverter, respectively [119]. The maximum carbon dioxide emissions are made by the breaker and the inverter, other two constituents essential to produce electric energy that can be utilized.

In conclusion, when designing an LCA for the assessment of a photovoltaic panel it is not enough to analyse the impact of the solar panel itself, but is important the deep understanding of all the technologies that must be used for the correct function of the overall system.

Apart from the greenhouse emissions and other pollutants and toxic molecules observed, there are other indicators that must be understood in order to evaluate the environmental impact of a system, such as the acidification of lands and oceans, the eutrophication of watery environments and the ozone layer depletion [119].

4.3) Final considerations

In this work the possibility of recycling the material of the first generation solar cells, in particular the active layer of the solar cell was exploited. The choice to focus on the active layer of the solar cells has both economic and technical reasons: first of all, the precious materials are contained for the majority in the active layer, making more profitable processes that focus on recycling it.

Furthermore, what isn't manufactured in the active layer can easily be taken apart with simple mechanical processes, apart from the EVA layer that must undergo a pyrolysis step in order to recover the glass coated with the ITO and the active layer itself. Although pyrolysis is indeed a process which has an impact, the pyrolysis is conducted at 400 °C [120], a temperature that is reached mandatorily in other steps of the manufacturing in order to ensure the final quality. The device itself needs to be not just green under an environmental point of view, but also needs to ensure the quality and the performance of the actual devices available in the market in order to be seen as an alternative to the actual choices.

In this sense, it is possible to foresee what the next step of this research will be:

- Research on annealing processes to reduce the defects present in the film
- Research on alternative dopants to improve the electrical properties
- Research on alternative thermomechanical approaches
- Characterization of films deposited with different techniques (e.g. Sputtering)
- Scale-up of the material in a pilot plant

There is still room for improvement with the initial results promising for the future.

It is essential to underline that the properties of the material characterized are slightly different if compared to the ones of virgin silicon, doped or intrinsic. However, the goal of this research was not to copy the silicon material, something which can be done effectively just with leaching processes, but trying to exploit the advantages of the new material deposited and characterized, which for sure lower the impact of the manufacturing process.

In order to better purify the silicon it is indeed possible to use several steps of shutter instead of just one step as in this work, but some doping and trap effect on the final thin film will always be present due to the interactions within the powder during the intermediate steps.

The most evident difference between the material characterized in this study and the virgin semiconductors is evident in the spectra of absorbance, which is unusually high in the near UV range and has an absorption tail not seen in semiconductors, probably due to the free metals of the system: a comparison can be seen in fig 4.6:

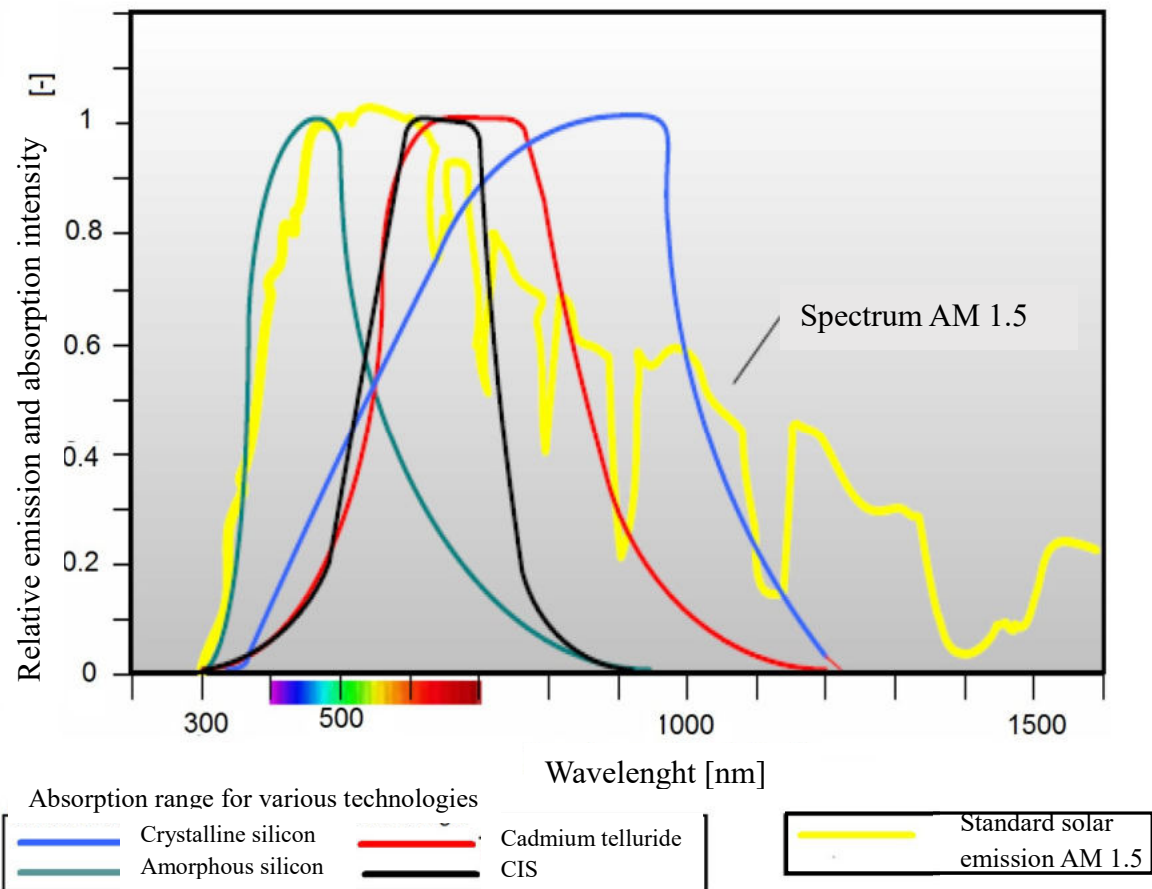


Fig 4.6 Comparison between absorption spectra of semiconductors and Sun's emission [121]

Considering the comparison of the absorption spectra there are some similarities between the amorphous silicon and the monolayer of the recycled powder because of the position of the absorption peak. It is for sure possible that the structure of the deposited layer is more similar to the one of amorphous silicon and not to the crystalline one, considering the deposition technique and the fact that aluminium induced crystallization is exploitable at temperature of more than 600 °C as discussed before in this work.

It is also missing the absorption tail, which however results in a temporary excitation due to the free metals present resulting in huge thermal losses.

The percentage of absorption are quite higher if compared to the ones of the study, but the absorbance spectra of the monolayer is enough to think about photovoltaic applications.

In conclusion, in this work the main goal was not to produce new silicon from the recycled waste but try to find some uses for the material deposited just with thermomechanical methods, in order to find a minimum on the environmental impact guaranteeing decent performances.

Ringraziamenti:

Non è facile ringraziare tutte le persone che mi hanno permesso di arrivare a questo momento: proverò comunque a farlo, tenendo in conto il più possibile che ogni traguardo non è mai frutto dell'impegno di un singolo individuo, ma è uno sforzo congiunto di più persone che si sono prodigate in diversi modi per renderti la persona che sei oggi, nel bene e nel male. Pertanto, ogni traguardo e obiettivo che ci prefissiamo e che riusciamo a raggiungere è reso possibile da ciò che siamo diventati nel corso della nostra vita, e la laurea non è un'eccezione: al di là dello studio e dell'impegno accademico profuso in questi anni, ci sono delle qualità che ho appreso in questo mio percorso di vita che non si possono imparare in ambito accademico, ma soltanto in un contesto sociale: in tal senso ringrazio tutte le persone che hanno deciso di loro spontanea volontà di lasciarmi qualcosa di loro, che sia un insegnamento, una riflessione o un ricordo gradevole, poiché è grazie a loro che sono diventato quel che sono oggi. Passando nello specifico, per prima cosa ringrazio i miei relatori che hanno deciso di supportarmi con i loro consigli nella parte più dedicata della mia carriera accademica, ovvero la stesura della tesi di laurea magistrale: ringrazio dunque il professor Matteo Pavese del politecnico di Torino e la professoressa Isabel Ferreira dell'università NOVA di Lisbona, sezione FCT. Poiché in questi mesi la parte sperimentale del mio lavoro di tesi è stata effettuata a Lisbona, ringrazio l'istituto della NOVA per avermi permesso di usufruire in piena libertà dei loro laboratori accademici, consentendomi di sviluppare delle vere e proprie competenze tecniche lavorando con la loro strumentazione.

Successivamente, ringrazio tutte le persone della mia vita che mi sono state vicine in questi anni dal punto di vista umano, senza chiedere nulla in cambio. La mia famiglia prima di tutto, poiché da essa è derivato un supporto costante durante la mia intera vita, sotto ogni aspetto immaginabile. Ringrazio poi tutte le amicizie che mi è stato possibile coltivare nel corso della mia vita, nella mia città natale ed in ogni altra località in cui ho deciso di vivere per un periodo, per quanto breve possa essere. Ogni nazionalità, ogni personalità che ho incontrato mi è stata fondamentale per maturare un pensiero più profondo, e per comprendere un po' meglio come funziona il mondo.

Infine, mi sento di ringraziare anche me stesso, perché non è scontato riuscire a superare gli ostacoli che la vita ci pone dinnanzi: tutte le persone che ti stanno vicino possono darti consigli, supportarti e provare ad indirizzarti verso la strada che loro ritengono corretta, ma nessuno può capire cosa veramente vuoi nel profondo se non te stesso, e dentro di sé bisogna trovare la forza per affrontare tutte le sfide che qualsiasi essere umano, in piccolo o in grande, deve affrontare nell'arco della propria esistenza. Grazie a tutte queste persone e mi auguro di aver restituito, almeno in parte, ciò che voi avete lasciato a me.

Bibliography

- [1] LCA study of photovoltaic systems based on different technologies Wesley M. Soares, Daniel D. Athayde, and Eduardo H.M. Nunes
- [2] Overview of global status and challenges for end-of-life crystalline silicon photovoltaic panels: A focus on environmental impacts: Bora Seo , Jae Young Kim , Jaeshik Chung
- [3] A Review on Design and Performance Evaluation of Solar Cells and Panels SumanLataTripathi, SobhitSaxena,SushmitaKumari
- [4] Solar photovoltaic technology: A review of different types of solar cells and its future trends Mugdha V Dambhare et al
- [5] Overview of the solar industry, Leonard Wagner
- [6] A Study of Materials for Solar PV Technology and Challenges Mallikarjun G. Hudedmani, Vishwanath Soppimath, Chaitanya Jambotkar
- [7] Solar energy—A look into power generation, challenges, and a solar-powered future Muhammad Badar Hayat, Danish Ali, Keitumetse Cathrine Monyake, Lana Alagha,Niaz Ahmed
- [8] Data on total and spectral solar irradiance Ann T. Mecherikunnel, James A. Gatlin, and Joseph C. Richmond
- [9] Exceeding the Shockley–Queisser Limit in Solar Energy Conversion Cory A. Nelsona, Nicholas R. Monahana, and X.-Y. Zhua
- [10] The schockley-Queisser limit, Susanne Siebentritt
- [11] Guide for the perplexed to the Shockley–Queisser model for solar cells, Jean-Francois Guillemoles, Thomas Kirchartz, David Cahen and Uwe Rau
- [12] Tabulated values of the Shockley–Queisser limit for single junction solar cells Sven Ruhle
- [13]Materials research and opportunities in solar (photovoltaic) cells Sudip K Saha
- [14] Investigation of basic principles and technologies of solar cells Kardelen Gundogdu, Meryem Tugce Ozel , Meryem Sena Akkus
- [15] Photovoltaics Reaching for the Sh^oCkley–Queisser Limit Bruno Ehrler,Esther Alarcon Llado,Stefan W Tabernig,Tom Veeken,Erik C Garnett,Albert Polman
- [16] High-Efficiency Crystalline Silicon Solar Cells: Status and Perspectives Corsin Battaglia, Andres Cuevas, Stefaan De Wolf
- [17] Silicon Solar Cells S. R. Wenham and M. A. Green
- [18] Crystalline solar cells: state of the art and future developments. Stefan W Glunz,Ralf Preu, Daniel Biro
- [19] P-Type Versus n-Type Silicon Wafers: Prospects for High-Efficiency Commercial Silicon Solar Cells J. E. Cotter, J. H. Guo, P. J. Cousins, M. D. Abbott, F. W. Chen, and K. C. Fisher
- [20] An overview of crystalline silicon solar cell technology: Past, present, and future K. Sopian, S. L. Cheow, and S. H. Zaidi
- [21] Crystalline Si thin-film solar cells: a review R.B. Bergmann

- [22] Metallurgical silicon from high purity sand critical issues and potential developments, Louis Parous, Valdiney Domingos de Oliveira
- [23] High Purity Polycrystalline Silicon Growth and Characterization, Uda Hashim, Abang A. Ehsan, and Ibrahim Ahmad
- [24] Review of status developments of high-efficiency crystalline silicon solar cells Jingjing Liu, Yao Yao, Shaoqing Xiao and Xiaofeng Gu
- [25] Thin-film Solar Cells W. H. Bless, F. Pfisterer, M. Schubert and T. Walter
- [26] Flexible CIGS, CdTe and a-Si:H based thin film solar cells: A review, Jeyakumar Ramanujam, Douglas M Bishop, Teodor K Todorov, Oki, Gunawan, Jatin Rath, Reza Nekovei, Elisa Artegiani, Alessandro Romeo
- [27] A review of thin film solar cell technologies and challenges Taesoo D. Leea,, Abasifreke U. Ebongb
- [28] Silicon Thin-Film Solar Cells Guy Beaucarne
- [29] Thin-film solar cells: review of materials, technologies and commercial status Martin A. Green
- [30] Thin-Film Solar Cells: An Overview K. L. Chopra, P. D. Paulson, and V. Dutta
- [31] Recent advances and applications of solar photovoltaics and thermal Technologies Lujean Ahmad, Navid Khordehghah, Jurgita Malinauskaite, Hussam Jouhara
- [32] The CdTe thin film solar cell-an overview Dieter Bonnet
- [33] Third-Generation Solar Cells: Concept, Materials and Performance - An Overview Soosaimanickam Ananthakumar, Jeyagopal Ram Kumar, and Sridharan Moorthy Babu
- [34] Flexible and Semitransparent Organic Solar Cells Yaowen Li, Guiying Xu, Chaohua Cui, and Yongfang Li
- [35] Organic solar cells: An overview Harald Hoppea and Niyazi Serdar Sariciftci
- [36] Recent Advances in Organic Solar Cells Thomas Kietzke
- [37] Organic Solar Cells—The Path to Commercial Success Moritz Riede, Donato Spoltore, and Karl Leo
- [38] Study and characterization of Graetzel solar cells Luísa Manuela Madureira Andrade
- [39] Panchromatic engineering for dye-sensitized solar cells Jun-Ho Yum, Etienne Baranoff, Sophie Wenger, Md. K. Nazeeruddin and Michael Graetzel
- [40] Dye-sensitized solar cells: A brief overview Md. K. Nazeeruddin, Etienne Baranoff, Michael Graetzel
- [41] Recent progress on quantum dot solar cells: a review Tomah Sogabe Qing Shen Koichi Yamaguchi
- [42] Colloidal quantum dot solar cells Saim Emin, Surya P. Singh, Liyuan Han, Norifusa Satoh, Ashraful Islam
- [43] Quantum dot solar cells A.J. Nozik
- [44] Silicon quantum dot/crystalline silicon solar cells Eun-Chel Cho, Sangwook Park, Xiaojing Hao, Dengyuan Song, Gavin Conibeer, Sang-Cheol Park and Martin A Green

- [45] Stability of Quantum Dot Solar Cells: A Matter of (Life)Time Miguel Albaladejo-Siguan, Elizabeth C. Baird, David Becker-Koch, Yanxiu Li, Andrey L. Rogach, and Yana Vaynzof
- [46] Frontiers, opportunities, and challenges in perovskite solar cells: A critical review Mohammed Istafaul Haque Ansaria, Ahsanulhaq Qurashib, Mohammad Khaja Nazeeruddin
- [47] Perovskite solar cells: an emerging photovoltaic technology Nam-Gyu Park
- [48] Perovskite Solar Cells: From Materials to Devices Hyun Suk Jung and Nam-Gyu Park
- [49] Recent progress in perovskite solar cells M. Khalaji Assadia, S. Bakhodaa, R. Saidurb,c, H. Hanaeia
- [50] The Future of Perovskite Photovoltaics—Thermal Evaporation or Solution Processing? Yana Vaynzof
- [51] Advances in Perovskite Solar Cells Chuantian Zuo, Henk J. Bolink, Hongwei Han, Jinsong Huang, David Cahen, and Liming Ding
- [52] Addressing the stability issue of perovskite solar cells for commercial applications Lei Meng, Jingbi You & Yang Yang
- [53] Material and Device Stability in Perovskite Solar Cells Hui-Seon Kim, Ja-Young Seo, and Nam-Gyu Park
- [54] Selecting tandem partners for silicon solar cells Zhengshan, Jason Yu, Mehdi Leilaoui, and Zachary Holman
- [55] Properties of high efficiency silicon heterojunction cells D.L. Bätzner, Y. Andraut, L. Andretta, A. Büchel, W. Frammelsberger, C. Guerin, N. Holm, D. Lachenal, J. Meixenberger, P. Papet, B. Rau, B. Strahm, G. Wahli, F. Wünsch
- [56] Monolithic Perovskite Tandem Solar Cells: A Review of the Present Status and Advanced Characterization Methods Toward 30% Efficiency Marko Jošt, Lukas Kegelmann, Lars Korte, and Steve Albrecht
- [57] Multi-junction solar cells and novel structures for solar cell applications Masafumi Yamaguchi
- [58] Japanese R&D Activities of High Efficiency III-V Compound Multi-Junction and Concentrator Solar Cells Masafumi Yamaguchi
- [59] Radiation-resistant and high-efficiency InGaP/GaAs/Ge 3-junction solar cells Masafumi Yamaguchi, Nobuaki Kojima, Auranzeb Khanb, and Tatsuya Takamoto, Koshi Andod
- [60] Environmental and economic evaluation of solar panel wastes recycling Çağdaş Gönen and Elif Kaplanoğlu
- [61] Global status of recycling waste solar panels: A review Yan Xu, Jinhui Li, Quanyin Tan, Anesia Lauren Peters, Congren Yang
- [62] The application of organic solvents and thermal process for eliminating EVA resin layer from waste photovoltaic modules Wei Sheng Chen, Yen Jung Chen, and Yu An Chen
- [63] A Simple Green Process to Recycle Si from Crystalline-Si Solar Cells Wen-Hsi Huang and Meng Taob

- [64] Chemical treatment of crystalline silicon solar cells as a method of recovering pure silicon from photovoltaic modules Ewa Klugmann-Radziemska, Piotr Ostrowski
- [65] Recycling perovskite solar cells to avoid lead waste Andreas Binek, Michiel L. Petrus, Niklas Huber, Helen Bristow, Yinghong Hu, Thomas Bein, and Pablo Docampo
- [66] Recycling progress of organic-inorganic perovskite solar cells for eco-friendly fabrication Fengjiu Yang, Shenghao Wang, Pengfei Dai, Luyang Chen, Atushi Wakamiya, Kazunari Matsuda
- [67] Recovery of FTO coated glass substrate via environment-friendly facile recycling perovskite solar cells M. S. Chowdhury,abe Kazi Sajedur Rahman,b Vidhya Selvanathan, A. K. Mahmud Hasan,b M. S. Jamal,bc Nurul Asma Samsudin,d Md. Akhtaruzzaman, Nowshad Amin and Kuaanan Techato
- [68] Current trends in recycling of photovoltaic solar cells and modules waste Stan Obeckny
- [69] Solvothermal synthesis,deposition and characterization of cadmium selenide (CdSe) thin films bythermal evaporation technique T.S. Shyju,S.Anandhi,R.Indirajith,R.Gopalakrishnan
- [70] Deposition of Nanostructured CdS Thin Films by Thermal Evaporation Method: Effect of substrate temperature
- [71] Fabrication of ZnO ring-like nanostructures at a moderate temperature via a thermal evaporation process XiangWua, Fengyu Qua, Xu Zhanga,Wei Caib, Guozhen Shenc
- [72] Preparation of large-scale cupric oxide nanowires by thermal evaporation method L.S. Huang, S.G. Yanga, T. Lia, B.X. Gua, Y.W. Dua, Y.N. Lub, S.Z. Shi
- [73] Diffusional Reactions Between MO and Si in the Synthesis and Densification of MoSi₂, Seetharama C. Deevi
- [74] Hall Effect Measurements in Materials Characterization Robert Green
- [75] The Al-Si (Aluminum-Silicon) System By J. L. Murray and A. J. McAlister
- [76] Temperature dependence of the optical properties of silicon H. A. Weakliem, and D. Redfield
- [77] Experimental and theoretical investigations of structural and optical properties of CIGS thin films M. Chandramohana, S. Velumanib, T. Venkatachalame
- [78] Synthesis and optical characterization of nan^oCrystalline CdTe thin films A.A. Al-Ghamdi a,n, ShamshadA.Khan a, A.Nagat b, M.S.AbdEl-Sadek
- [79] Photovoltaic Self-Powered Gas Sensor Based on Single-Walled Carbon Nanotubes Si Heterojunction L. Liua,b, G. H. Lic, Y. Wangd,e, Y. Y. Wangb, T. Lia, T. Zhang,a, S. J. Qin
- [80] Thermal Conductivity, Electrical Resistivity, and Seebeck Coefficient of Silicon from 100 to 1300 K W Fulkerson, J. P. Moore, R. K. Williams, R. S. Graveb, and D. L. Mcelroy
- [81] Temperature and Irradiance Dependence of the I-V Curves of Various Kinds of Solar Cells Yuki Tsuno, Yoshihiro Hishikawa and Kosuke Kurokawa
- [82] Aluminum induced crystallization and counterdoping of phosphorous doped hydrogenated amorphous silicon at low temperatures M. S. Haque, H. A. Naseem, and W. D. Brown

- [83] Solid phase epitaxial thickening of boron and phosphorus doped polycrystalline silicon thin films formed by aluminium induced crystallization technique on glass substrate Ö. Tüzün Özmena,b, M. Karamanc,d, S.H. Sedanic,d,e, H.M. Sağbanb, R. Turand
- [84] Electronic Transport in Phosphorus-Doped Silicon Nanocrystal Networks A. R. Stegner, R.N. Pereira, K. Klein, R. Lechner, R. Dietmueller, M. S. Brandt, and M. Stutzmann
- [85] Electrical conductivity of amorphous silicon doped with rare-earth elements J. H. Castilho, I. Chambouleyron, F. C. Marques, C. Rettori, and F. Alvarez
- [86] Efficiency Potential of n-Type Silicon Solar Cells With Aluminum-Doped Rear p+ Emitter Marc Rüdiger, Christian Schmiga, Michael Rauer, Martin Hermle, and Stefan W. Glunz
- [87] Recombination lifetimes in highly aluminum-doped silicon Jan Schmidt, Nils Thiemann, Robert Bock, and Rolf Brendel
- [88] Hall effect and impurity conduction in substitutionally doped amorphous silicon P. G. Le Comber a , D. I. Jones a & W. E. Spear
- [89] Influence of deep defects on device performance of thin-film polycrystalline silicon solar cells M. Fehr, P. Simon, T. Sontheimer, C. Leendertz, B. Gorke, A. Schnegg, B. Rech, and K. Lips
- [90] A variety of microstructural defects in crystalline silicon solar cells Pavel Škarvadaa, Pavel Tománek, Pavel Koktavya, Robert Mackua, Jiri Šicnera, Marek Vondraa, Dinara Dallaevaa, Steve Smithb, Lubomír Grmelaa Faculty
- [91] Defect induced non-ideal dark I-V characteristics of solar cells O. Breitenstein, J. Bauer, A. Lotnyk, J.-M. Wagner
- [92] Research on efficiency limiting defects and defect engineering in silicon solar cells - results of the German research cluster SolarFocus Stephan Riepe, Isolde E. Reis, Wolfram Kwopil, Marie Aylin Falkenberg, Jonas Schön, Herfried Behnken, Jan Bauer, Denise Kreßner-Kiel, Winfried Seifert, and Wolfgang Koch
- [93] Effect of metal electrode on Seebeck coefficient of p- and n-type Si thermoelectrics Osamu Yamashita
- [94] Intrinsic concentration, effective densities of states, and effective mass in silicon Martin A. Green
- [95] Hall mobility of polycrystalline silicon H. Paul Maruska, Amal K. Ghosh, Albert Rose, and Tom Feng
- [96] Development of a Phosphorus Spray Diffusion System for Low-Cost Silicon Solar Cells D. S. Kim,a M. M. Hilali, A. Rohatgi,a,z K. Nakano,b A. Hariharan,b and K. Mattheib
- [97] Understanding the sprayed boric acid method for bulk doping of silicon ribbons J.A. Silva a,n, David Pera, Miguel C. Brito, Jorge Maia Alves, Joao Serra, A.M. Vallera
- [98] Investigation on phosphorus doping using H₃PO₄ as doping source by simple dip method and its electrical characterisation I. Moon, M. Gunasekaran, K. Kim, M. Ju, S. Han and J. Yi

- [99] Low temperature doping of poly-SiGe films with boron by co-sputtering Emil V. Jelenkovic, K.Y. Tonga, W.Y. Cheungb, I.H. Wilsonb, S.P. Wongb, M.C. Poon
- [100] Nonequilibrium boron doping effects in lowtemperature epitaxial silicon films B. S. Meyerson, F. K. LeGoues, T. N. Nguyen, and D. L. Harnage
- [101] Binary copper oxide semiconductors: From materials towards devices B. K. Meyer, A. Polity, D. Reppin, M. Becker, P. Hering, P. J. Klar, Th. Sander, C. Reindl, J. Benz, M. Eickhoff, C. Heiliger, M. Heinemann, J. Blasing, A. Krost, S. Shokovets, C. Muller, and C. Ronning
- [102] Copper Oxides (Cu₂O, CuO) Carl G Ribbing and Arne Roos
- [103] Fabrication and Characterization of CuO-based Solar Cells Hiroki Kidowaki, Takeo Oku, Tsuyoshi Akiyama, Atsushi Suzuki Balachandran Jeyadevan & Jhon Cuya
- [104] A Review: Synthesis, Characterization and Cell Performance of Cu₂O Based Material for Solar Cells Hafsa Siddiqui, Mohammad Ramzan Parra, Padmini Pandey, Neha Singh, M. S. Qureshi and Fozia Haque
- [105] Optimization of Cuprous Oxides Thin Films to be used as Thermoelectric Touch Detectors Joana Figueira, Joana Loureiro, José Marques, Catarina Bianchi, Paulo Duarte, Mikko Ruoho, Ilkka Juhani Tittonen, and Isabel Ferreira
- [106] Understanding the p-n Junction by Dr. Alistair Sproul
- [107] Extraordinary Mobility in Semiconducting Carbon Nanotubes T. Duirkop, S. A. Getty, Enrique Cobas, and M. S. Fuhrer
- [108] Electron mobility in 2-6 semiconductors D.L.Rode
- [109] Enhancing hole mobility in III-V semiconductors Aneesh Nainani, Brian R. Bennett, J. Brad Boos, Mario G. Ancona, and Krishna C. Saraswat
- [110] Conductivity in Semiconductors K. Lark Horovitz
- [111] Electrical Conductivity of Organic Semiconductors Hiro Inokutchi and Hideo Akamatu
- [112] Photovoltaic device on a single ZnO nanowire p-n homojunction Hak Dong Cho, Anvar S Zakirov, Shavkat U Yuldashev, Chi Won Ahn, Yung Kee Yeo and Tae Won Kang
- [113] Designing CdS/Se heterojunction as high-performance self-powered UV-visible broadband photodetector Jianyuan Wang, Yu Chang, Linfeng Huang, Kexin Jin, and Wei Tian
- [114] Characterization of CuO/n-Si pn junction synthesized by successive ionic layer adsorption and reaction method Adel H. Omran Alkhayatt · Mustafa D. Jaafer · Hassan Hadi Ali Al Alak Asala H. Ali
- [115] Prospects of life cycle assessment of renewable energy from solar photovoltaic technologies: A review Norasikin Ahmad Ludina, Nur Ifthitah Mustafaa, Marlia M. Hanafiahb, Mohd Adib Ibrahima, Mohd Asri Mat Teridia, Suhaila Sepeaia, Azami Zaharime, Kamaruzzaman Sopiana
- [116] Evaluating the Environmental Performance of Solar energy Systems Through a combined Life Cycle assessment and cost analysis maria milousi, manolis souliotis, george arampatzis and spiros papaefthimiou

[117] Comparative Life Cycle Assessment of End-of-Life Silicon Solar Photovoltaic Modules

Marina M. Lunardi, J. P. Alvarez-Gaitan, J. I. Bilbao and Richard Corkish

[118] LCA study of photovoltaic systems based on different technologies Wesley M. Soares, Daniel D. Athayde & Eduardo H.M. Nunes

[119] Environmental Impacts of Solar-Photovoltaic and Solar-Thermal Systems with Life-Cycle Assessment M. A. Parvez Mahmud, Nazmul Huda, Shahjadi Hisan Farjana and Candace Lang

[120] Demanufacturing photovoltaic panels: Comparison of end-of-life treatment strategies for improved resource recovery Joost R. Duflou, Jef R. Peeters, Diego Altamirano, Ellen Bracquene, Wim Dewulf

[121] Courtesy of energy hunters website 13/07/2023 <https://www.energyhunters.it/>